

**DRAFT FINAL REPORT**

**EXPERIMENTAL AND ANALYTICAL EVALUATION OF  
FLEXIBLE PIPES FOR CULVERTS AND STORM SEWERS**

---

**VOLUME I – LITERATURE REVIEW**

Submitted to:

Director, Research Center  
Florida Department of Transportation  
605 Suwannee St., MS 30  
Tallahassee, Florida 32399-0450

**CONTRACT No. BC-775**

By

**Dr. M. Arockiasamy**  
Principal Investigator  
Professor and Director  
Center for Infrastructure and Constructed  
Facilities  
Department of Civil Engineering  
Florida Atlantic University  
Boca Raton, FL 33431

**T. Limpeteprakarn**  
Graduate Research Assistant

**Dr. O. Chaallal**  
Co-Principal Investigator  
Professor and Director  
Dev. & Research for Str. and Rehab. (DRSR)  
Department of Construction Engineering  
University of Quebec/  
Ecole de Technologie superieure  
Montreal, Quebec, Canada H3C1K3

**N. Wang**  
Graduate Research Assistant

**August 2002**

## **DISCLAIMER**

---

The opinions, findings and conclusions expressed in this publication are those of the authors who are responsible for the facts and accuracy of the data presented herein. The contents do not necessarily reflect the views or policies of the Florida Department of Transportation or the Federal Highway Administration. This report does not constitute a standard, specification or regulation.

The report is prepared in cooperation with the Florida Department of Transportation and the Federal Highway Administration.

## ACKNOWLEDGEMENTS

---

The authors would like to express sincere thanks to Dr. S. J. Nix, Chairman, Department of Civil Engineering and Dr. K. Stevens, Interim Dean, College of Engineering, Florida Atlantic University for their continued interest and encouragement.

The authors are grateful to N. Butrieng, P. Charoenruengkit, V. Joshi and L. Banda research assistants for their assistance in the report preparation.

# TABLE OF CONTENTS

---

**ACKNOWLEDGEMENTS** .....

**LIST OF TABLES**.....

**LIST OF FIGURES**.....

**TABLE OF CONVERSION** .....

## **1.1 STRUCTURAL DESIGN**

- i) Calculating Loads on Buried Culverts Based on Pipe Hoop Stiffness ..... 1-1
- ii) Structural Design of Buried Culverts with Slotted Joints..... 1-3
- iii) Design Methodology for Corrugated Metal Pipe Tiedowns: Phase 1 ..... 1-6
- iv) Design Methodology for Corrugated Metal Pipe Tiedowns: Phase 2 ..... 1-8

## **1.2 STRUCTURAL PERFORMANCE**

- i) Comparison of Structural Response of 762 mm (30in.) Diameter Thermoplastic Pipes under Deep Burial..... 1-12
- ii) Comparison of Tests and Analysis of 1050 mm (42 in.) Diameter High Density Polyethylene (HDPE) Thermoplastic Pipe ..... 1-16
- iii) Structural Performance of HDPE Profile-wall Pipe ..... 1-20
- iv) Corrugated HDPE Pipe: Laboratory Testing and Two-Dimensional Analysis to Develop Limit States Design ..... 1-23
- v) Earth Pressure and Surface Load Effects on Buried Pipelines ..... 1-30
- vi) Boundary Effects on Response of Polyethylene Pipe Under Simulated Live Load ..... 1-33
- vii) Performance of Thermoplastic Culvert Pipe Under Highway Vehicle Loading ..... 1-42

## **1.3 SOIL STIFFNESS**

- i) Laboratory Determination of Soil Stiffness Data for Buried Plastic Pipe ..... 1-47

## **1.4 SOIL-PIPE INTERACTION**

- i) Modulus of Soil Reaction Values For Buried Flexible Pipe ..... 1-51
- ii) The Peripheral Movement of Soil Around a Buried Flexible Pipe ..... 1-55

## **1.5 LONGITUDINAL STRENGTH AND STIFFNESS**

- i) Longitudinal Strength and Stiffness of Corrugated Steel Pipe ..... 1-57

<b>1.6</b>	<b>STATE-OF-THE-ART IN UNITED KINGDOM</b>	
	i) Structural Performance of Profile-Wall Drainage Pipe-Stiffness Requirements Contrasted with Results of Laboratory and Field Tests .....	1-61
	ii) Laboratory and Field Testing of Large-Diameter Plastic Pipe .....	1-68
	iii) The Influence of Surrounding Soil on Flexible Pipe Performance.....	1-73
	iv) Some Observations on Flexible Pipe Response to Lo .....	1-77
<b>1.7</b>	<b>FINITE ELEMENT ANALYSIS</b>	
	i) Nonlinear Finite Element Analysis for Thermoplastic Pipes .....	1-82
	ii) Three Dimensional Analysis of Flexible Circular Culverts .....	1-87
	iii) Three Dimensional Response of Deeply Buried Profiled Polyethylene Pipe.....	1-92
	iv) Analysis of Buried Flexible Pipe Using CANDE and ANSYS .....	1-98
<b>1.8</b>	<b>TIME-DEPENDENT BEHAVIOR</b>	
	i) Time-Dependent Deflection of Thermoplastic Pipes Under Deep Burial .....	1-101
	ii) Long-term Behavior of Flexible Large-Span Culverts .....	1-104
	iii) New Method of Time-Dependent Analysis for Interaction of Soil and Large-Diameter Flexible Pipe .....	1-107
	iv) Stress Relaxation Characteristics of the HDPE Pipe-Soil System.....	1-116
	v) Three Dimensional Time Dependent Model for Buried HDPE Pipe .....	1-119
<b>1.9</b>	<b>LIFETIME PREDICTION OF POLYETHYLENE PIPES</b>	
	i) New Method of Lifetime Prediction for Brittle Fracture of Polyethylene .....	1-125
	ii) Methodology for Durability Analysis of HDPE Pipe .....	1-129
	iii) Accelerated Fracture Mechanics Evaluation of Slow Crack Growth Potential in Corrugated Polyethylene Pipes.....	1-134
	iv) Time-Temperature Superposition in Mechanical Durability Testing of Polyethylene Geomembranes .....	1-144

**REFERENCES**

## LIST OF TABLES

1.1.1- Elastic Solution Equation for Pressure on Pipe Response for Bounded and Frictionless Interface .....	1-5
1.1.2- Comparison of Yield Moment Values.....	1-7
1.1.3- Comparison of Ultimate Moment Values .....	1-7
1.1.4- Comparison of EI Factor Values .....	1-7
1.2.1- Pipe Properties.....	1-13
1.2.2- Description of Backfill on Test Pipes .....	1-13
1.2.3- Summary of 762-mm (30-inch) Pipes under 6-m (20 ft) Cover .....	1-14
1.2.4- Description of Backfill Material on Test Pipes.....	1-17
1.2.5- Comparison of Pressure and Deflection for Pipes 13, 14, and 15 Calculated Using Burns and Richards Equations (Full Slip Interface) with the Field Data .....	1-18
1.2.6- Comparison of Pressure and Deflection for Pipes 13, 14, and 15 Calculated Using Burns and Richards Equations (Full Bonded Interface) with the Field Data .....	1-18
1.2.7- Performance Limit for 60-inch ADS HDPE Pipes.....	1-21
1.2.8- Performance Limit for 42-inch ADS HDPE Pipes.....	1-21
1.2.9- Change in Vertical Diameter (mm) (% Difference from Measured Values in Parentheses) ..	1-26
1.2.10- Conduit Thrusts and Moments with HS-20 Surface Loading).....	1-31
1.2.11- Pipe Deflections at 479 kPa (10,000 psf).....	1-35
1.2.12- Pipe Deflections at Ultimate Strength.....	1-38
1.2.13- Test Variables.....	1-42
1.2.14- Summary of Pipe Installations and Instrumentation .....	1-43
1.2.15- Crown Deflections from Static Live Load Tests.....	1-45
1.2.16- Crown Deflections from Dynamic Static Live Load Tests .....	1-46
1.3.1- Values of E' Determined by Empirical and Analytical Means .....	1-49
1.3.2- Backcalculated Values of E' for Lightly Compacted Sand Surround.....	1-49
1.3.3- Backcalculated Values of E' for Gravel Surround.....	1-50
1.3.4- Backcalculated Values of E' for Heavily Compacted Sand Surround.....	1-50
1.4.1- Bureau of Reclamation Value of E' for Iowa Formula (for Initial Flexible Pipe Deflection)	1-54
1.5.1- Comparison of Experimental and Theoretical Values .....	1-59
1.6.1- Experimental Data at Critical Points of Tests .....	1-65
1.6.2- Vertical Diametrical Strains Recorded in Laboratory Tests .....	1-70
1.6.3- Vertical Diametrical Strains Recorded in Field Test .....	1-72
1.7.1- Pipe and Soil Properties Used in the Analysis .....	1-98
1.8.1- Pipe Properties.....	1-102
1.8.2- Stabilized Deflection for the Pipes.....	1-103
1.8.3- Exponents of Relaxation Power Law for Soils and Pipe Materials .....	1-114
1.9.1- Correspondence Between Notation on Panels and Panel Designations .....	1-136
1.9.2- Information of Slow Crack Growth Tests .....	1-137
1.9.3- SCG Post Test Data .....	1-139
1.9.4- SCG Incubation Material Parameters for Virgin PE Material at A Reference Temperature of 70°F. Parameters for Virgin Material are used as Lower Bound Estimates for Those of Recycle PE Material .....	1-140

## LIST OF FIGURES

1.1.1- Standard Keyhole Slot Dimensions.....	1-3
1.1.2- Potential Failure Modes .....	1-6
1.1.3- Flowchart for Design Process to Determine Restraining Force.....	1-10
1.1.4- Finite Element Models .....	1-10
1.1.5a- Cross Sectional View of Assumed Flow Conditions .....	1-11
1.1.5b- Influence of Flow Condition on Restraining Force.....	1-11
1.2.1- Pressure Cell Configuration .....	1-15
1.2.2- Orientation of Potentiometers .....	1-15
1.2.3- Overall Layout of Thermoplastic Pipes at Deep Burial Test Site.....	1-19
1.2.4- Installation of Pressure Cells.....	1-19
1.2.5- Pipe Burial in the Soil Cell, and Load Being Applied to Soil Surface .....	1-22
1.2.6- Vertical Deflection Curves for 60-Inch HDPE Pipe at Various Soil Densities. The Dashed Lines are Approximated Curves for Intermediate Densities .....	1-22
1.2.7- Pipe Installation (Schematic) .....	1-23
1.2.8- Pipe Profile and Location of Strain Gauges.....	1-24
1.2.9- Finite Element Mesh .....	1-24
1.2.10- Circumferential Strain at the Springline .....	1-27
1.2.11- Circumferential Strain at the Crown .....	1-27
1.2.12- Deformed Shape of the Pipe for Different Soil Support (Deflection x 5) .....	1-28
1.2.13- Distribution of Circumferential Strains on HDPE Pipe .....	1-29
1.2.14- Thrusts and Moments: 60-inch Pipe with HS-20 Surface Load.....	1-32
1.2.15- Cross Sections of Backfill Envelopes Used in Field Tests: (a) Tests 7 and 8; (b) Tests 9, 11, and 12; (c) Tests 10 and 13.....	1-34
1.2.16- Service Loading of 900-mm (36-in.) Diameter Pipes: (a) Vertical Deflection (b) Horizontal Deflection .....	1-36
1.2.17- Service loading of 1200-mm (48-in.) Diameter Pipes: (a) Vertical Deflection, (b) Horizontal Deflection .....	1-37
1.2.18- Vertical Deflection of Pipes with Varying Levels of Backfill: (a) No Backfill, (b) Backfill to Springline of Pipe, (c) Backfill to 70 Percent of Outside Diameter, (d) Backfill to Crown of Pipe .....	1-39
1.2.19- Failure Loading of 900-mm (36-in.) Diameter Pipes: (a) Vertical Deflection, (b) Horizontal Deflection .....	1-40
1.2.20- Failure Loading of 1200-mm (48-in.) Diameter pipes: (a) Vertical Deflection, (b) Horizontal Deflection .....	1-41
1.2.21- Actual Corrugated PE Wall Profiles .....	1-43
1.2.22- Truck Configuration and Axle Loads.....	1-44
1.2.23- Typical Dynamic Response, 0.3 m (1 ft) Cover, 107 kN Axle Load Truck .....	1-46

1.3.1- Cross Section Through Test Apparatus.....	1-51
1.4.1- Comparison of Actual and Predicted Deflections for (A) Dumped and Slightly Compacted Beddings (< 85%)(B) Moderately Compacted Beddings (85%-95%)(C) Highly Compacted Beddings (>95%).....	1-53
1.4.2- Peripheral Soil Movement and $V_z$ for Small Diameter Pipes.....	1-55
1.4.3- Visible Movement Zone/Pipe Diameter $V_z/D$ for Small Diameter Pipes (D = Pipe Diameter).....	1-56
1.5.1- Description Of CMP: (a) Corrugation Detail; (b) Free Body Diagram of One-Quarter Corrugation Cycle; (c) Transverse Cross Section .....	1-60
1.6.1- Diametral Strains due to Installation and 70-Kpa Static Stress Phases .....	1-66
1.6.2- Diametral Strains due to Installation and 70-Kpa Cyclic and 140-Kpa Static Stress Phases .	1-66
1.6.3- Twin Wall Strains Caused by the Complete Stress Sequence (End of Test Minus Installation) and Parallel Plate Testing.....	1-67
1.6.4- Single Wall Strains Caused by the Complete Stress Sequence (End of Test Minus Installation).....	1-67
1.6.5- The Effect of Surround Conditions on the Pipe Deformation.....	1-71
1.6.6- Increase in Vertical Diametrical Strain for A Twin-Wall Pipe in A Trodden Sand Surround Under Repeated Loading in the Field Test.....	1-72
1.6.7- Vertical Diametral Strains (VDS) for Five Sidefill Types in the Pit (Uncompacted Backfill / UCPG: Pea Gravel; UCCB: Concrete Ballast; UCQT: Quarry Tailings; UCBS: Building Sand; UCRS: Reject Sand) .....	1-74
1.6.8- Influence of Bedding on VDS Measurements in the Pit .....	1-75
1.6.9- Influence of Empirical Soil Factor, Compaction Fraction .....	1-76
1.6.10- Pipe-Wall Strain Profiles Under 55 kN Static Load Using Four Sidefill Materials .....	1-79
1.6.11- Pipe-Wall Strain Profiles Under 55 kN Static Load Using Four Combinations of Gravel and Clay.....	1-80
1.6.12- Types of Deformation and Associated Strain Profiles.....	1-81
1.7.1- Load Deflection Response for Plain Pipe at 12-Mm/Min Vertical Deflection Rate Until 20 Percent Decrease in Vertical Diameter: Measurements and Finite Element Predictions .....	1-84
1.7.2- Load Deflection Response for Plain Pipe at Two Different Rates of Vertical Diameter Decrease: Measurements and Finite Element Predictions.....	1-84
1.7.3- Load Relaxation with Time for Plain at Fixed Vertical Deflection after Abrupt Change Deflection Rate: Measurements and Nonlinear Finite Element Predictions.....	1-85
1.7.4- Radius Decrease Versus Air Bladder Pressure: Test Measurements and Finite Element Predictions .....	1-85
1.7.5- Axial Strain at Corrugation Valley: Finite Element Estimates and Experimental Measurements.....	1-86
1.7.6- Axial Strain at Corrugation Crown: Finite Element Estimates and Experimental Measurements.....	1-86

1.7.7- Shallow Buried Culvert with Prismatic Geometry and Location of Tire Loads from Vehicle on Ground Surface.....	1-87
1.7.8- Semianalytic Finite-Element Model for Shallow Buried Culvert.....	1-88
1.7.9- Axle and Wheel Loads under Test Vehicle: (a) x Direction, Eccentricity, $e_x$ (b) z Direction, Eccentricity, $e_z$ .....	1-89
1.7.10- Finite Element Mesh to Model Deux Rivieres Culvert.....	1-89
1.7.11- Thrust Distribution for Deux Rivieres Culvert (a) $E'=30\text{mpa}$ (b) $E'=80\text{mpa}$ .....	1-90
1.7.12- Effect of Orthotropic Structural Theory on Thrust Predictions $E_x=0$ (a) $E_z=0$ ; (b) $E_z=2.74$ 1-91	1-91
1.7.13- 2D and 3D Thrust Predictions $E_z=0$ (a) $E_x=0$ ; (b) $E_x=1.52\text{m}$ .....	1-91
1.7.14a- Exposed View Showing the Deeply Buried Pipe .....	1-95
1.7.14b- Detail of the Pipe with Annular Corrugation and Smooth Internal Liner.....	1-95
1.7.15- Finite Element Mesh Close to the 460mm Diameter Pipe .....	1-96
1.7.16- Circumferential Pipe Stresses at Crown/Invert, Springlines and Quarter Points.....	1-96
1.7.17- Radial Pipe Stresses at Crown/Invert, Springlines and Quarter Points.....	1-97
1.7.18- Axial Pipe Stresses at Crown/Invert, Springlines and Quarter Points .....	1-97
1.7.19- PE Pipe Crown Vertical Deflection with Respect to Position on Pipe Circumference for Different Height of Soil Covers (1 foot = 0.305m, 1 inch = 25.4mm).....	1-99
1.7.20- PE Vertical Deflection using Duncan Chang Model for both ANSYS and CANDE (1 foot = 0.305m, 1 inch =25.4 mm) .....	1-100
1.7.21- PE Vertical Deflection Percent using Duncan Chang Model for both ANSYS and CANDE (1 foot = 0.305m).....	1-100
1.8.1- Cross-Sections of The Test .....	1-103
1.8.2- Measured Earth Pressure Around the Structure (Tolpinrud) .....	1-105
1.8.3- Long-Term Deformations (Tolpinrud).....	1-106
1.8.4- Measured Thrust Force in the Steel Structure (Dovre).....	1-106
1.8.5- Measured Earth Pressure around the Structure (Dover) .....	1-107
1.8.6- Typical Configuration of A Pipe Trench.....	1-109
1.8.7- Vertical Deflections for Pipes of Different Stiffness.....	1-109
1.8.8- Vertical Deflection of Pipes in Different Soils .....	1-110
1.8.9- Soil Moduli for Different Depths of Cover.....	1-110
1.8.10- Arching Factor of A Soil-Pipe System in Different Soils .....	1-111
1.8.11- Effects of Groundwater on Pipe Deflection .....	1-111
1.8.12- Ratio of Pipe Horizontal Deflection to Vertical Deflection.....	1-112
1.8.13- Pipe Strains at Crown for Different In Situ Soils.....	1-113
1.8.14- Variation of Pipe Vertical Deflection over Time.....	1-114
1.8.15- Variation of Bending Moment at Crown over Time .....	1-114
1.8.16- Predicted and Measured Pipe Vertical Deflection for Different Depths of Cover .....	1-115
1.8.17- Predicted and Measured Pipe Vertical Deflection for Different Time Periods .....	1-115
1.8.18- Stress Relaxation Modulus vs. Time for HDPE.....	1-117
1.8.19- Crown Bending Moment vs. Time for HDPE Pipe in Clay and in Sand .....	1-118
1.8.20- Typical Buried HDPE Pipe .....	1-119
1.8.21- Finite Element Model for Axisymmetric Pipe Analysis .....	1-120

1.8.22- Multi-Kelvin model .....	1-120
1.8.23a- Loading Conditions for the Parallel Plate Test .....	1-121
1.8.23b- Finite Element Mesh for the Parallel Plate Test .....	1-122
1.8.24- Experimental Measurement and Finite Element Predictions for the Parallel Plate Test .....	1-123
1.8.25- Field Installation for Deeply Buried HDPE Pipe .....	1-123
1.8.26- Measurement and Theoretical Prediction of Pipe Deformation and Circumferential Strain .....	1-124
1.9.1- Schematic Presentation of Crack Layer in PEs .....	1-126
1.9.2- Experimental Observations (points) and Theoretical Predictions (lines) .....	1-128
1.9.3- SEM Image of Fracture Surface. The Primary Crack Initiation Site is Located at Bottom-Center in the Figure and is Near the Inner Wall of the Pipe .....	1-130
1.9.4- Particle Size Distribution of Defect Particles Observed From Fracture Surfaces of Two Pipes with Quite Different Lifetimes (6 Times Difference) Under Test.....	1-130
1.9.5- The Defect Sizes vs. the Crack Sizes in Tested Pipes.....	1-131
1.9.6- Creep Behavior of a HDPE Material Under the Stress of Drawing Stress .....	1-133
1.9.7- Schematic of the SCG Experimental Setup.....	1-136
1.9.8- Raw SCG Test Data for Recycle Sample A-1. The Point of Inflection at 89 Hours Denotes Transition from Incubation to Crack Propagation.....	1-138
1.9.9- SCG Incubation Test Data For Virgin and Recycle Material Tests. The Line Represents The Best Power Law Fit to the Virgin Material Data .....	1-139
1.9.10- Estimated Lifetime of 18 Inch Diameter Virgin Pipe Buried at A Depth of 36 Feet versus Service Temperature for Three Defect Depths.....	1-143
1.9.11- Notched Constant Load Specimen and Crack Growth Rate $\dot{a}$ (da/dt) versus Stress Intensity Factor (K) Curve.....	1-145
1.9.12- Experimental NCTL Test Results for a HDPE Geomembrane .....	1-147

## TABLE OF CONVERSIONS

To convert from	To	Multiply by
<b>Length</b>		
Inch (in.)	Millimeter (mm)	25.4
Foot (ft)	Meter (m)	0.3048
<b>Area</b>		
Square inch (sq. in.)	Square millimeter (sq. mm)	645.2
Square foot (sq. ft.)	Square meter (sq. m)	0.0929
<b>Volume</b>		
Cubic inch (cu. in.)	Cubic meter (cu. m)	0.00001639
Cubic foot (cu. ft.)	Cubic meter (cu. m)	0.02832
Cubic yard (cu. yd.)	Cubic meter (cu. m)	0.7646
Gallon (gal)	Liter	3.785
<b>Force</b>		
Kip	Kilogram (kgf)	453.6
Kip	Newton (N)	4448.0
Pound (lb)	Newton (N)	4.448
<b>Pressure or Stress</b>		
Kip/square inch (ksi)	Megapascal (MPa)**	6.895
Pound/square inch (psi)	Megapascal (MPa)**	0.006895
**One Pascal equals one newton/square meter		
<b>Mass</b>		
Pound	Kilogram (kg)	0.4536
Ton (short, 2000 lb)	Kilogram (kg)	907.2
<b>Mass (weight per length)</b>		
Kip/linear foot (klf)	Kilogram/meter (kg/m)	0.001488
Pound/linear foot (plf)	Kilogram/meter (kg/m)	1.488
Pound/linear foot (plf)	Newton/meter (N/m)	4.593

# Literature Review

## 1.1 Structural Design

**Calculating Loads on Buried Culverts Based on Pipe Hoop Stiffness, McGrath, T.J.,  
*Transportation Research Record 1656 , Paper No.99-0909, 1999, pp. 73-79.***

Flexible pipe has traditionally been designed based on the assumption that vertical soil load is the weight of soil directly over the pipe, known as “soil prism load”. Field experience and research have shown that the pipe with low cross-sectional area and low modulus of elasticity can be buried at depths greater than calculated by using the soil prism load. Burns and Richard elasticity solution for a circular tube embedded in an elastic medium shows that the ratio of the soil stiffness to the pipe hoop stiffness ( $EA/R$ ) is often the controlling factor in determining the load on a buried pipe instead of the flexural stiffness of the pipe.

The weight of soil directly over the pipe is calculated as follows:

$$W_{sp} = \gamma_s (H + 0.11D_o) D_o$$

Where

$W_{sp}$  = soil prism load, kN/m (lb/ft)

$\gamma_s$  = unit weight of soil, kN/m<sup>3</sup> (lb/ft<sup>3</sup>)

H = depth of fill over top of pipe, m (ft), and

$D_o$  = outside diameter of pipe, m (ft)



Under typical embankment conditions, theories for flexible pipe generally predict loads to be less than or equal to the soil prism load and theories for rigid pipe generally predict loads to be greater than the soil prism load.

The load on the pipe is expressed as a function of the soil prism load:

$$W_p = VAF \times W_{sp}$$

Where

VAF= vertical arching factor, and

$W_p$  =load on the pipe, kN/m (lb/ft)

The Burns and Richard equation for VAF based on thrust at the spring line is:

No slip:  $VAF = B(1 - a_0) + C(1 + a_2)$

Full slip:  $VAF = B(1 - a_0) + \frac{C}{3}(1 + 3A_2 - 4B_2)$

Where

The parameters  $A_2$ ,  $B$ ,  $B_2$ ,  $C$ ,  $a_0$ , and  $a_2$ , usually depend on bending stiffness, Poisson's ratio of the soil and hoop stiffness of the pipe.

Burns and Richard equations are somewhat cumbersome. The simplified Burns and Richard equations to predict load on buried pipe are suitable for use in design. The VAF values are consistent with past practice for traditional pipe, with the keyhole slotted designs used in the corrugated steel pipe industry, and with recent research on corrugated polyethylene pipe under deep fills.

The modified and simplified design equations are:

No slip:  $VAF = 1.06 - 0.96 \frac{(S_H - 0.7)}{(S_H + 1.75)}$

Full slip:  $VAF = 0.76 - 0.71 \frac{(S_H - 0.7)}{(S_H + 1.75)}$

Where  $S_H$  = hoop stiffness factor.



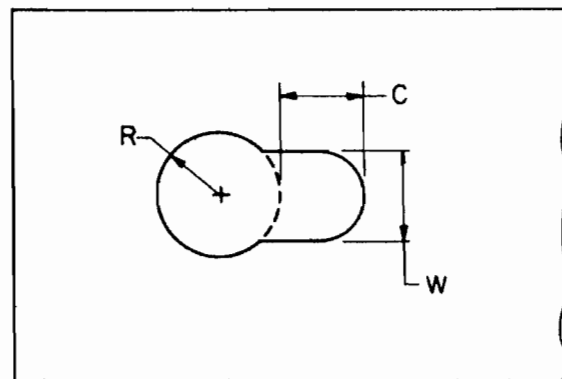
Simplified version of Burns and Richard method is proposed for computing loads based solely on the pipe hoop stiffness and soil stiffness. Little accuracy is lost by disregarding the flexural stiffness of the pipe in the calculations.

**Structural Design of Buried Culverts With Slotted Joints**, Katona, M.G. and Akl, A.Y., *ASCE Journal of Structural Engineering*, Vol .113, No.1, 1987, pp. 44-60.

The purpose of slotted bolt hole connections for corrugated metal culvert installations is to relieve the thrust stress and, thereby, achieve a deeper allowable burial depth, or alternatively, reduce the required wall thickness. By removing little bits of metal next to the bolt holes, the design capacity of the culvert is significantly improved.

The objective of this paper is to provide a set of design tables, listing the maximum allowable fill height for 152.4 x 50.8 mm (6 x 2-in) corrugated steel pipes with slotted joints and, for comparative purposes, standard joints as well.

The “keyhole” slot configuration is shown in Fig.1.1.1.



R = Bolt Hole Radius ( 7/16 in. )  
C = Key - Slot Length ( 1/2 in. )  
W = Slot Width ( 5/8 in. )

**Fig. 1.1.1 Standard Keyhole Slot Dimensions**

Table 1.1.1 summarizes Burn’s solutions for the key responses of the pipe for both interface assumptions. In adapting the elasticity solutions to simulate slotted-joint behavior, the authors apply the equations in an incremental fashion to accommodate changes in the circumferential stiffness  $E^*A$ , as overburden pressure increases.  $E^*A$ , which is a smeared average of the elastic pipe wall and all slotted joints, has four possible values corresponding

to the four zones of slotted-joint behavior. Initially,  $E^*$  is the elastic steel modulus  $E_e$ . When the average thrust stress exceeds  $\sigma_e$  (initial slipping stress),  $E^*$  is reduced to represent joint slipping, and this value is retained until the total circumferential contraction of the pipe is equal to the sum of all slot lengths. Upon further loading, the  $E^*$  is increased to represent post-slipping until the average thrust stress reaches  $\sigma_f$  (joint failure) after which the incremental modulus is zero.

$$E^* = \frac{E_j}{\left[ (1 - J_r) \frac{E_j}{E_e} + J_r \right]}$$

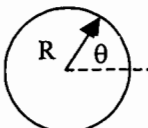
$$J_r = \frac{C_{\max}}{2\pi R}$$

$C_{\max}$  = the sum of all slot lengths.

Increments of overburden pressure are prescribed, and incremental responses (e.g., thrusts, moments, displacements, etc.) are computed from Table 1.1.1 using the current value of  $E^*$  to define a dimensionless parameters,  $\alpha$ . The allowable fill heights for both slotted-joint and standard-joint construction based on the preceding design method and assumptions are listed in Table 3-6 of Ref. (Katona, et, al. 1987)

The use of slotted bolt hole joints in large diameter corrugated pipe culverts permits substantial increases of burial depth up to a factor of 2 or more over that of unslotted pipes providing that high quality backfill soil is employed. For low quality soil and/or smaller diameter-to-thickness ratios, the benefits of slotted-joint construction are marginal. The authors believe that the maximum allowable fill-height tables presented here can be used with conservative confidence providing that the slotted-joint culvert system conforms to the stated guidelines and assumptions.

**Table 1.1.1 Elastic Solution Equation for Pressure on Pipe Response for Bounded  
and Frictionless Interface.**

Structural Response of Pipe 	Common Factor	Bonded Interface, $A^*=(1+K) + 3(5-K)\beta$ $+(3+K)\alpha + 12(3-K) \alpha\beta$	Frictionless Interface, $A^*=(1+K) + 3(5-K)\beta$
Radial pressure on pipe, $P_r$	$P_o$	$\alpha/(1+\alpha)-[(1-K)(-2\alpha +18\beta+24\alpha\beta)/A^*]\cos 2\theta$	$\alpha/(1+\alpha)-[18(1-K)\beta/A^*]\cos 2\theta$
Tangential pressure on pipe $P_\theta$	$P_o$	$[(1+K)(4\alpha +18\beta)/A^*]\sin 2\theta$	0.0
Radial disp. of pipe $w$	$P_o R(1-K)/2G$	$1/((1-K)(1+\alpha)) - [(2 +4\beta)/A^*]\cos 2\theta$	$1/((1-K)(1+\alpha)) - (2/A^*)\cos 2\theta$
Tangential disp. of pipe, $v$	$P_o R(1-K)/2G$	$[(2+2\alpha+6\beta)/A^*]\sin 2\theta$	$(1/A^*)\sin 2\theta$
Moment in pipe wall, $M$	$P_o R^2$	$\beta/(1+\alpha)+[(6\beta(1-K) +12\alpha\beta(1-K))/A^*]\cos 2\theta$	$\beta/(1+\alpha)-[6(1-K)\beta/A^*]\cos 2\theta$
Thrust in pipe wall, $N$	$P_o R$	$\beta/(1+\alpha)+[(6\beta(1-K) +12\alpha\beta(1-K))/A^*]\cos 2\theta$	$\alpha/(1+\alpha)-[6(1-K)\beta/A^*]\cos 2\theta$
Shear resultant in pipe, $Q$	$P_o R$	$[(1-K)(-12\beta-24\alpha\beta)/A^*]\sin 2\theta$	$[-12(1-K)\beta/A^*]\sin 2\theta$

<sup>a</sup> Soil lateral pressure coefficient is related to Poisson ratio,  $\nu_s$ , by  $K = \nu_s / (1 - \nu_s)$ .

<sup>b</sup> Plane-strain modulus of pipe,  $E = E_{steel} / (1 - \nu^2)$

Note: Soil Properties:  $G$  = shear modulus,  $K$  = lateral pressure coefficient,<sup>a</sup>  $P_o$

= overburden pressure; Pipe Properties:  $E$  = plane-strain Young's modulus,<sup>b</sup>  $I$

= moment of inertia,  $a$  = thrust area,  $R$  = average radius; Dimensionless parameter:

$\alpha = EA/2GR^3$ , and  $\beta = EI/2GR^3$

**Design Methodology for Corrugated Metal Pipe Tiedowns: Phase 1, Klaiber, F.W., Lohnes, R.A., Zachary, L.W., Austin, T.A., Havens, B.T., Mccurnin, B.T., Iowa DOT Project HR-332, ISU-ERI-Ames-9340, Engineering Research Institute, Iowa State University, 1993.**

The objective of this study was to develop a rational method for the design of tiedowns for corrugated metal pipe (CMP) and provide standard designs. In the study in phase I, the focus was to determine the longitudinal stiffness of CMP and obtain experimental data on soil-CMP interaction.

Possible failure modes for CMP are the following: i) Excessive deflection if the foundation soil is highly compressible or the side fill has not been properly compacted as shown in Fig. 1.1.2a. ii) Yielding of the wall section occurs when the soil has considerable passive resistance and CMP wall thickness is insufficient to resist the superimposed loads (Fig. 1.1.2b). iii) The pipe wall may buckle under high load with inadequate passive resistance from the soil (Fig. 1.1.2c). iv) Seam failure includes shear of bolts, rivets, or welds at seams and occurs if the pipe is adequate to carry the loads but the fasteners are either substandard or spaced incorrectly (Fig. 1.1.2d). v) Corrosion may create holes which prevent the CMP from remaining watertight.

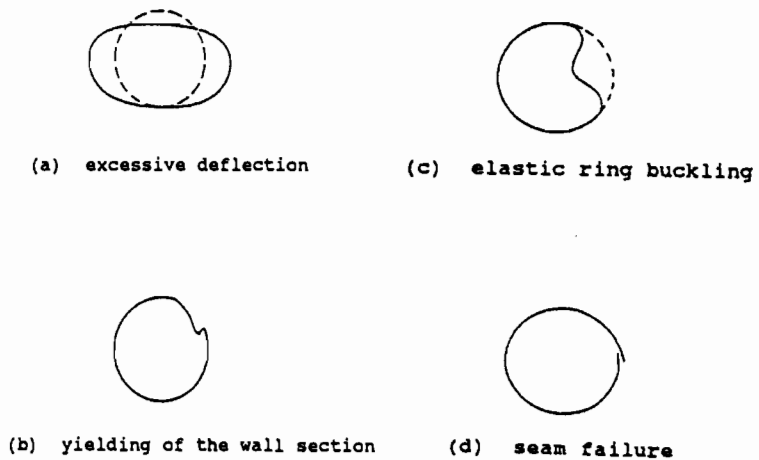


**Fig 1.1.2 Potential Failure Modes**

Three CMPs (ISU1), (ISU2), and (ISU3) were loaded to failure to determine experimental values for the “stiffness” EI, yield moments, and ultimate moments. Tables

1.1.2, 1.1.3 and 1.1.4 show respectively the yield moments, ultimate moments, and EI values. “Stiffness” EI, yield moments, and ultimate moments for other CMPs (different diameter, gages, corrugation geometry, etc.) can be determined using theoretical relationships derived in this study.

**Table 1.1.2 Comparison of Yield Moment Values**

Test	Experimental Yield Moment (k-ft)	Theoretical Yield Moment (k-ft)	Difference from Experimental (%)
ISU1	22.6	25.4	+12.4
ISU2	20.7-27.5	28.7	+4.4 to +38.6
ISU3	32.3-42.7	47.7	+11.7 to +47.7

**Table 1.1.3 Comparison of Ultimate Moment Values**

Test	Experimental Ultimate Moment (k-ft)	Theoretical Ultimate Moment (k-ft)	Difference from Experimental (%)
ISU1	67.5	66.5	-1.5
ISU2	71	74.0	+4.2
ISU3	109.1	126.4	+15.9

**Table 1.1.4 Comparison of EI Factor Values**

Test	Experimental EI Factor ( $\times 10^{-6}$ in <sup>2</sup> -lb)	Theoretical EI Factor (k-ft)	Difference from Experimental (%)
ISU1	911	840	-7.8
ISU2	1060	994	-17.2
ISU3	3443	2062	-40.1

The study also included investigation of the soil-structure interaction based on field tests. Changes in the pipe’s cross sectional shape are evident during backfilling as a result of

the lateral soil pressure acting on the sides of the CMP. A majority of the deformations take place when backfilling the middle half of the height. The primary strains developed during backfilling are those in the hoop direction; this is as a direct result of the cross sectional deformations that occur during backfilling. The longitudinal strains during backfilling were insignificant in comparison to the hoop strains. The hoop strains developed on top of the pipe during backfilling are greater than those on the bottom as the bottom of the pipe is firmly set in a compacted saddle and prevented from deforming while the upper portion of the pipe is free of any external restraints during the early stages of the backfill.

The soil-structure interaction developed during uplift with minimum cover requirements (2 feet) is significant enough to cause longitudinal bending of the CMP. Longitudinal strains are the primary strains during uplift. Hoop strains are insignificant in comparison to the longitudinal strains during uplift. In regions where the soil covers the entire pipe, the top regions receive additional stiffness from the interacting soil during uplift. On the other hand, the bottom of the pipe is separated from the soil and receives no benefit from the surrounding soil. This behavior results in smaller strains being developed on top of the pipe than on the bottom. Cross sectional deformations during uplift are very small in comparison to the deformations experienced during backfilling.

**Design Methodology for Corrugated Metal Pipe Tiedowns: Phase 2, Lohnes, R.A., Klaiber, F.W., Kjartanson, B.H., Austin, T.A., Heilers, G.A., Morgan, B.C., Peiffer E.A., Iowa DOT Project HR-362, ISU-ERI-Ames-9640, Engineering Research Institute, Iowa State University, 1995.**

Pore water pressures acting beneath the CMP cause the longitudinal uplifts. The objective of this research was to develop a design method to determine the required force for restraining a CMP against inlet uplift. Five field tests were conducted on a 2.43-m (8.1- ft.) diameter CMP specimen.

The CMP was modeled in a three dimensional FEM analysis as a smooth shell pipe with equivalent properties and the soil is assumed to be linearly elastic. The model was applied for different combinations of pipe stiffness, pipe diameter, soil characteristics, foreslopes, depth of cover, and hydraulic conditions. A hydraulic load was included in the model, with the inlet restrained, to determine the amount of resisting force needed to prevent uplift. Analysis conducted with varying depths of cover indicated that the depth of soil is not critical in determining the required restraining force. The largest resistance to the uplift occurs within the foreslope; therefore, increases in the depth of cover have no effect on the restraining force. The design process to determine restraining force is shown as Fig. 1.1.3.

In the soil-structure interaction finite element model, four-noded isoparametric shell elements were used to idealize the pipe and 2-noded linear beam elements accounted for the loading straps. The soil was modeled using 8-noded isoparametric solid elements. The finite element models are shown in Fig.1.1.4.

Many factors are involved in the soil-CMP interaction and the bending characteristics of CMP including the influence of the backfill properties. The response for different foreslope conditions during the field tests has been compared with the analytical results and it has been shown that the foreslope has a significant effect on the CMP bending characteristics.

Another factor that significantly affects the required tiedown force is the amount of water flowing in the pipe. The influence of flow in the pipe on the restraining force is shown in Fig. 1.1.5, where the restraint forces for 14 gage pipe and clayey alluvium backfill are plotted versus the amount of flow in the pipe. The results indicate a decrease in the restraining force from 60 KN (13,490lb) to 1.2 KN (270lb) as the flow level increases from 0 to 75% of the pipe diameter. The design process suggested here provides an easy to follow procedure based upon experiment and analysis and allows the engineer to make final design considerations based on their judgment and experience. The method also indicates that in situations where the soil and/or pipe is sufficiently stiff or where total blockage of the pipe is unlikely, tiedowns may not be required.

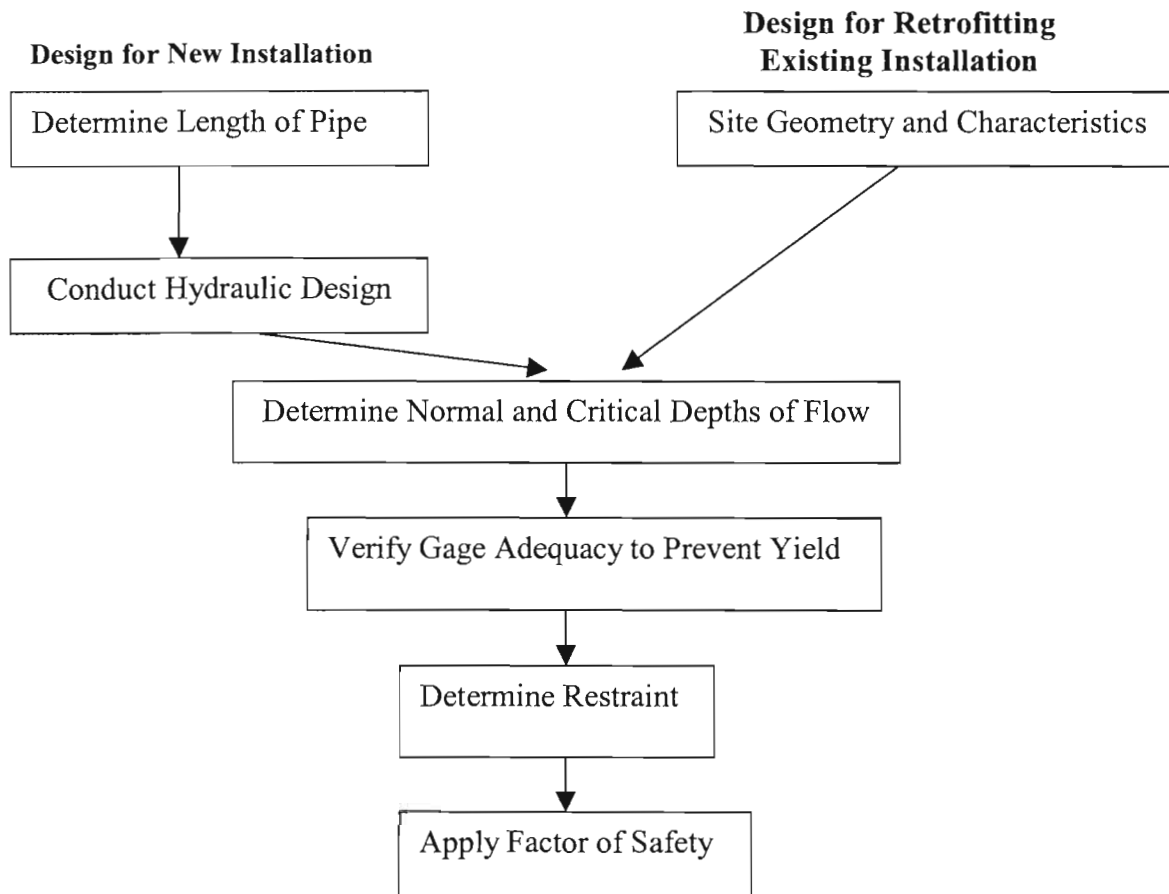


**Fig. 1.1.3 Flowchart for Design Process to Determine Restraining Force**

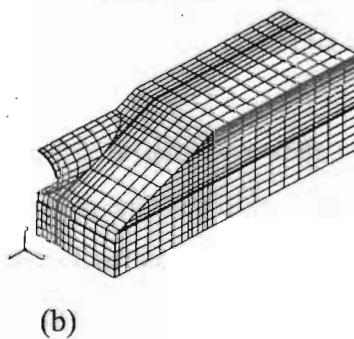
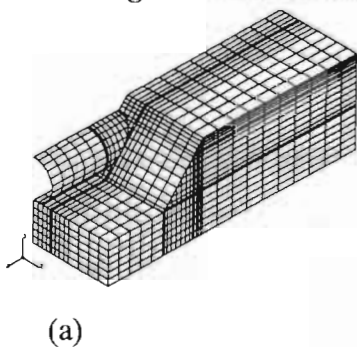
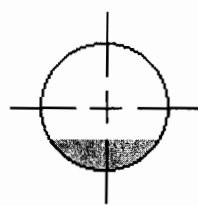


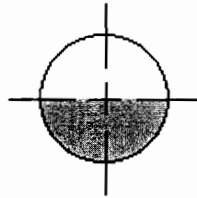
**Fig 1.1.4 Finite Element Models**

a) Finite element model for uplifting the pipe with a soil cover and a foreslope of 2:1, referred to as 8SC (8 ft diameter CMP with soil cover)

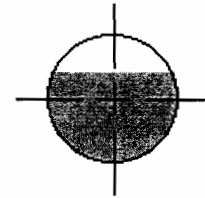
b) Finite element model for the pipe that is backfilled without a foreslope to leave the upstream end of the pipe without soil restraint, referred to as 8NF



a) Flow at 25% of pipe diameter



b) Flow at 50% of pipe diameter



c) Flow at 75% of pipe diameter

**Fig. 1.1.5a Cross Sectional View of Assumed Flow Conditions**

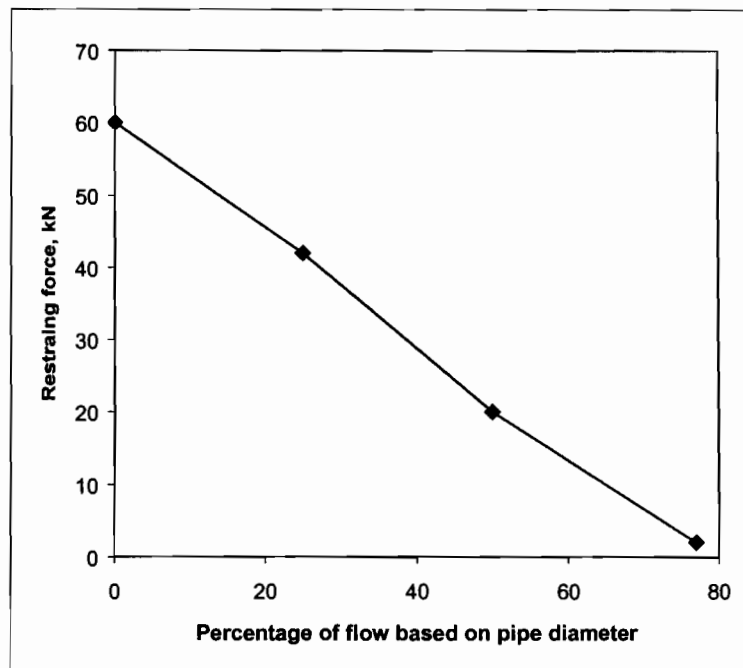


**Fig. 1.1.5b Influence of Flow Condition on Restraining Force**

## 1.2 Structural Performance

**Comparison of Structural Response of 762 mm (30 in.) Diameter Thermoplastic Pipes under Deep Burial**, Sargand, S. M., Hazen, G. A., Moran, A. P., *Transportation Research Board 80<sup>th</sup> Annual Meeting, Jan. 2001.*

The objectives of this paper were to compare vertical and horizontal diameter changes and circumferential shortening of the test pipes. The soil pressures at the crown and springline of pipe were also compared.

Pipes of 762 mm (30-inch) diameter from four different manufacturers were buried under 6 m (20-ft) and 12 m (40-ft) cover using different backfill materials and compactions. Before the placement of the test pipes, a trench width of two times the outside diameter was excavated meeting the ODOT specifications. Two different backfill materials were used in this study for pipe backfill and bedding granular material. Tables 1.2.1 and 1.2.2 present the pipe properties and the description of backfill on test pipes. Soil pressure cells were placed at the springline and crown of the pipes (Fig. 1.2.1) The pressure cells were located approximately 25.4 to 38.1 mm (1 to 1.5 in.) away from the face of the pipe. Displacement potentiometers were placed in the pipes to measure vertical and horizontal and circumferential shortenings of the pipe (Fig. 1.2.2). During the backfill process around the pipe, deflection and pressure readings were taken at 203 mm (8 in) lifts until placement of 12 inch of backfill over each pipe. Table 1.2.3 presents the summary of deflections for the 762 mm (30-in.) pipes. The data collected over 8 months period only are presented here.

The following observations and conclusions were reached in this study:

- i) Deflections and pressures stabilized in a short duration of two months from the end of construction.
- ii) The circumferential shortening was greater in HDPE pipes as compared to PVC pipes.
- iii) Under the same backfill conditions, the PVC pipes experienced greater pressure than the HDPE pipe.

iv) Well-compacted sand induced higher peaking deflections and provided greater lateral support to corrugated pipes than the loosely compacted sand.

**Table 1.2.1 Pipe Properties**

Make	Inside Diameter (mm)	Pipe Material	Corrug. Spacing (mm)	Wall thickness			Moment of Inertia (mm <sup>4</sup> /mm)
				Outside Face (mm)	Inside Lining (mm)	Between Corrugations (mm)	
A	762	PVC	----	5.08	5.08	3.5	69.7
B	762	PVC	56.1	3.8	3.8	3.8	71.6
C	762	HDPE	106	2.7	2.7	4.2	142.6
D	762	HDPE	108	3.0	2.8	6.1	221.9

\*Pipe A: Lamson & Sessions Vylon – 762-mm (30-inch)

\*Pipe B: Contech A2000 – 762-mm (30-inch)

\*Pipe C: Lane HDPE – 762-mm (30-inch)

\*Pipe D: ADS N12 – 762-mm (30-inch)

**Table 1.2.2 Description of Backfill on Test Pipes**

Pipe	Pipe Type	Compaction	Backfill	Bedding (cm)	Cover (m)
1	A	96%	ODOT 310 Sand	15.2	6
2	A	96%	ODOT 304 Crushed Limestone	15.2	12
3	A	86%	ODOT 304 Crushed Limestone	15.2	6
4	B	86%	ODOT 310 Sand	15.2	6
5	B	96%	ODOT 304 Crushed Limestone	15.2	12
6	B	96%	ODOT 304 Crushed Limestone	15.2	6
7	C	96%	ODOT 310 Sand	15.2	6
8	C	96%	ODOT 310 Sand	15.2	12
9	C	86%	ODOT 304 Crushed Limestone	15.2	6
10	D	86%	ODOT 310 Sand	15.2	6
11	D	96%	ODOT 304 Crushed Limestone	15.2	12
12	D	96%	ODOT 304 Crushed Limestone	15.2	6

**Table. 1.2.3 Summary of 762-Mm (30-Inch) Pipes under 6-M (20 Ft) Cover**

Pipe	Backfill	Comp.	Pressure (kPa)#				Stabilized Deflection (mm)**			
			Crown	Spgl.	Change Crown	Change Spgl.	Days*	Vert	Spgl.	Circum
1	310	96%	102.8	94.5	33.8	12.3	20	-7.1	3.56	-
3	304	86%	117.7	142.3	30.5	49.3	100	-17.8	14.0	-
4	310	86%	111.0	86.8	32.1	22.3	10	-12.7	7.11	-
6	304	96%	88.2	84.1	25.9	19.9	14	-6.35	8.38	-
7	310	96%	55.1	54.9	1.31	9.72	50	-6.35	0.635	-6.10
9	304	86%	60.4	63.2	6.34	-1.72	12	-17.8	7.37	-5.33
10##	310	86%	60.3	60.4	-3.52	-4.83	9	-26.2	19.1	-10.2
12	304	96%	66.4	61.6	7.52	13.5	30	-15.0	5.08	-5.84

\* The number of days is the difference between when the laying of overburden was completed and when the values of pressure and deflection stabilized.

\*\* The value for the deflection is the absolute difference between the deflection at 0-m (at the top of the pipe) of cover and the stabilized deflection after the construction of overburden.

#The values of the pressure are about 250 days after the start of construction. The change in the pressure is the difference between the pressure after 250 days and the pressure when the final height of overburden was reached.

##Pipes 10 and 11- Part of the backfill was replaced during construction due to a heavy rain washout.

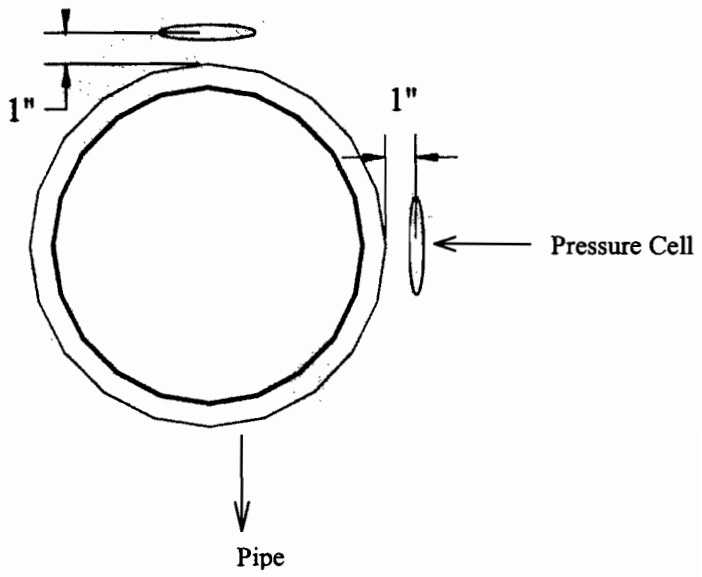


**Fig. 1.2.1 Pressure Cell Configuration**

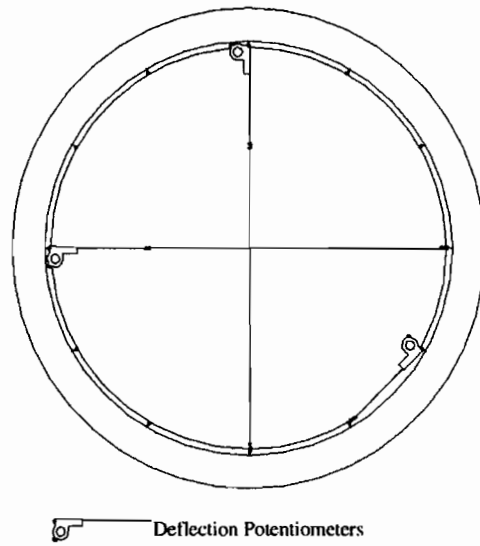


**Fig. 1.2.2 Orientation of Potentiometers**

**Comparison of Tests and Analysis of 1050 mm (42 in.) Diameter High Density Polyethylene (HDPE) Thermoplastic Pipe, Sargand, S. M., Hazen, G.A., White. K. and Bhargava, A., Transportation Research Board 80<sup>th</sup> Annual Meeting, Jan. 2001.**

The objectives of this paper were to present the pressure distribution around the perimeter of the pipe, the deflection at crown and springline and circumferential shortening of the pipes, subjected to deep cover and long-term loading condition. In addition, the results obtained from the Burns and Richards equations for both slip and full bonding interface conditions between the soil and pipe were also compared with the field data.

Three thermoplastic HDPE pipes of 1050-mm (42-inch) diameter were buried under 6-m and 12-m (20-ft and 40-ft) cover using different backfill materials. Fig. 1.2.3 shows the layout of the pipes and the overburden placement. The description of the two different backfill materials is given in Table 1.2.4. The backfilling was done in eight layers of thickness varying between 15.24 to 20.32 cm (6 to 8 in). To measure the pressure at the pipe-soil interface, Geokon pressure cells were placed in 7.62-cm (3-in.) thick sand lenses that were trenched in the backfill material, as shown in Fig. 1.2.4. The vertical and horizontal deflections of the pipe under loading were monitored by using displacement potentiometers. Another potentiometer was installed along the circumference of the pipe to determine the circumferential shortening of the pipe. After construction of overburden was completed, the readings were taken once every month for pressure cells and automatically at 48 hr. intervals for potentiometers. The data presented here was collected during installation and over a period of 8 months.

The parameters used for the solutions to Burns and Richards equation were based on the AASHTO specifications. The equations were solved for the following conditions:

- The soil is fully bonded with the pipe.
- There is slippage of soil around the pipe.

Tables 1.2.5 and 1.2.6 present the comparison of the calculated pressures and deflections using Burns and Richards equation with the field data.

The following observations and conclusions were reached in this study:

i) The deflections and pressures with crushed limestone backfill stabilized more quickly than that with sand backfill.

ii) The lateral force exerted on the pipe by ODOT sand induced more vertical deflection and it had a smaller friction angle. It was also interesting to note that the horizontal deflections for pipes embedded were negative on the completion of backfill and it then stabilized in a positive direction.

iii) The pressure calculated using the Burns and Richard Equations are questionable when compared to field measurements.

iv) The deflections from the field data (both full slip interface and the full bonded interface) and the results from the Burns and Richards' equations are in good agreement.

**Table 1.2.4 Description of Backfill Material on Test Pipes**

Pipe #	Pipe Type	Compaction	Backfill	Bedding (mm)	Cover (m)
13	ADS N12-42"	90%	ODOT 310 Sand	0-305	6
14	ADS N12-42"	96%	ODOT 310 Sand	76-381	12
15	ADS N12-42"	90%	ODOT 304 Crushed	0-305	6

**Table 1.2.5 Comparison of Pressure and Deflection for Pipes 13, 14, and 15 Calculated Using Burns and Richards Equations (Full Slip Interface) with the Field Data**

	Values using Burns & Richards Equation				Field Data			
	Pressure (kPa)		% Deflection		Pressure (kPa)		% Deflection	
Pipe	Crown	Spring-line	Vertical	Spring-line	Crown	Spring-line	Vertical	Spring-line
13	94.0	84.1	-1.66	0.68	55.2	62.1	-2.00	0.57
14	144.7	133.8	-2.05	0.51	93.1	65.5	-2.38	0.71
15	71.2	66.0	-1.00	0.24	58.6	63.8	-1.64	0.35

**Table 1.2.6 Comparison of Pressure and Deflection for Pipes 13, 14, and 15 Calculated Using Burns and Richards Equations (Full Bonded Interface) with the Field Data**

	Values Using Burns & Richards Equation				Field Data			
	Pressure (kPa)		% Deflection		Pressure (kPa)		% Deflection	
Pipe	Crown	Spring-line	Vertical	Spring-line	Crown	Spring-line	Vertical	Spring-line
13	57.7	120.52	-1.50	0.52	55.2	62.1	-2.00	0.57
14	81.2	197.4	-1.90	0.36	93.1	65.5	-2.38	0.71
15	39.7	97.4	-0.93	0.17	58.6	63.8	-1.64	0.35

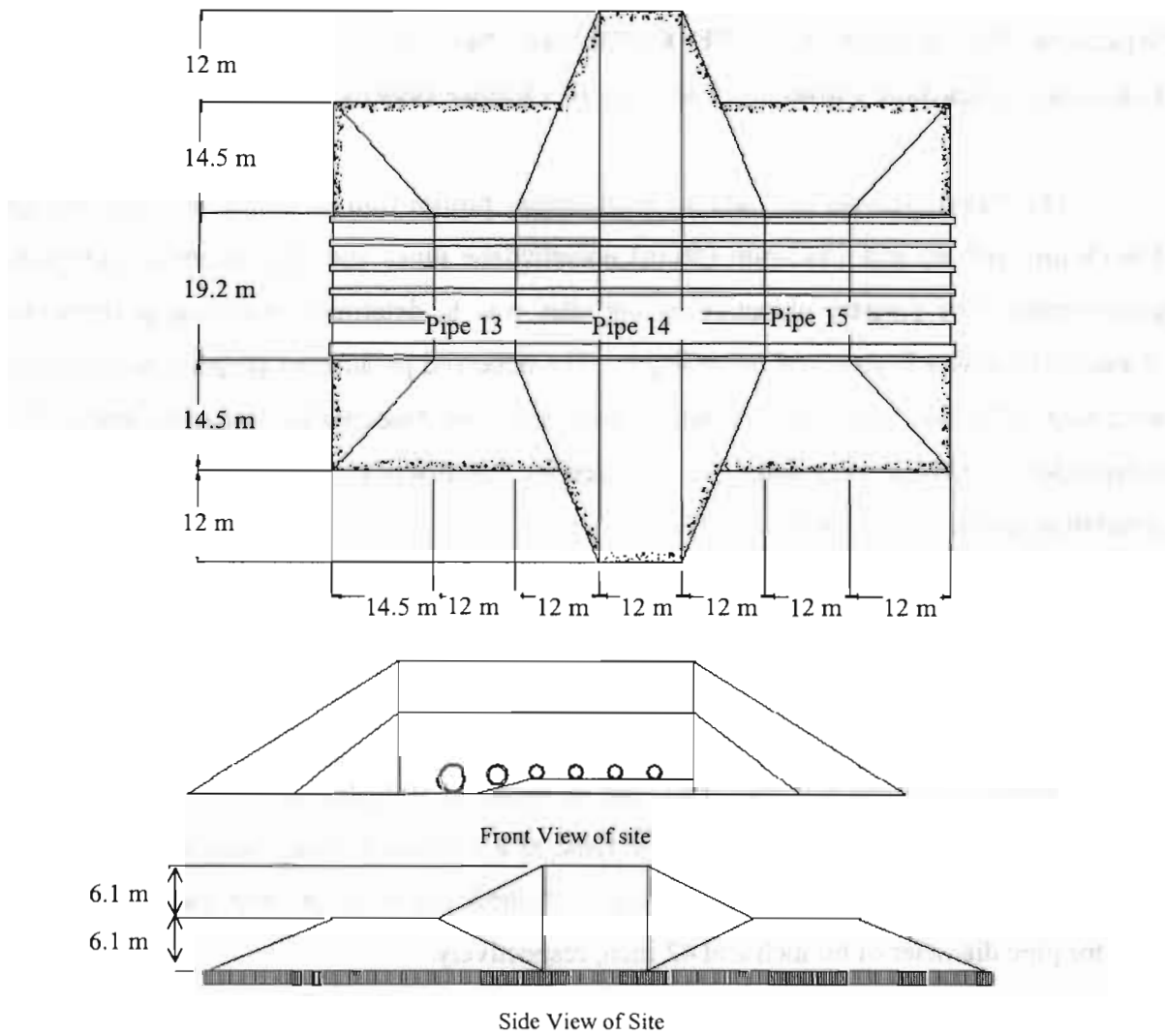


**Fig. 1.2.3 Overall Layout of Thermoplastic Pipes at Deep Burial Test Site**

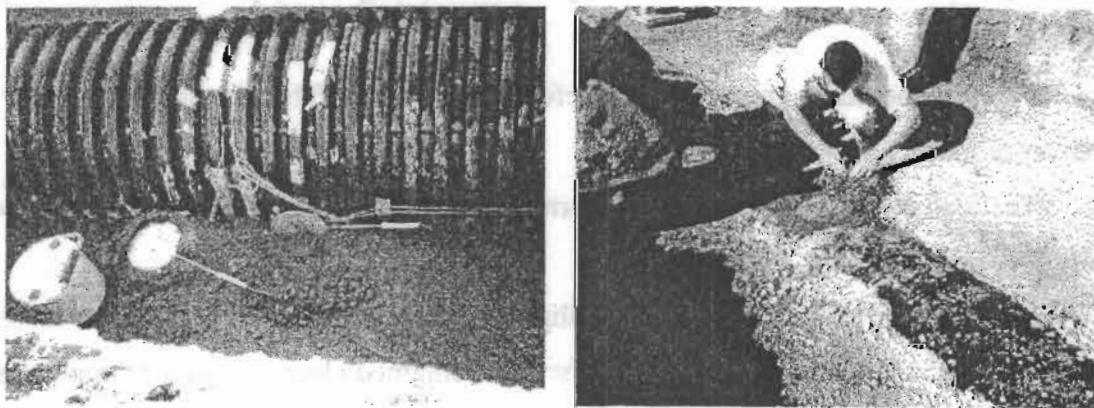


**Fig. 1.2.4 Installation of Pressure Cells**

**Structural Performance of HDPE Profile-wall Pipe, Moser, A. P., Buried Structures Laboratory, Utah State University, Logan, Utah, October 1999.**

The report presents test data for high density profile-wall (Honeycomb Wall Design) 1066.8-mm (42-in) and 1542-mm (60-in) polyethylene pipes and discussions on structural performance. The primary objective of the tests was to determine structural performance characteristics as a function of cover depth. The observed parameters (dependent variables) were ring deflection, any visual evidence of distress, and structural performance limits. The independent variables were soil type, soil density (compaction), and the vertical soil load simulating height of soil cover.

The pipes were tested at three levels of compaction, 75%, 83%, and 95%. The basic soil type was silty-sand, usually considered as lesser quality than most soils specified as backfill (a worst case test). Tests were performed in a large soil cell into which the sample pipe is buried. A vertical soil load is applied by means of 50 hydraulic cylinders (Fig. 1.2.5). The applied hydraulic pressures were converted to a soil cover depth scale based on a soil weight of 120 lbs/ft<sup>3</sup>. Table 1.2.7 and Table 1.2.8 show performance limit obtained from the field for pipe diameter of 60 inch and 42 inch, respectively.

The following conclusions were achieved from the test:

- The pipes deflect more in loose soil than in dense soil and Fig. 1.2.6 shows graphically the importance of soil density in controlling the pipe deflection in typical installations.

- The soil should be granular and carefully compacted, if the pipe is buried under high soil cover or under heavy surface loads.

- The load at which a structural performance limit takes place is a function of the soil density (Tables 1.2.7 and 1.2.8).

- The pipe cross-section became elliptical as the height of the cover increased; however, for 95 % dense soil, the shape of the pipe remained closer to circular shape even for extremely high heights of cover.

-None of the test pipes ever exhibited a so-called squaring or a square shape at any load.

-The ratio of ring-compression stress to bending stress is very low (much less than one) close to one, and much greater than unity for 75 %, 83% and 95% standard Proctor density.

**Table 1.2.7: Performance Limit for 60-Inch ADS HDPE Pipes**

Proctor Density	Load at Performance Limit	Deflection at Performance Limit
75%	Excessive Deflection and Dimpling* 55 feet of cover	17 percent
83%	Cracks at 72 feet of cover	17 percent
95%	Excessive Dimpling at 143 feet of cover	5.7 percent

**Table 1.2.8 Performance Limit for 42-Inch ADS HDPE Pipes**

Proctor Density	Load at Performance Limit	Deflection at Performance Limit
75%	Excessive Deflection at 55 feet of cover	17 percent
	Hinging* at 69 feet of Cover	20 percent
83%	Hinging at 69 feet of Cover	15.6 percent
	Cracks at 76 feet of cover	18 percent
95%	Cracks at 168 feet of cover	9.3 percent

“Dimpling” refers to the wavy pattern that occurred in inner wall of the pipe due to local instability of the wall. This is not general bucking and is not a structural performance limit. The term “hinging” refers to yielding of the material due to an excessive bending moment in the wall. These hinges usually take place at the 3 and 9 o’ clock positions. These plastic hinges can be influenced by a combination of localized buckling and wall yielding caused by thrust in the wall of the pipe. Hinging is usually considered to be a structural performance limit.

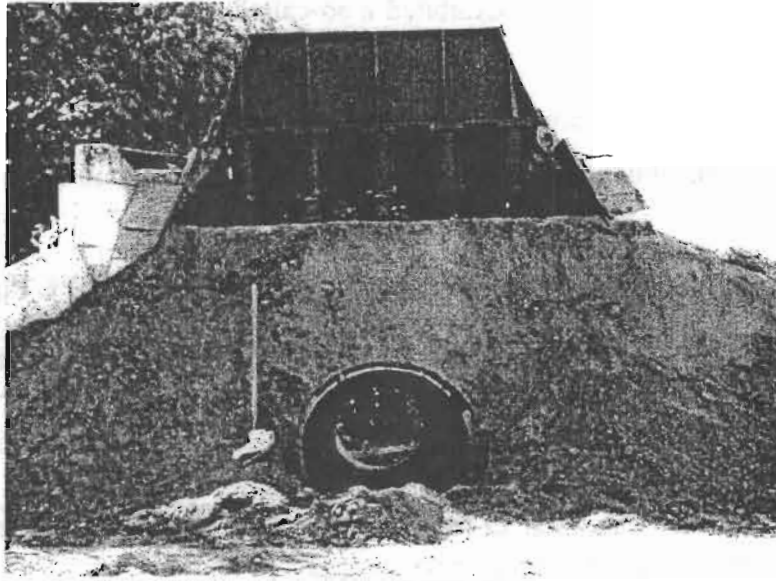


**Fig. 1.2.5 Pipe Burial in the Soil Cell, and Load Being Applied to Soil Surface**

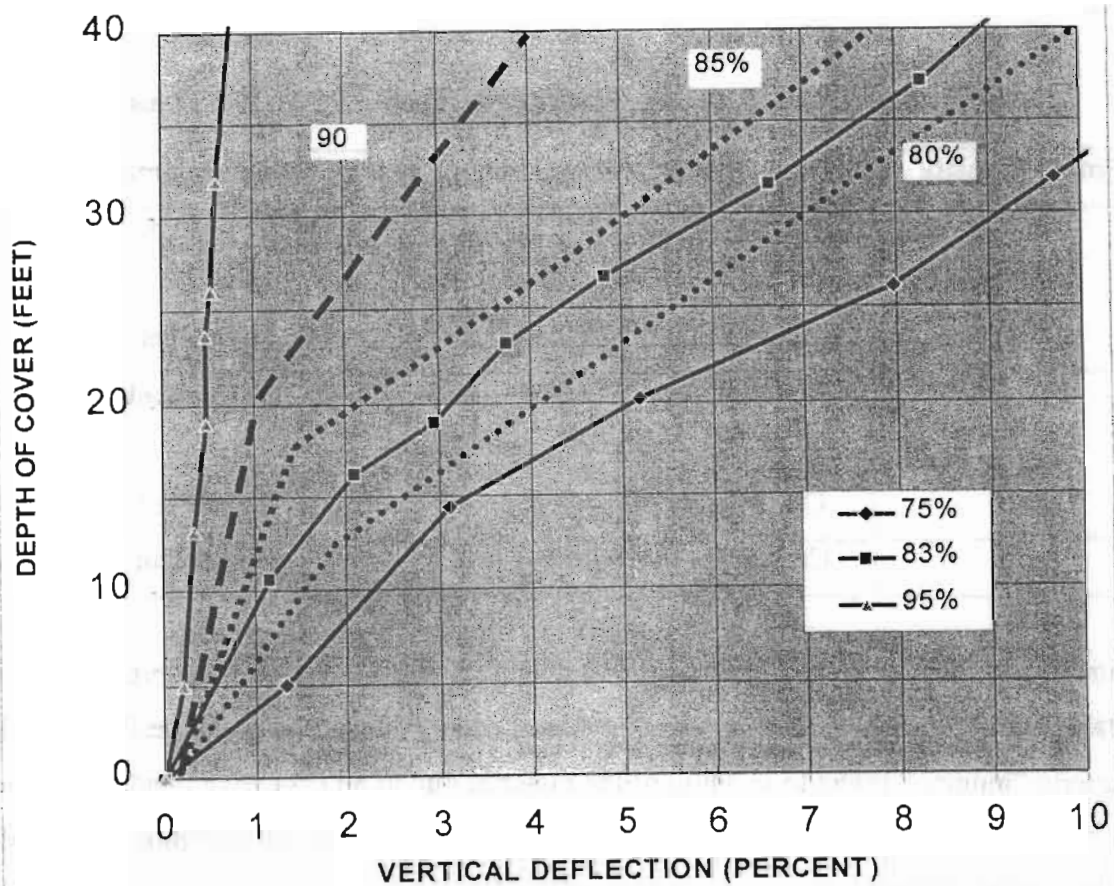


**Fig.1.2.6 Vertical Deflection Curves for 60-Inch HDPE Pipe at Various Soil Densities. The Dashed Lines are Approximated Curves for Intermediate Densities**

**Corrugated HDPE Pipe: Laboratory Testing and Two-Dimensional Analysis to Develop Limit States Design, Dhar, A. S. and Moore, I. D., Transportation Research Board 81<sup>st</sup> Annual Meeting, Jan. 2002, pp. 22.**

The objective of this research is to develop baseline information on buried pipe behavior in a controlled laboratory environment for use in verification of the pipe design models. Deflections and local wall strains of a lined corrugated high-density polyethylene pipe with an inside diameter of 610 mm. are also reported. Test results are then compared with calculations using two-dimensional finite element analysis and the simplified design method, to evaluate the effectiveness of both methods. The pipe was tested in the biaxial test cell. The cell is a high strength steel box with dimensions 2m x 2m in plan and 1.6m in height. Arrangement of the pipe and the instrumentation in the test cell are shown in Fig. 1.2.7. Earth pressure cells were used to measure both vertical and horizontal soil stresses. Two settlement plates (A&B) were used to monitor the vertical soil moment at the springline. Poorly graded sand was used as the backfill material in the cell. The soil was compacted to a density of about 1625-kg/m<sup>3</sup>, which is 85% of the maximum standard Proctor density. An air bladder was used to apply uniform pressures on top of the soil. Sidewall friction of the cell was minimized using special sidewall treatment.

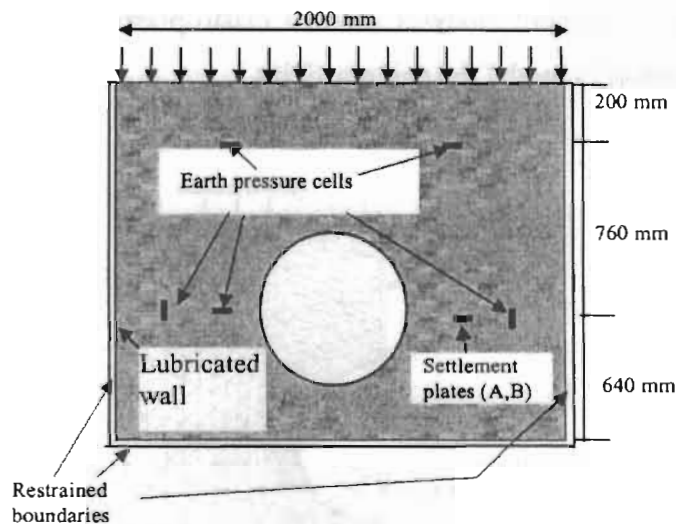


**Fig. 1.2.7 Pipe Installation (Schematic)**

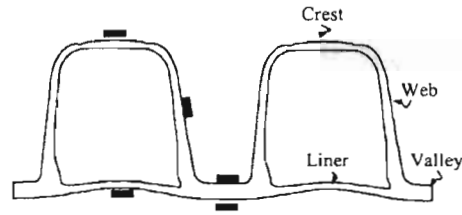


**Fig. 1.2.8 Pipe Profile and Location of Strain Gauges**

Wall strains on different positions shown in Fig. 1.2.8 of the profile were measured using resistance strain gages. Tests were conducted in pressure increments of 25 kPa with each increment allowed to remain for 20 minutes. Loading continued for about 6 hours until limit states like local buckling were observed and a vertical pressure of 500 kPa was reached.

### **Finite Element Modeling**

Small strain finite element analysis has been employed to study the interaction of the pipe with the backfill soil in the test cell (Fig. 1.2.9). An elastic secant modulus has been used with modulus of elasticity for the high-density polyethylene pipe taken as 450 MPa. The area and moment of inertia for the pipe section were  $10.1 \text{ mm}^2/\text{mm}$  and  $3978 \text{ mm}^4/\text{mm}$  respectively. The finite element analysis uses an elasto-plastic model based on the Mohr-Coulomb failure criterion to model the soil plasticity.

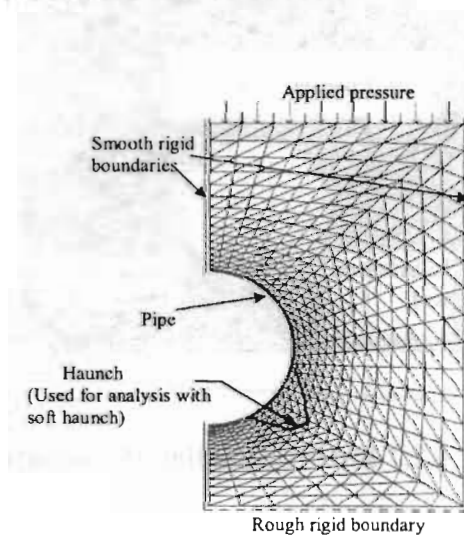


**Fig 1.2.9 Finite Element Mesh**

## Deflections

In this study, the simplified design equation proposed by McGrath<sup>1</sup> based on the continuum approach<sup>2</sup> is shown below to calculate the vertical deflection of flexible pipe.

$$\frac{\Delta_v}{D} = \left[ \frac{q_v}{\frac{EA}{R} + 0.57M_s} \right] + \left[ \frac{D_1 K q_v}{\frac{EI}{R^3} + 0.061M_s} \right]$$

where,

$\Delta_v$  = vertical deflection (mm)

D = pipe diameter (mm)

A = area per unit length of the pipe (mm<sup>2</sup>/mm)

I = moment of inertia per unit length (mm<sup>4</sup>/mm)

$q_v$  = overburden pressure at springline (MPa)

E = pipe material modulus (MPa)

R = radius of the centroid of the pipe section (mm)

$M_s$  = one dimensional soil modulus (N/mm)

K = bedding coefficient (dimensionless)

$D_1$  = deflection lag factor (dimensionless)

Calculations of pipe deflections have been obtained using the simplified and FEM methods at 100 kPa and 400 kPa of vertical earth pressure. Calculations along with the measurements of deflection due to the pressures are shown in Table 1.2.9

<sup>1</sup> McGrath, T.J., Design Method for Flexible Pipe, Report to the AASHTO Flexible Culvert Liaison Committee, Simpson Gumpertz & Heger Inc., Arlington, MA, 1998.

<sup>2</sup> Burns, J.Q., and Richard, R.M., Attenuation of Stresses for Buried Cylinders, Proc. of the Symposium on Soil Structure Interaction, University of Arizona, 1964, pp.379-392.

**Table 1.2.9 Change in Vertical Diameter (mm) (% Difference from Measured Values in Parentheses)**

Stress kPa	Expt.	FE		Simplified	Continuum
		Linear	GN*		
100	-9.9	-10.3 (4%)	-10.5 (6%)	-9.6 (-3%)	-10.0 (1%)
400	-48.8	-41.1 (-15.6%)	-45.1 (-7.6%)	-38.3 (-21.5%)	-40.1 (-17.8%)

\* Geometrical non-linearity

### Pipe Strains

Simple beam theory has been used to calculate the strains from hoop thrust and the moment values obtained from the finite element analysis. The finite element method calculates the thrust and bending moments at the Gauss (numerical integration) points of the elements. Hoop strain,  $\epsilon$ , on a fiber located at a distance  $y$  from the neutral axis of the section is given by;

$$\epsilon = \frac{N}{EA} + \frac{My}{EI}$$

where,

N = thrust (N/mm)

M = bending moment (N-mm/mm)

E = pipe material modulus (MPa)

A = area of the cross-section (mm<sup>2</sup>/mm)

I = moment of inertia (mm<sup>4</sup>/mm)

Comparisons of the hoop strains at the springline and the crown of the pipe are shown in Figures 1.2.10 and 1.2.11 respectively. Invert strain is similar to that of the crown. It appears from the figures that the valley strains from the finite element method are reasonably estimated, whereas the strain at the springline is overestimated by about 12%. Also, the method substantially overestimates the strains on the crests at the invert and at the crown. Local bending on the profile elements might be responsible for this overestimation.

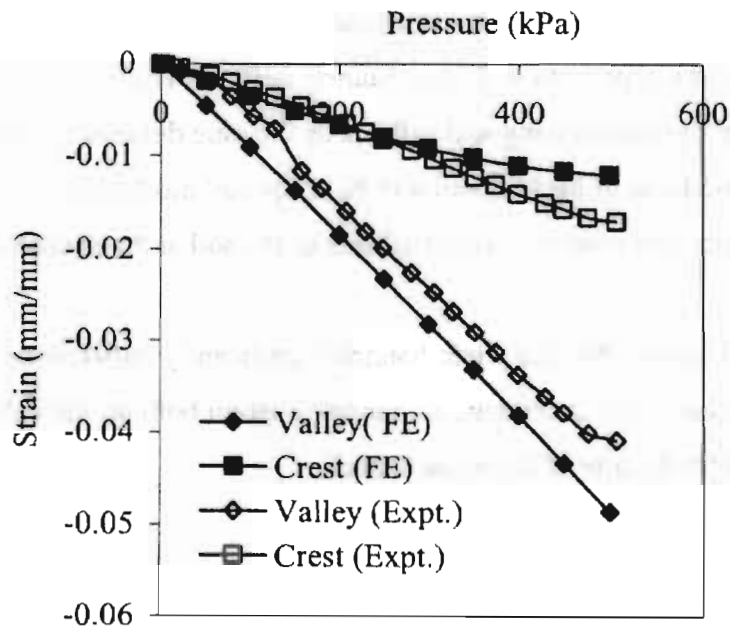


Fig. 1.2.10 Circumferential Strain at the Springline

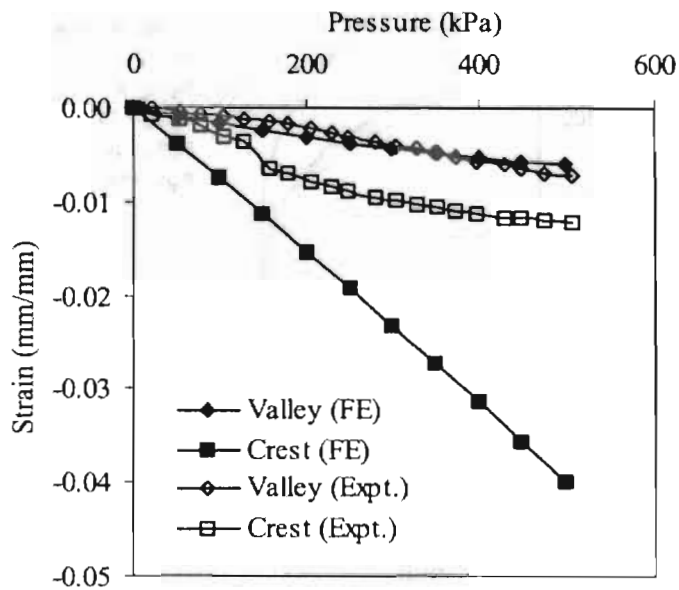


Fig. 1.2.11 Circumferential Strain at the Crown

## Influence of Weak Haunch Support

Fig. 1.2.9 shows the zone of low stiffness haunch soil considered in the analysis. The deflected shape of the pipe with different haunch stiffness ( $E_s/E_h = 1$  to 100) demonstrates that the stiffness of the surrounding soil influences the pipe deformation (Fig. 1.2.12), where  $E_s$  represents the modulus of backfill soil and  $E_h$  is the soil modulus at the haunch zone. The invert of the pipe gets flattened when the stiffness of the soil at the haunch is reduced.

Fig. 1.2.13 shows that the weak haunch significantly redistributes the strain around the pipe circumference. The maximum compressive strain both on the valley and crest of the profile occurs near the middle of the weak haunch.

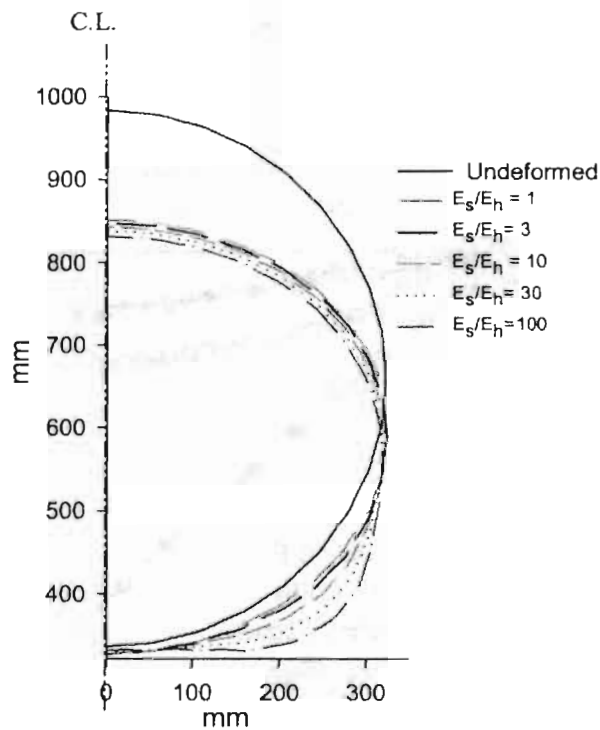
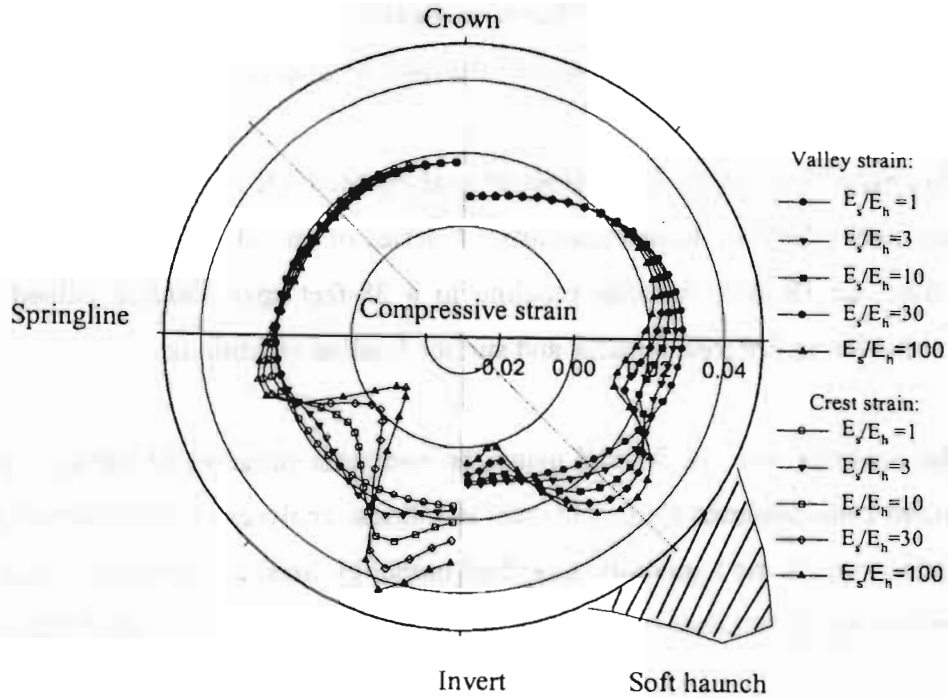


Fig. 1.2.12 Deformed Shape of the Pipe for Different Soil Support (Deflection x 5)



**Fig. 1.2.13 Distribution of Circumferential Strains on HDPE Pipe**

### Conclusions

The local bending and local buckling in the profile cannot be considered in the two-dimensional analysis. However, the method can successfully be used to calculate the response of the elements on which the three dimensional effects are not significant.

Non-uniform soil support has a significant effect on the behavior of buried pipe. Finite element analysis supports Roger's<sup>1</sup> experimental observation that weak support at the haunch induces "inverted heart shape" deformation of the pipes. For the case considered, the crest strain appeared to govern the design when the stiffness of the haunch soil was less than one tenth of the stiffness of the surrounding backfill.

<sup>1</sup> Rogers, C.D. , Some Observations on Flexible Pipe Response to Load, Transportation Research Record 1191, TRB, National Research Council, Washington, D.C., 1988, pp. 1-11.

**Earth Pressure and Surface Load Effects on Buried Pipelines**, Seed, R. B. and Duncan, J. M., *Advances in Underground Pipeline Engineering*, Jeyapalan, J.K. ed., 1985, pp. 320-329.

This paper reviews the finite element analysis methods used to analyze earth pressure and surface load effects on buried conduits. A series of buried conduits ranging in size and stiffness from an 18-inch diameter pipeline to a 38-foot span flexible culvert have been analyzed considering different backfill and surface loading conditions.

The analyses were performed using the computer program SSTIPN<sup>1</sup>, a plane-strain finite element code designed for incremental non-linear analyses of soil-structure interaction. The analysis employs the hyperbolic modified model by Seed and Duncan<sup>2</sup>, to idealize non-linear stress-history-dependent stress-strain, strength, and volumetric strain behavior of soils.

### **Surface Loads**

The surface load is applied as an “equivalent” line load at the surface of the fill. The magnitude of the “equivalent” line loading is selected, based on three-dimensional linear elastic analyses using Boussinesq theory. The peak vertical stress increase at the elevation of the top of the buried conduit due to the actual concentrated loading considered, is set equal to the peak vertical stress increase at the same depth due to the plane strain “equivalent” line loading.

Table 1.2.10 shows the thrusts and moments calculated for a 60-inch diameter steel pipe with walls 0.5 inches thick and interior coal-tar lining. These values correspond to placement of an HS-20 vehicle over the crown of the pipe considered with fill cover heights of 1.5, 3.0 and 6.0 ft. above the crown.

---

<sup>1</sup> User's Guide for SSTIPN, Unnumbered Geotechnical Research Report, University of California, Berkeley, January, 1979.

<sup>2</sup> Seed, R. B., and Duncan, J.M., Soil- Structure Interaction Effects of Compaction-Induced Stresses and Deflection, Geotechnical Research Report No. UCB/GT/83-06, University of California, Berkeley, Dec., 1983

**Table 1.2.10 Conduit Thrusts and Moments with HS-20 Surface Loading**

H <sub>c</sub> (ft)	Location	60-In. Pipe	
		P	M
1.5	Invert	1,128	-203.0
	Haunch	2,788	691.8
	Crown	1,609	-2,145
3.0	Invert	1,439	-120.9
	Haunch	2,574	287.3
	Crown	1,123	-849.1
6.0	Invert	2,349	108.9
	Haunch	3,317	157.5
	Crown	1,954	-242.6

Table 1.2.10 and Fig. 1.2.14 show that the application of surface loads with only shallow cover thickness over the conduit crown can induce very large increases in conduit thrusts and bending moments, most notably near the conduit crown.

Comparison between the results presented in Table 1.2.10 shows that the application of a load representing an HS-20 vehicle with 1.5 feet of cover dramatically increases thrusts and moments in the crown regions, but that with only six feet of cover this loading results in an almost negligible increase in thrust, and approximately a three-fold increase in crown moment.

### **Conclusions**

The stresses induced by surface load effects increase with increasing pipe diameter and surface load magnitude, and decrease as the depth of burial of the pipe increases.

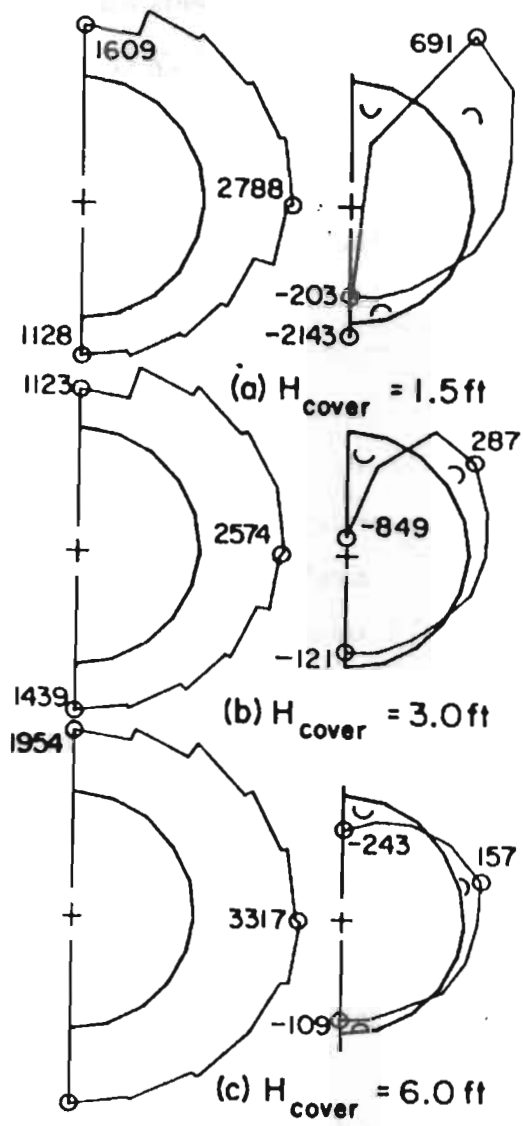


Fig. 1.2.14 Thrusts and Moments: 60-inch Pipe with HS-20 Surface Load

**Boundary Effects on Response of Polyethylene Pipe Under Simulated Live Load,**  
*Conard, B. E., Lohnes, R. A., Klaiber, F. W., and Wipf, T. J., Transportation Research Record 1624, Paper No. 98-0588, 1998, pp. 196-205.*

The objective of this paper is to evaluate the deflection response of polyethylene pipes when loaded near the pipe ends. The paper describes tests on 900-mm (36-in.) and 1200-mm (48-in.) diameter pipes with 610 mm (2 ft) of cover and a variety of backfills. The overall objective of this investigation was to determine the deflection response of the PE pipes to overloads and marginal backfills.

**Backfill Characteristics**

Seven configurations of backfill (tests 7 through 13) consisting of glacial till and granular material were tested to evaluate the response of PE pipes. In tests 7 and 8, the backfill was glacial till compacted to about 80 percent and 95 percent Standard Proctor density, respectively, around the pipes. In tests 9, 11, and 12, sand backfill was compacted to 70 percent of the pipe diameter. In tests 10 and 13, flowable fill was poured on top of the sand. Schematics of the backfill envelopes used in each test are shown in Fig. 1.2.15.

Tests 7 through 10 were conducted on 900-mm (36-in.) pipe from Manufacturer A. Tests 11 and 13 were conducted on 1200-mm (48-in.) pipe from Manufacturer A, and test 12 was conducted on 1200-mm (48-in.) pipe from Manufacturer C.

**Test Equipment and Procedures**

In all the tests, the cover above the top of the pipe was 610 mm (2 ft) deep and the pipes were 6100 mm (20 ft) long. Service load tests were conducted to simulate contact stresses that would be expected for truck tire pressures of 460 kPa (9,360 psf) to 690 kPa (14,400 psf). Beyond those stresses, the pipes were loaded to failure. Failure was defined by a decrease in load with increasing deflections.

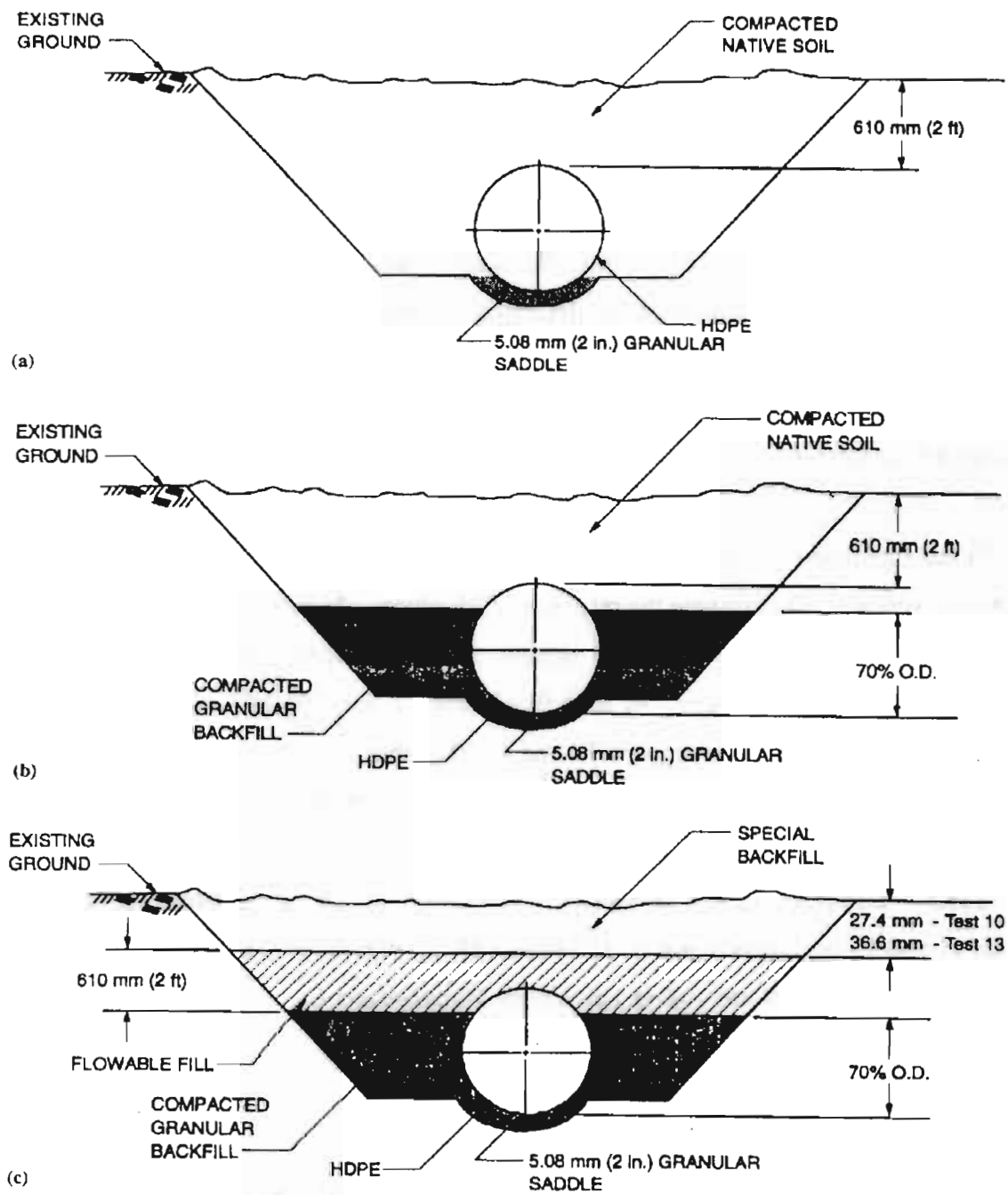


**Fig. 1.2.15 Cross Sections of Backfill Envelopes Used in Field Tests: (a) Tests 7 and 8; (b) Tests 9, 11, and 12; (c) Tests 10 and 13**

## Test Results

### *Pipe Response Under Service Load*

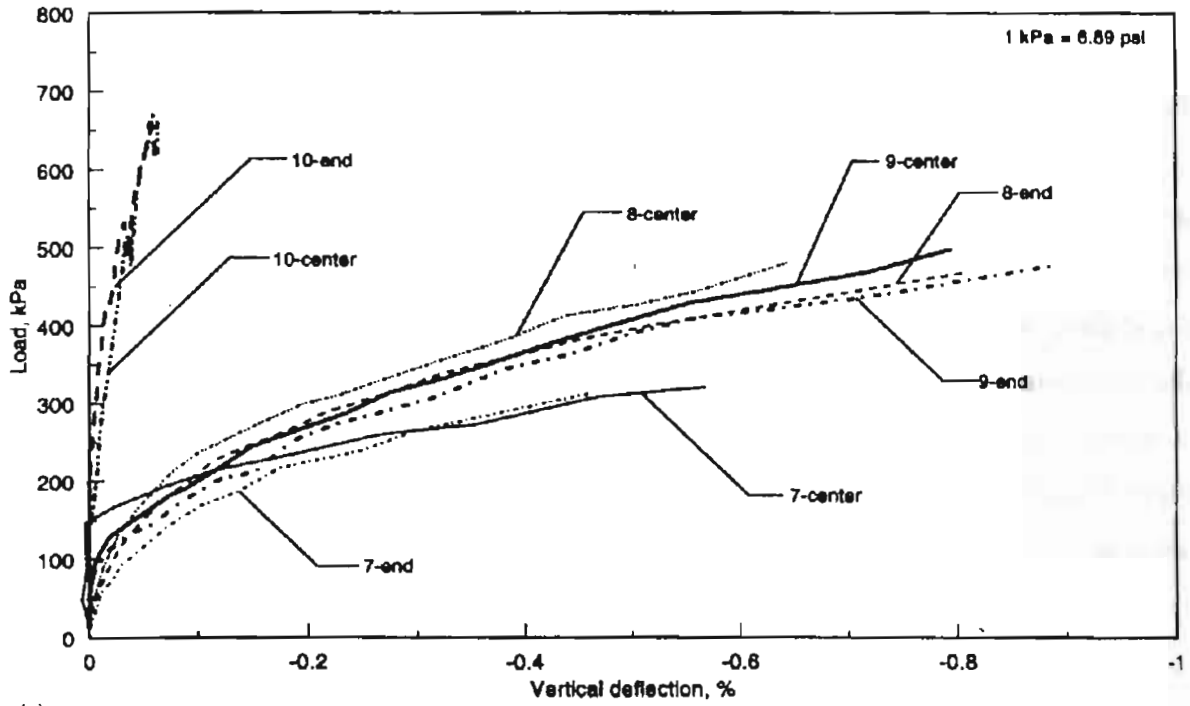
Fig. 1.2.16 shows the load-versus-deflection response for the 900-mm (36-in.) pipes, and Fig. 1.2.17 shows the load-versus-deflection response for the 1200-mm (48-in.) pipes. A comparison of the deflections at the center and the ends of the pipes in all cases shows that the deflections are somewhat higher at the ends of the pipes than at the centers. In general, the variation in deflections between the center loading and end loading in tests 7 through 10 is small. The percent deflections at 480 kPa (10,000 psf) are compared in Table 1.2.11. For pipes loaded at the center, except for the low-density glacial till (test 7), the deflections are less than 0.5 percent.

**Table 1.2.11 Pipe Deflections at 479 kPa (10,000 psf)**

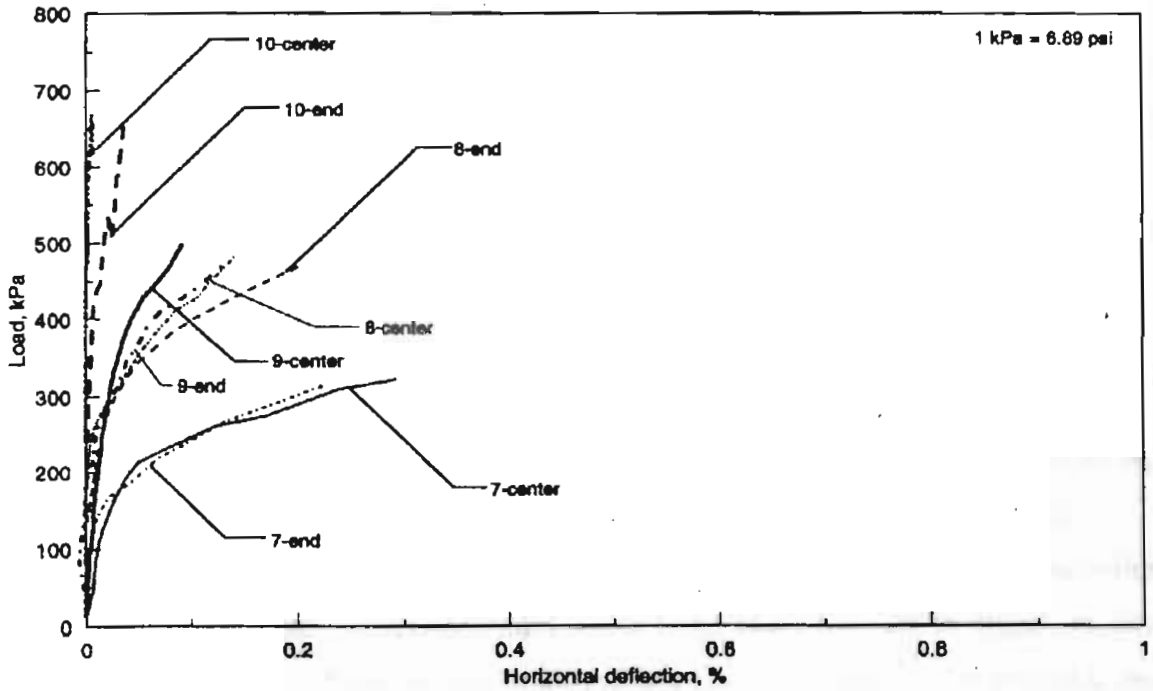
Field Test	Center Loading	End Loading
7	1.4%	1.9%
8	0.4%	0.4%
9	0.4%	0.5%
10	0.02%	0.05%
11	0.3%	0.5%
12	0.5%	1.8%
13	0.01%	0.03%

### *Pipe Dependence on Backfill Envelope*

In four tests on 900-mm and 1200-mm pipes from Manufacturers A and C, the load application system was identical to that used in the tests on 6100-mm (20-ft) long pipes; however, length of the pipes was equal to the pipe diameter. In each set of tests, the pipes were subjected to loading with four backfill conditions: no backfill with pipes resting in the bedding saddle, sand backfill to the springline, sand backfill to 70 percent pipe diameter, and sand backfill to the crown of the pipe.

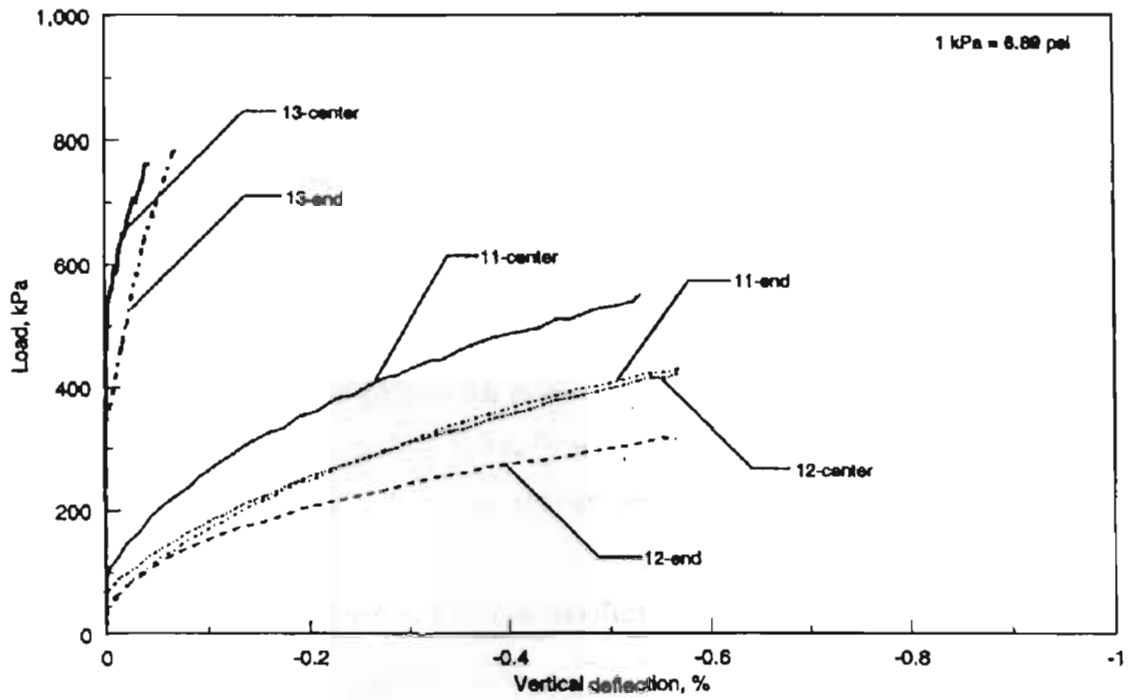


(a)

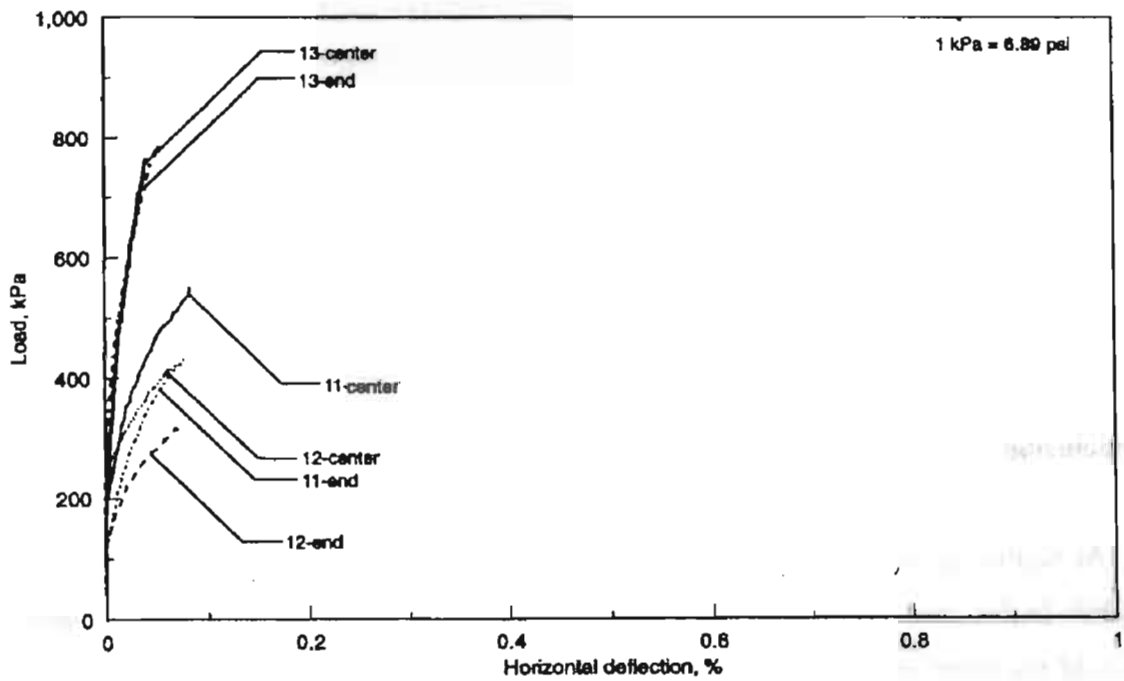


(b)

Fig. 1.2.16 Service Loading of 900-mm (36-in.) Diameter Pipes: (a) Vertical Deflection  
(b) Horizontal Deflection



(a)



(b)

Fig. 1.2.17 Service loading of 1200-mm (48-in.) Diameter Pipes: (a) Vertical Deflection, (b) Horizontal Deflection

In Fig. 1.2.18(b) where the backfill is at the springline, the pipes' responses become nonlinear and the loads to cause 5 percent vertical deflection are nearly twice the values observed in Fig. 1.2.18(a). As the backfill height becomes larger, the pipes exhibit greater stiffness.

#### *Ultimate Capacity of Pipe-Soil System*

Figures 1.2 .19 and 1.2.20 show the curves for loading to failure for the 900-mm (36-in.) and 1200-mm (48-in.) pipes, respectively. Table 1.2.12 summarizes the ultimate contact stresses and failure deflections. Most pipe failures occurred at vertical deflections between 2 and 2.5 percent.

**Table 1.2.12 Pipe Deflections at Ultimate Strength**

Field Test	Center Loading		End Loading	
	Load , kPa (psf)	Deflection	Load , kPa (psf)	Deflection
7	579 (12,000)	2.6%	527 (11,000)	2.4%
8	718 (15,000)	2.1%	622 (13,000)	1.2%
9	622 (13,000)	2.0%	622 (13,000 )	2.9%
10	1,484 (31,000)	1.1%	1,436 (30,000)	1.0%
11	862 (18,000)	2.3%	670 (14,000)	2.6%
12	718 (15,000)	2.6%	479 (10,000)	1.9%
13	1,436 (30,000)	0.8%	1,341(28,000)	1.0%

#### **Conclusions**

At contact stresses equivalent to moderate highway tire pressures, pipe deflections are slightly higher near the ends of the pipes than at the center. The increased deflections at the ends of the pipes are caused by pipe's end effects and lower effective soil modulus due to lower soil restraint. Except for low-density till, the percent deflections are not excessive and the pipe-soil systems have adequate stiffness. For contact stresses near the upper limit of truck tire pressure and when loaded near their ends, the pipes with sand and till backfills fail with localized wall bending.

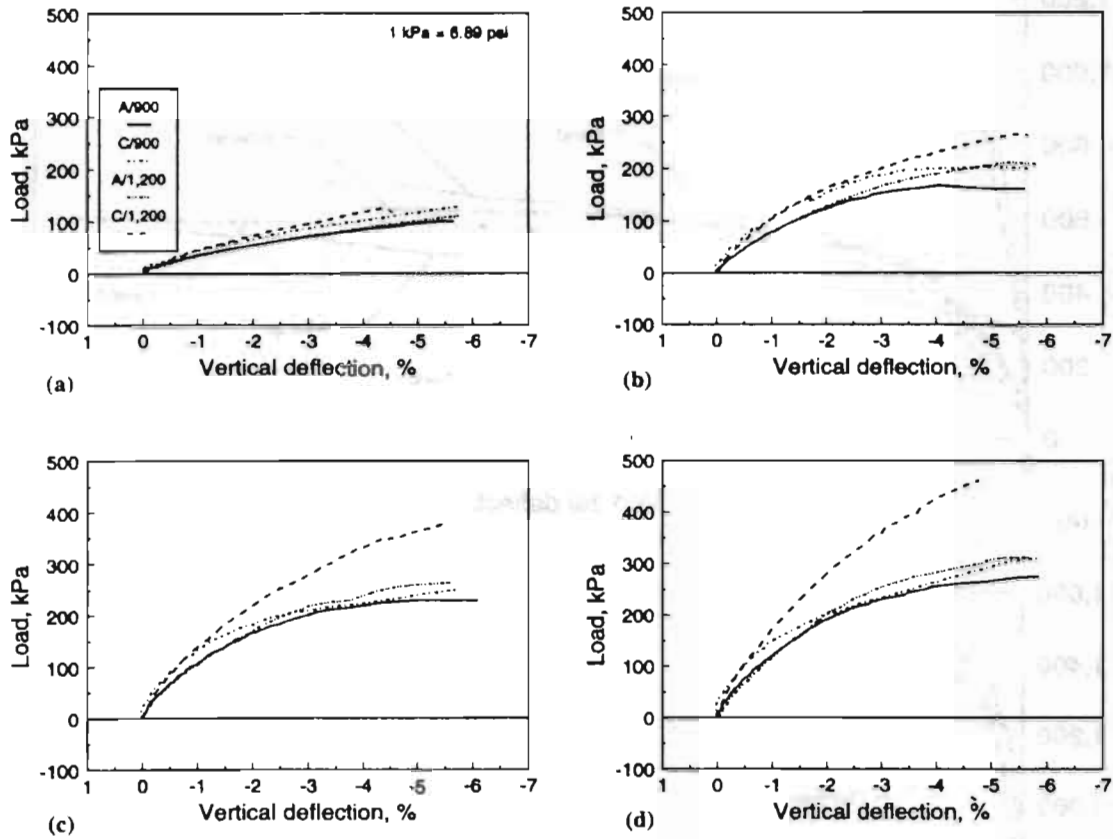
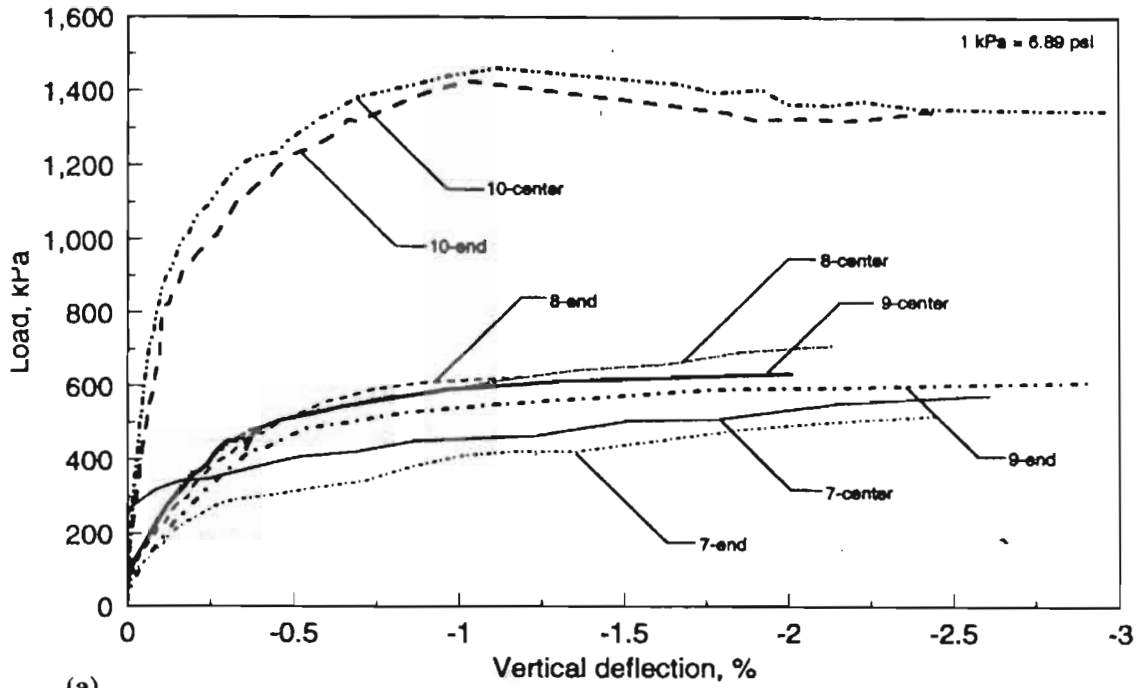
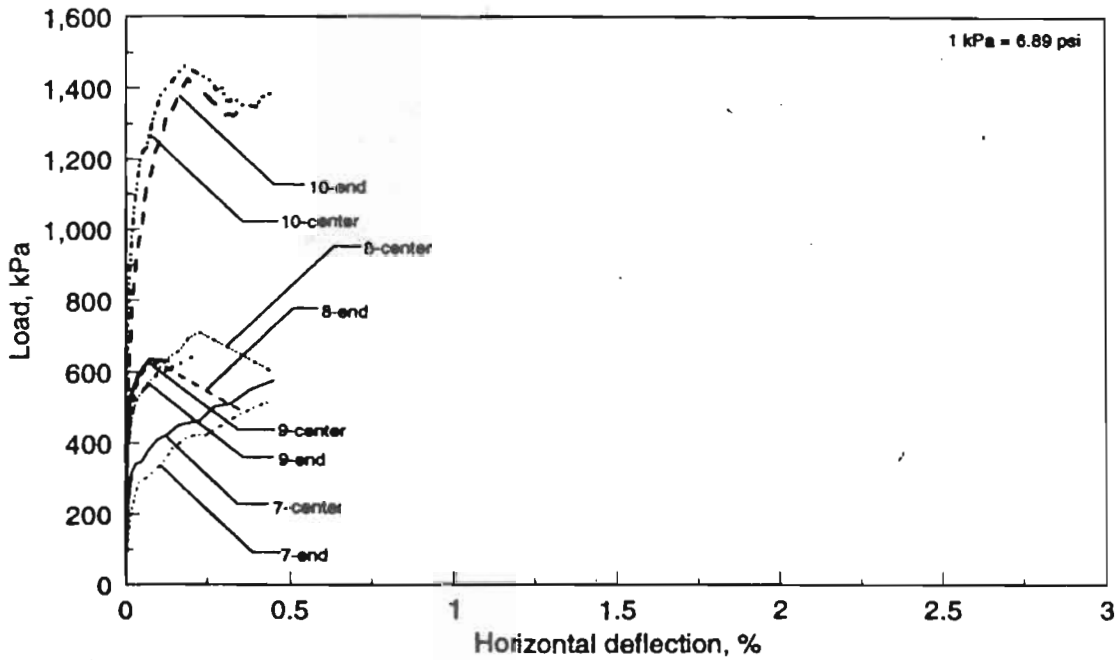


**Fig. 1.2.18 Vertical Deflection of Pipes with Varying Levels of Backfill: (a) No Backfill, (b) Backfill to Springline of Pipe, (c) Backfill to 70 Percent of Outside Diameter, (d) Backfill to Crown of Pipe**



(a)



(b)

Fig. 1.2.19 Failure Loading of 900-mm (36-in.) Diameter Pipes: (a) Vertical Deflection, (b) Horizontal Deflection

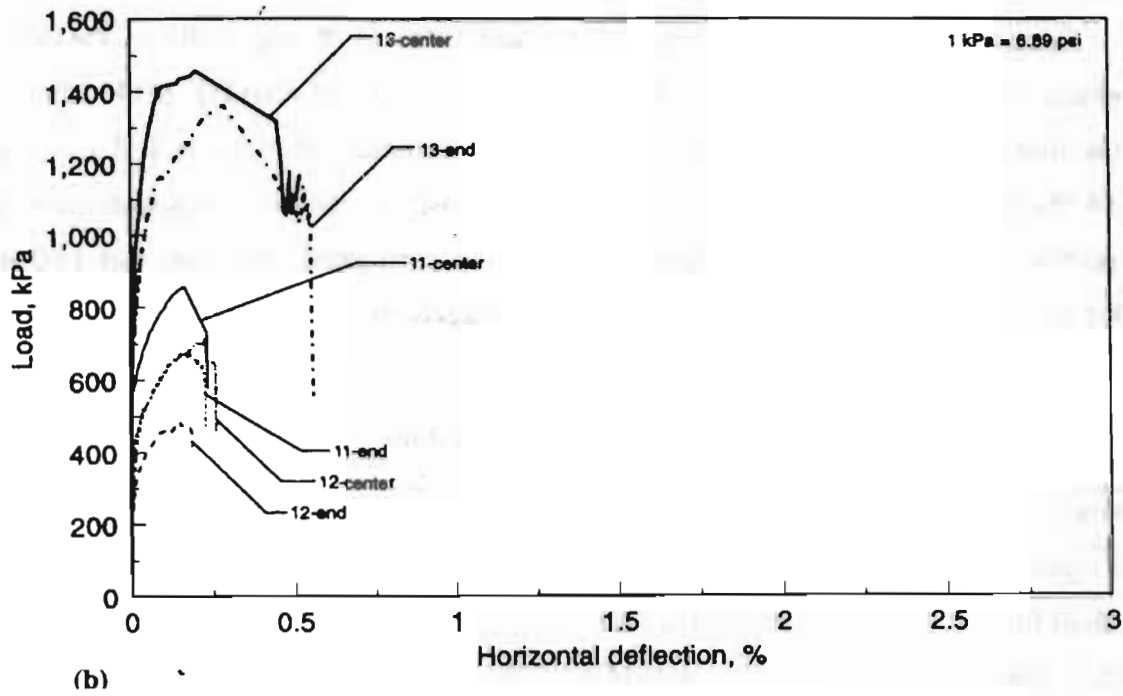
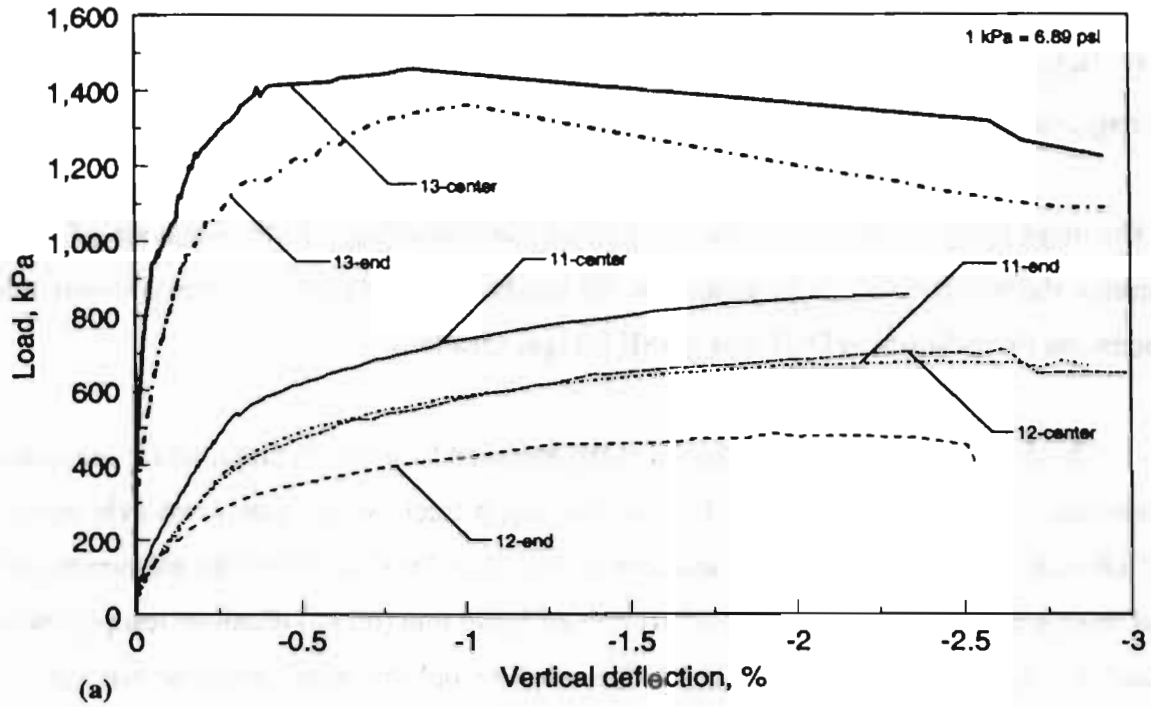


Fig. 1.2.20 Failure Loading of 1200-mm (48-in.) Diameter pipes: (a) Vertical Deflection, (b) Horizontal Deflection

**Performance of Thermoplastic Culvert Pipe Under Highway Vehicle Loading**, McGrath, T. J., DelloRusso, S. J., and Boynton, J., *Transportation Research Board 81<sup>st</sup> Annual Meeting*, Jan. 2002, pp. 14.

The objectives of the study are to improve understanding of the behavior of large diameter thermoplastic culverts under low fill heights, and develop design and installation procedures for inclusion in DOT and AASHTO specifications.

The field tests are being conducted at the MnRoad Research Facility, which maintains a two-lane test road traversed only by test vehicles, a truck with a maximum axle load of 107 kN (24,000 lb) travels in one lane and a truck with 80 kN (18,000 lb) maximum axle load travels in the other. Ten 20 m (65 ft) runs of 1,500 mm (60 in.) diameter test pipe were installed. Test pipe consisted of eight runs of thermoplastic pipe, and one run each of reinforced concrete and corrugated steel pipe.

Nominal installation depths were 0.3m and 0.6m (1 ft and 2 ft) to the top of pavement. Backfill materials were A-1 and A-2 soils per AASHTO M145. Backfill compaction effort was minimal. All test variables are summarized in Table 1. 2.13. Table 1.2.14 shows the summary of pipe installations and instrumentation. Cross-sections of the PE profile types are presented in Figure 1.2.21. The corrugated steel pipe was 1.63 mm (0.064 in.), with 75 mm by 25 mm (3in. by 1 in.) corrugations.

**Table 1.2.13 Test Variables**

Parameter	Values
Pipe type (1)	Type S PE, Type D PE, corrugated steel, reinforced concrete
Depth of fill	0.3m, 0.6m (1ft, 2 ft)
Backfill type	A-1, A-2 per AASHTO T99
Live Load	80 kN maximum axle load, 107 kN maximum axle load

1. PE Profile types as defined by AASHTO M294.

**Table 1.2.14 Summary of Pipe Installations and Instrumentation**

Pipe Run No.	Pipe Type	Nominal Fill Height m (ft)	Backfill Material
1	PE, Type S	0.3 (1)	A-1
2	PE, Type S	0.3 (1)	A-1
3	PE, Type S	0.3 (1)	A-2
4	PE, Type S	0.3 (1)	A-2
5	Reinforced Concrete	0.3 (1)	A-2
6	Corrugated Steel	0.3 (1)	A-2
7	PE, Type S	0.6 (2)	A-2
8	PE, Type D	0.6 (2)	A-2
9	PE, Type S	0.6 (2)	A-1
10	PE, Type D	0.6 (2)	A-1

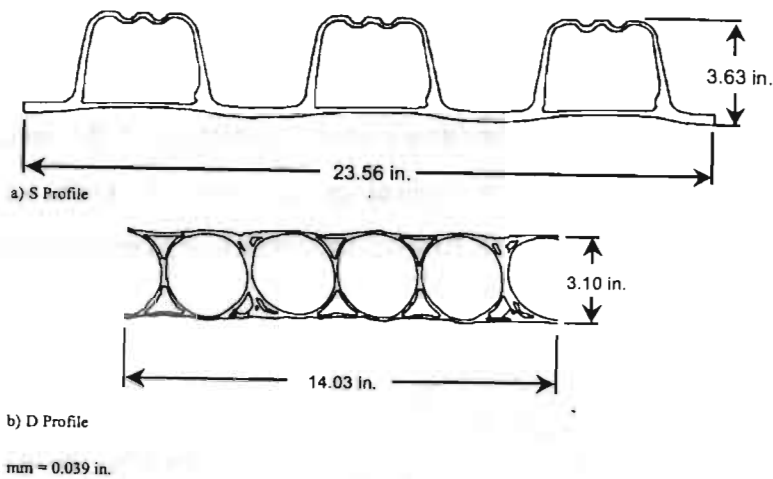


**Fig. 1.2.21 Actual Corrugated PE Wall Profiles**

**Installation**

The ten culvert runs are oriented south to north and spaced approximately 4.9 m (16 ft). The pipe installation proceeded as described below:

- i) The trench cross-section extended nominally 150 mm (6 in.) below the pipe invert as well as 450 mm (18 in.) clear from the pipe outer diameter at the springline.

ii) Compaction levels of 85% to 90% were achieved using foot traffic with the A-1 select fill, and a single pass with an impact type compactor for the A-2 material.

iii) All pipes were initially backfilled to approximately 300 mm (1 ft) below final grade.

iv) Pavement consisted of approximately 200 mm (8 in.) of MN/DOT Class 5 aggregate base followed by a total of 100 mm (4 in.) of bituminous paving material placed in two equal lifts to final grade.

### Static Live Load Tests

Static live load tests were performed at each pipe run with the 107 kN axle load and 80 kN axle load trucks in their appropriate lane on 10/24/00 (first load cycle) and after the spring thaw on 5/15/01. Figure 1.2.22 presents a schematic of the axle arrangement and axle loads of the test trucks. The truck was aligned with the driver's side wheels 0.9 m (3 ft) from the centerline of the roadway, thus aligning the truck wheels with the instrumented cross-sections.

### Dynamic Live Load Tests

Dynamic live load tests were conducted after completion of the static tests. The truck operator traversed the pipe runs at the typical speed of 40 to 50 km/hr (25 to 30 mph) with the driver's wheel as close to 0.9 m (3 ft) from the centerline as practicable.

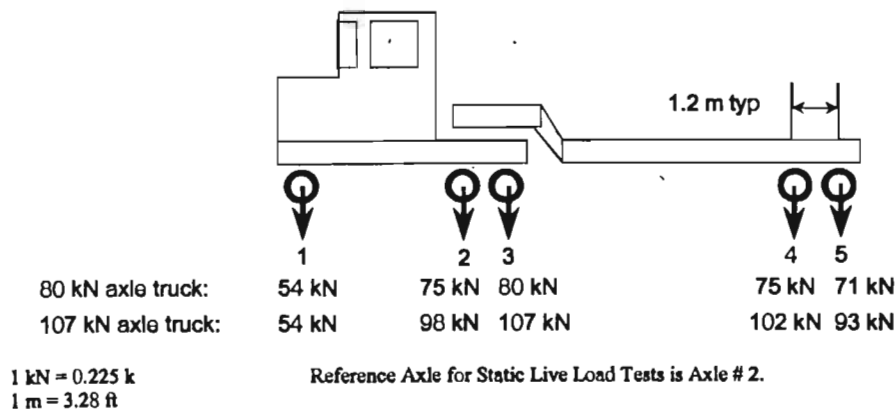


Fig. 1.2.22 Truck Configuration and Axle Loads

## Findings

Response to static live load is summarized for each pipe in Table 1.2.15, which shows the deflection due to the first load cycle (Oct-00), and after the spring thaw (May-01). A typical response to dynamic live load is shown in Figure 1.2.23. Table 1.2.16 summarizes for each pipe. The initial data from the live load tests suggests that the response to live loads for the test PE pipe is small.

**Table 1.2.15 Crown Deflections from Static Live Load Tests**

Pipe Run No.	Pipe Type	Nominal Fill Height m (ft)	Truck Lane	Static Deflection, %(1)		
				Oct-00	May-01	Change
1	PE, Type S	0.3 (1)	107 kN	0.23	0.16	-0.07
			80 kN	0.14	0.13	-0.01
2	PE, Type S	0.3 (1)	107 kN	0.16	0.20	0.04
			80 kN	0.17	0.18	0.01
3	PE, Type S	0.3 (1)	107 kN	0.12	0.14	0.02
			80 kN	0.07	0.07	0.00
4	PE, Type S	0.3 (1)	107 kN	0.16	0.14	-0.02
			80 kN	0.13	0.03	-0.10
6	Corrugated Steel	0.3 (1)	107 kN	0.10	0.07	-0.03
			80 kN	0.08	0.05	-0.03
7	PE, Type S	0.6 (2)	107 kN	0.07	0.02	-0.05
			80 kN	0.05	0.03	-0.02
8	PE, Type D	0.6 (2)	107 kN	0.06	0.04	-0.02
			80 kN	No data	0.02	
9	PE, Type S	0.6 (2)	107 kN	0.09	0.06	-0.03
			80 kN	0.03	0.03	-0.00
10	PE, Type D	0.6 (2)	107 kN	0.09	0.06	-0.03
			80 kN	0.08	0.04	-0.04

1. Based on nominal 1500 mm (60 in.) diameter.

**Table 1.2.16 Crown Deflections from Dynamic Static Live Load Tests**

Pipe Run No.	Pipe Type	Nominal Fill Height m (ft)	Truck Lane	Dynamic Deflection, %		
				Oct-00	Nov-00	May-01
1	PE, Type S	0.3 (1)	107 kN	0.08	0.01	0.13
4	PE, Type D	0.3 (1)	107 kN	0.05	0.01	0.08
8	PE, Type D	0.6 (2)	80 kN	0.03	0.01	0.03
9	PE, Type S	0.6 (2)	80 kN	0.03	0.01	0.03

**Conclusions**

Comparisons of static and dynamic deflections suggest that the static load produces more deflection than the same load applied as a moving truck. No changes in the general condition of the pipes have been observed. The increase in the dynamic load response at 0.3m (1 ft) fill is a concern. If this response continues to increase, then it suggests a degradation of the quality of soil support and an increased minimum depth of fill.

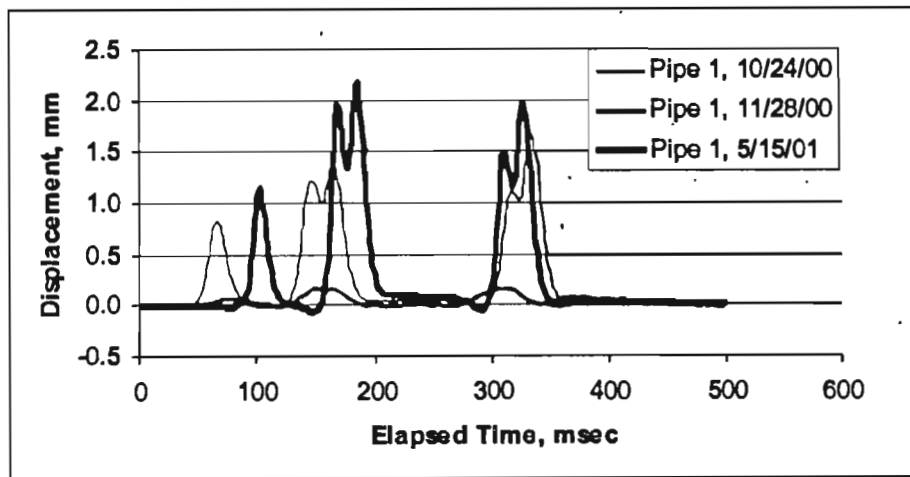


**Fig. 1.2.23 Typical Dynamic Response, 0.3 m (1 ft) Cover, 107 kN Axle Load Truck**

### 1.3 Soil Stiffness

**Laboratory Determination of Soil Stiffness Data for Buried Plastic Pipe**, Faragher, E., Rogers, C.D.F., and Fleming, P.R., Transportation Research Record 1624, Paper No.98-0773, 1998, pp. 231-236.

The paper reports on the results of an laboratory study based on testing of structured-wall plastic pipes in a large test tank to simulate burial in a trench wherein both gravel and sand surrounds were used.

Tests were conducted in a steel test tank measuring 1.8 m x 1.5 m (5.9 ft x 4.9 ft) in plan and 2.2 m (7.2 ft) in height and supported by a relatively rigid steel framework (Fig. 1.3.1). To the underside of the steel lid was affixed a rubber membrane, clamped at the edges. Water was forced between the membrane and the tank lid to create additional vertical stress up to a maximum of 140 kPa (20.3 psi). The applied loading aimed at simulating relatively severe practical conditions. The changes in the vertical and horizontal pipe diameters were recorded during the installation and loading phases. Linear variable differential transformers (LVDTs) were used, via datalogger, to record the pipe wall movement. Measurements were taken every second during application of the static stress, when the pipes deflected rapidly, and at 15-minute intervals thereafter.

The stiffness of the surrounding soil (quantified by  $E'$ ) is numerically a much larger value in general than the stiffness of the pipe when used in the Iowa formula, and thus has a dominant effect on the magnitude of the calculated pipe deformation. The authors cited the values of  $E'$  based on studies conducted by other researchers (Table 1.3.1) for three different surround types.

The most widely used design method for flexible pipes is Spangler's "Iowa" formula for the static loading phases given by

$$\delta x = \frac{KW_c D_L}{(EI/r^3) + 0.06E'}$$

where,

$\delta x$  = change in horizontal pipe diameter (m)

$W_c$  = load per unit length applied to pipe ( $\text{Nm}^{-1}$ )

$r$  = radius of pipe (m)

$E$  = elastic modulus of pipe material ( $\text{Nm}^{-2}$ )

$I$  = second moment of area of pipe wall per unit length ( $\text{m}^4$ )

$E'$  = modulus of soil reaction ( $\text{Nm}^{-2}$ )

$K$  = bedding factor (dimensionless)

$D_L$  = deflection lag factor (dimensionless)

The modulus of soil reaction  $E'$  was calculated in four ways:

i)  $E'(1)$ : value obtained using the (horizontal) diametral reduction recorded at the end of the 70-kPa static loading phase;

ii)  $E'(2)$ : value obtained using the diametral change recorded during the 70-kPa (10.15 psi) static loading phase;

iii)  $E'(3)$ : value obtained using the cumulative diametral reduction recorded at the end of the 140-kPa (20.3 psi) static loading phase; and

iv)  $E'(4)$ : value obtained using the cumulative diameter reduction recorded during the 140-kPa (20.3 psi) static loading phase.

The computed results are given in Tables 1.3.2 –1.3.4 for the three surround types: lightly compacted sand (mean bulk unit weight of  $15.1 \text{ kNm}^{-3}$ ), rounded river gravel (unit weight of  $17.5 \text{ kNm}^{-3}$ ), and heavily compacted sand (unit weight of  $18.3 \text{ kNm}^{-3}$ ).

The following conclusions were reached in this study:

The determination of Spangler's modulus of soil reaction ( $E'$ ) from laboratory testing of buried plastic pipes has been described. The values of  $E'$  are significantly higher than those currently used in U.K. and U.S. practice and as such suggest a general underestimation of the support offered to a buried flexible structure by the soil that surrounds it.

The tests replicated the case of a pipe buried in a trench with strong, stiff, stable walls and subjected to static loading. They yielded global  $E'$  values of 16 MPa (2,320 psi) for

lightly compacted sand, 29 MPa (4,205 psi) for rounded river gravel, and 99 MPa (14,355 psi) for heavily compacted sand. These values must be adjusted downward in cases where the natural soil making up the trench wall is less competent and where repeated (e.g., cyclic) surface loading will occur at a cover depth that allows the pipe to be significantly affected by it. When an existing pipe is to be subjected to an additional loading, the values of E' recommended for design for the same case are approximately 20 MPa (2,900 psi) for lightly compacted sand, 40 MPa (5,800 psi) for uncompacted gravel, and 100 to 150 MPa (14,500 to 21,750 psi) for very dense granular soils.

**Table 1.3.1 Values of E' Determined by Empirical and Analytical Means**

Soil Classification	E' (Howard Empirical) (MPa)	E' (Selig-Analytical) (MPa)
CL (low plasticity clay)	2.8	3.4-15.2
ML (low plasticity silt)	7.0	9.6-40.0
SW (well graded sand)	14.0	28.0-82.0

**Table 1.3.2 Backcalculated Values of E' for Lightly Compacted Sand Surround**

Pipe Ref.	E'(1) (MPa)	E'(2) (MPa)	E'(3) (MPa)	E'(4) (MPa)
A	12.5	15.3	11.1	95.5
B	13.8	17.6	10.1	74.1
C	16.2	16.6	10.8	81.5
D	26.5	32.4	19.1	110.0
E	19.8	19.8	12.3	110.0
Mean	18	20	13	94

Where  $[E'(1)+E'(3)]/2 = 16$  MPa.

**Table 1.3.3 Backcalculated Values of E' for Gravel Surround**

Pipe Ref.	E'(1) (MPa)	E'(2) (MPa)	E'(3) (MPa)	E'(4) (MPa)
A	28.4	41.8	29.2	157.0
B	23.5	33.8	23.5	114.0
C	35.2	50.1	30.4	137.0
D	27.8	40.1	27.6	155.0
E	28.9	45.6	28.3	178.0
Mean	29	42	28	148

Where  $[E'(1)+E'(3)]/2 = 29$  MPa.

**Table 1.3.4 Backcalculated Values of E' for Heavily Compacted Sand Surround**

Pipe Ref.	E'(1) (MPa)	E'(2) (MPa)	E'(3) (MPa)	E'(4) (MPa)
A	-61.7	-154.0	-85.6	-118
B	-84.1	101	-49.1	140
C	-52.4	106	-48.9	68.2
D	86.9	122	111	138
E	-42.3	251	-81.8	207
Means*	87	145	111	129

Where  $[E'(1)+E'(3)]/2 = 99$  MPa.

\*Negative values of E' were omitted in the calculation of mean values

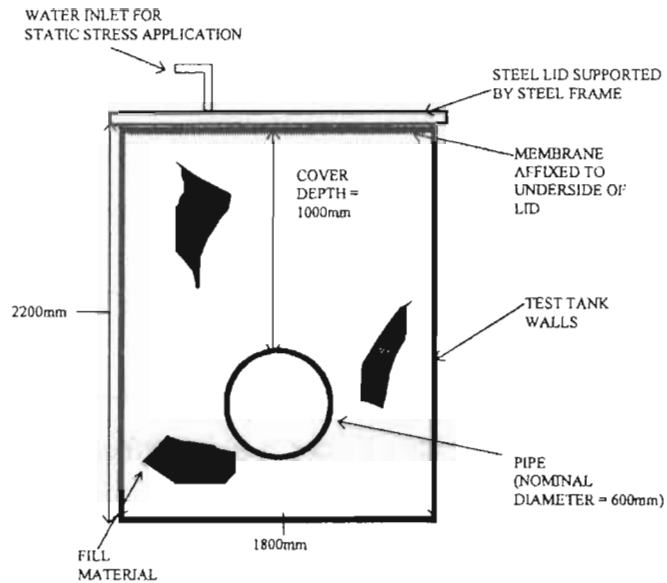


**Fig. 1.3.1 Cross Section Through Test Apparatus**

## 1.4 Soil-Pipe Interaction

**Modulus of Soil Reaction Values For Buried Flexible Pipe**, Howard, A.K., *ASCE Journal of the Geotechnical Engineering Division*, Vol.103, No.GT1, January 1977, pp.33-43.

The paper presents discussions on the investigation of the U.S. Bureau of Reclamation (USBR) on the load-deflection relationship of buried flexible pipe using laboratory soil container tests and special field installations.

The material modulus becomes a combination of the structural modulus (stiffness) of the pipe and the modulus (stiffness) of the soil, so that

$$\text{pipe deflection} = \frac{\text{load on pipe}}{\text{pipe stiffness} + \text{soil stiffness}}$$

The modified Iowa formula is given as

$$\Delta X = \frac{D_1 KW}{\frac{EI}{r^3} + 0.061E'}$$

in which

$$\Delta X = \frac{\text{Load Factor}}{\text{Ring Stiffness Factor} + \text{Soil Stiffness Factor}} =$$

$D_1 KW$  = load factor

$EI/r^3$  = ring stiffness factor

$0.061E'$  = soil stiffness factor

USBR experience with laboratory and field tests of buried flexible pipe has resulted in an empirical relationship between pipe deflection and soil stiffness values for different pipe bedding construction conditions. The values of the soil stiffness (modulus of soil reaction  $E'$ ) shown in Table 1.4.1 represent the types of soils and degrees of compaction for buried flexible pipe. The variations between the actual deflection and the deflection predicted using  $E'$  values from Table 1.4.1 appear to be affected more by the degree of compaction than any other factor.

The comparisons between the actual and predicted deflections are shown in Fig. 1.4.1(a) for the dumped and slightly compacted field tests. Fig. 1.4.1(b) shows the comparison for the field tests with moderate degrees of compaction and the comparison of actual deflection versus predicted deflection for the tests with a high degree of compaction is shown in Fig. 1.4.1(c).

E' values were established for specific soil types and degrees of compaction using data from over 100 field tests. The values of E' could be used to predict the actual pipe deflection for dumped and slight degrees of compaction to within  $\pm 2\%$ , for moderate degrees of compaction to within  $\pm 1\%$  deflection, and for high degrees of compaction to within  $\pm 0.5\%$  deflection.

The percentage deflection refers here to the variation in the actual deflection from the predicted deflection. For  $\pm 1\%$  deflection accuracy, if the predicted deflection were  $\pm 3\%$ , the actual deflection would be between  $\pm 2\%$  and  $\pm 5\%$ .

The data from the field measurements of buried pipe showed that the deflection along a pipeline can vary  $\pm 2\%$  deflection about the average deflection for any soil type or degree of compaction.

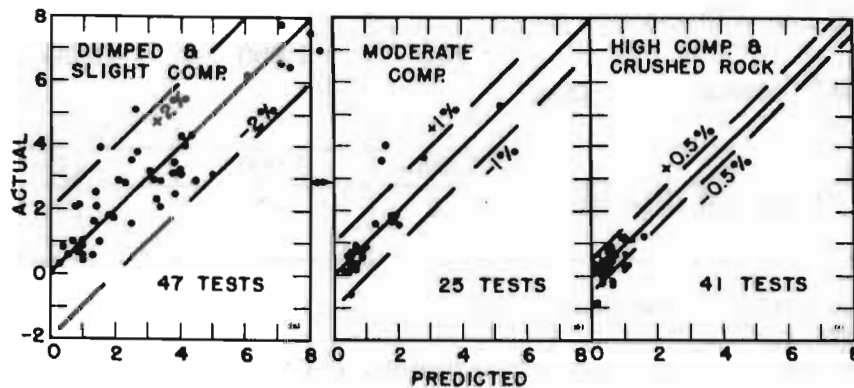


**Fig.1.4.1 Comparison of Actual and Predicted Deflections for**

- (A) Dumped and Slightly Compacted Beddings (< 85%)**
- (B) Moderately Compacted Beddings (85%-95%)**
- (C) Highly Compacted Beddings (>95%)**

**Table 1.4.1 Bureau of Reclamation Value of E' for Iowa Formula (for Initial Flexible Pipe Deflection)**

Soil Type-Pipe Bedding Material (Unified Classification System <sup>a</sup> )	E' For Degree of Compaction of Bedding, In Pounds Per Square Inch			
	Dumped	Slight,< 85% Proctor, <40% relative density	Moderated, 85%-95% Proctor, 40%-70% relative density	High,> 95% Proctor, >70% relative density
Fine-grained Soils, (LL>50) <sup>b</sup> Soils with medium to high plasticity CH, MH, CH-MH	No data available; consult a competent soils engineer; otherwise use E' = 0			
Fine-grained Soils, (LL<50) Soils with medium to no plasticity CL, ML, ML-CL, with less than 25% coarse-grained particles	50	200	400	1,000
Fine-grained Soils, (LL<50) Soils with medium to no plasticity CL, ML, ML-CL, with less than 25% coarse-grained particles Coarse-grained Soil with Fines GM,GC,SM,SC <sup>c</sup> contains more than 12% fines	100	400	1,000	2,000
Coarse-grained Soil with Little or No Fines GM,GC,SM,SC <sup>c</sup> contains less than 12% fines	200	1,000	2,000	3,000
Crushed Rock	1,000	3,000	3,000	3,000
Accuracy in Terms of Percentage Deflection <sup>d</sup>	±2	±2	±1	±0.5

<sup>a</sup> ASTM Designation D-2487, USBR Designation E-3

<sup>b</sup> LL = Liquid limit

<sup>c</sup> Or any borderline soil beginning with one of these symbols (i.e., GM-GC, GC-SC)

<sup>d</sup> For ±1 % accuracy and predicted deflection of 3%, actual deflection would be between 2% and 4%.

Note: Values applicable only for fills less than 50 ft (15 m). Table does not include any safety factor. For use in predicting initial deflections only, appropriate Deflection Lag Factor must be applied for long-term deflections. If bedding falls on the borderline between two compaction categories, select lower E' value or average the two values. Percentage Proctor based on laboratory maximum dry density from test standards using about 12,500 ft-lb/cu ft (598,000 J/m<sup>3</sup>) (ASTM D-698, AASHTO-99, USBR Designation E-11). 1 psi = 6.9 kN/m<sup>2</sup>.

**The Peripheral Movement of Soil Around a Buried Flexible Pipe, Duryee, W.A.,  
Master's Thesis, Department of Civil Engineering, Kansas State University, 1974.**

The purpose of this study was to determine the peripheral movement of the soil around a buried PVC pipe as it deflected under loading to a point beyond the performance limit. After the zone of visible movement was known, the relationship of pipe deflection and disturbance of the soil in the pipe-soil system was determined.

A testing program was set up to model test sections of four diameters (1.0, 1.30, 1.65 and 2.40 in.) of flexible pipe in a metal chamber. Two densities of backfill soil (clean river sand) were used for purposes of comparison. The soil was placed to a height of at least one diameter above the top of the pipe. During each test the pipe was loaded to various deflections and the visible movement zone was observed and measured.

The visible movement zone,  $V_z$ , (Fig. 1.4.2) is the visible peripheral movement of sidefill material caused by deflection of the pipe. This measurement was taken in all cases from the original position of the pipe to the furthest extent of the visible movement of the soil. The pipe sections were generally deflected vertically to at least 5% of their diameters, which is usually considered the performance limit for most flexible pipe in actual service.

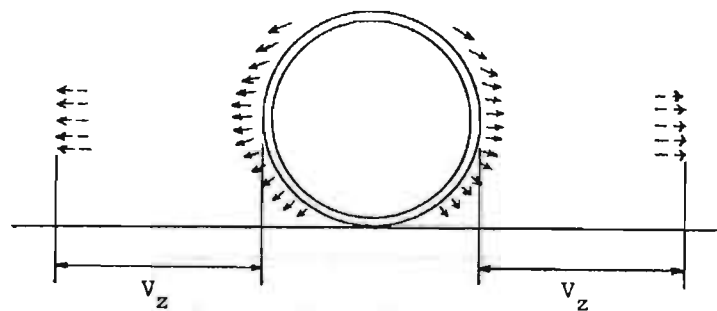


**Fig.1.4.2 Peripheral Soil Movement and  $V_z$  for Small Diameter Pipes**

The results from the tests indicate that the visible peripheral movement of the soil due to the deflection of the pipe is dependent upon the amount of deflection of the pipe, the size or diameter of the pipe, and the density of the soil.

The conclusions made are as follows:

i) As the deflection of the pipe increased, the visible movement zone,  $V_z$ , increased also.

ii) As the size of the pipe was increased for the same amount of deflection and the same original soil density, the value of  $V_z$  was generally found to be smaller.

iii) As the size of the pipe was changed for the same percent deflection,  $\Delta_y$ , and the same original soil density, the values of  $V_z/D$  could be seen to fall in the same range.

iv) As the original density of the fill was changed from loose to dense,  $V_z/D$  increased for all sizes of the pipe at a constant percent deflection. For the loose fill, the range of values of  $V_z/D$  for 5% deflection averages to about 1 and for the dense fill the range of values of  $V_z/D$  for 5% deflection averages to about 2. Intermediate densities should fall between these extremes (Fig.1.4.3).

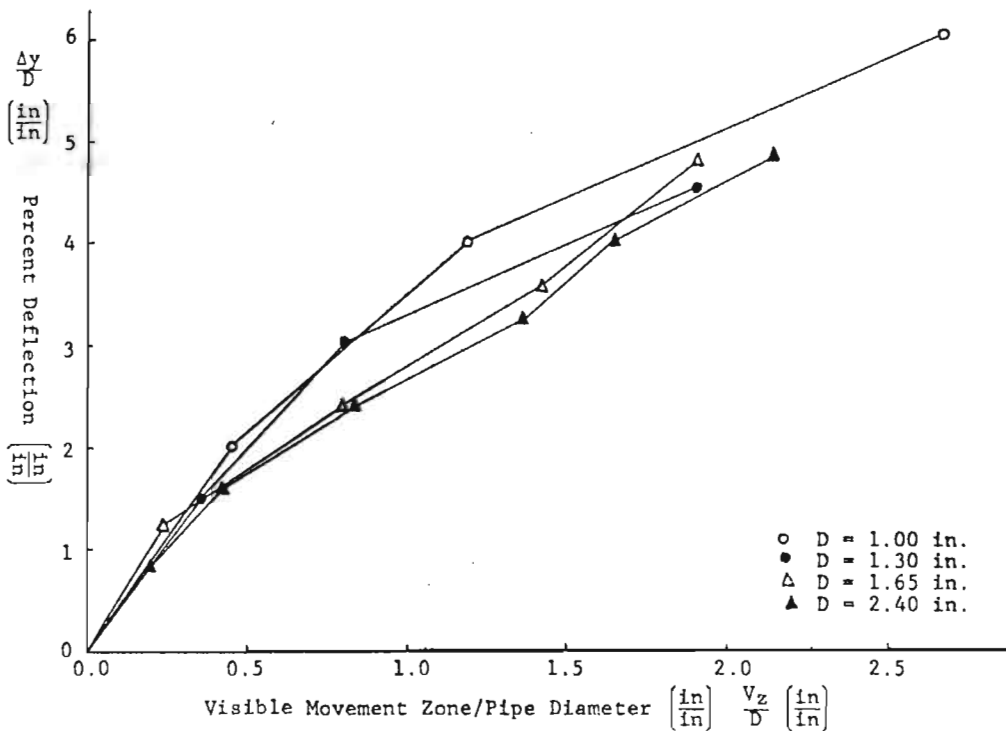


**Fig. 1.4.3 Visible Movement Zone/Pipe Diameter  $V_z/D$  for Small Diameter Pipes  
( $D =$  Pipe Diameter)**

Thus, it has been shown that the visible peripheral movement of the soil is a function of the pipe-soil system and can extend to a considerable distance under certain conditions. It

is not known what the side effects would be if the chamber walls of a model study interfered in any way with this movement, but it is felt that it could lead to misleading results about the performance of the pipe.

### 1.5 Longitudinal Strength and Stiffness

**Longitudinal Strength and Stiffness of Corrugated Steel Pipe, Havens, B.T. Klaiber, F.W., Lohnes, R.A., and Zachary, L.W., Transportation Research Record 1514, 1995, pp. 1-9.**

Analytical design procedures in use today frequently overlook or underestimate the possibility of longitudinal flexural failures, which may result from uneven settlement beneath the corrugated metal (CMP) pipe or inlet uplift because of pore water pressure. The objective of this study was to develop CMP design methods to prevent uplift failures. Theoretical relationships were developed for predicting the longitudinal stiffness, yield moment capacity, and ultimate moment capacity of CMP with any corrugation style, strength, and stiffness characteristics. Laboratory tests were conducted on steel pipes to experimentally evaluate the accuracy of the theoretical relationships. Two test specimens ISU1 (1.22 m (4-ft) diameter) and ISU2 (1.83 m (6-ft) diameter) were selected for testing. Each test specimen was instrumented with electrical-resistance strain gages, direct current displacement transducers, and dial gages. The CMP specimens were simply supported and a uniformly distributed load was applied in increments along the length of the pipe. The testing program included a service load test and a failure load test for each specimen.

#### Theoretical Longitudinal Moment Capacity

$$M_E = \frac{2\pi r t \sigma_L}{d_c} \left[ \frac{r t}{6} + K_\sigma \left( \frac{L_T^2 \cos \phi}{12} R_{TP} + K_\lambda R \right) \right]$$

Where

$\sigma_L$  = a limiting longitudinal stress within the elastic range

$K_\sigma$  = the ratio of hoop stress to longitudinal stress for any CMP element

$d_c$  = the corrugation depth indicated in Fig. 1.5.1(a)

$r$  = the CMP radius

$t$  = the CMP wall thickness

$L_T$  = the length of the tangent section in each corrugation cycle as indicated in Fig. 1.5.1(a)

$\phi$  = the tangent angle indicated in Fig. 1.5.1(a)

$R_{TP}$  = the ratio of the distance from the CAN to the tangent point to the distance from the CAN to the rest of the corrugation

$K_\lambda$  = the constant that depends on the corrugation geometry; the average value for all pipe gauge may be taken as 0.3828 in. for 3 x 1 CMP, 0.17 in. for 2 2/3 x 1/2 CMP, and 0.214 in. for 2 x 1/2 CMP; values for specific gages may be calculated using relationships presented in the work of Havens<sup>1</sup>

$R$  = the corrugation radius.

### Theoretical Longitudinal Ultimate Moment Capacity

$$M_u = \frac{4\sigma_{YL} r t}{\sin \phi} \left[ K_\sigma \left( R\phi + \frac{L_T}{6} \right) \cos \phi + \frac{r t}{2L_T} \right]$$

### Theoretical EI factor

$$EI = \frac{E \pi s_c r t}{4K_G} \left[ \frac{3}{1 + 3K_\sigma^2} \right] \left[ \frac{r t}{6} + K_\sigma \left( \frac{L_T^3 \sin \phi \cos \phi}{12d_c} + K_\lambda R \right) \right]^2$$

Where, except for  $K_G$  and  $s_c$ , all terms have been previously defined.

$K_G$  is the geometrical parameter which may be taken as 0.09215 in.<sup>3</sup> for 3 x 1 CMP, 0.01928 in.<sup>3</sup> for 2 2/3 x 1/2 CMP, and 0.01388 in.<sup>3</sup> for 2 x 1/2 CMP; note that these values are averages

---

<sup>1</sup> Havens, B. T., Determination of Longitudinal Strength and Stiffness of Corrugated Metal Pipe, M. S. Thesis, Iowa State University, Ames, Iowa, 1993

for all common pipe gages. Values for specific gages may be calculated using relationships presented in the work of Havens<sup>1</sup>. The corrugation crest spacing (length of one cycle) is denoted as  $s_c$ .

Experimental results and theoretical values calculated from above equations are shown in Table 1.5.1.

Two CMPs were loaded to failure to determine experimental values for yield moments, ultimate moments, and “stiffness” EI. Theoretical relationships were derived for determining the yield moment, ultimate moment, and the “stiffness” EI for CMPs of various diameters, gages, and corrugation geometry. The theoretical relationship for yield moments provides slightly unconservative values. Variation in the yield strength of steel is believed to be the main reason for the difference. Theoretical ultimate moment are in good agreement with the values that were obtained experimentally. The relationship for “stiffness” EI, provides values that are in good agreement with the experimental values.

**Table 1.5.1 Comparison of Experimental and Theoretical Values**

	ISU1	ISU2
Experimental Yield Moment, kN-m	30.7	28.1 to 37.3
Theoretical Yield Moment, kN-m	34.2	38.7
Difference from experimental value (%)	+11.5	+3.6 to + 37.7
Experimental Ultimate Moment, kN-m	91.5	96.3
Theoretical Yield Moment, kN-m	90.2	100
Difference from experimental Value (%)	-1.5	+4.2
Experimental EI Factor, MN-m <sup>2</sup>	2.49	2.61
Theoretical EI Factor, MN-m <sup>2</sup>	2.39	2.83
Difference from experimental value (%)	-4.3	+8.1

Note 1 kN = 737 lbf-ft ; 1 MN-m<sup>2</sup> = 2.42x10<sup>6</sup> lbf-ft<sup>2</sup>

<sup>1</sup> Havens, B. T., Determination of Longitudinal Strength and Stiffness of Corrugated Metal Pipe, M. S. Thesis, Iowa State University, Ames, Iowa, 1993

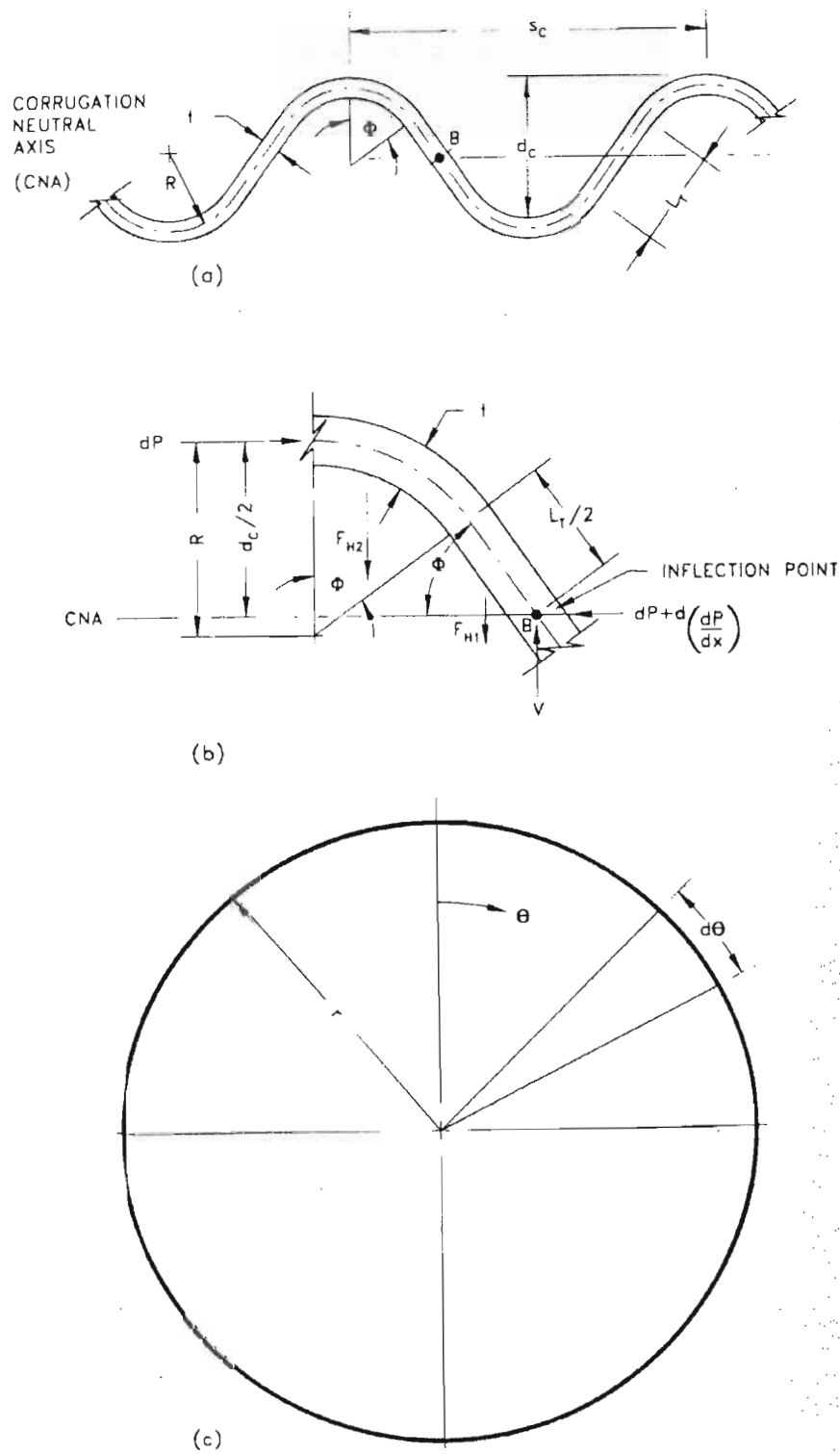


**Fig. 1.5.1 Description Of CMP: (a) Corrugation Detail; (b) Free Body Diagram of One-Quarter Corrugation Cycle; (c) Transverse Cross Section**

## 1.6 State-of-the Art in the United Kingdom

**Structural Performance of Profile-Wall Drainage Pipe-Stiffness Requirements Contrasted with Results of Laboratory and Field Tests, Rogers, C. D. F., Fleming, P. R., Loepky, M. W. J., and Faragher, E., *Transportation Research Record* 1624, 1995, pp. 83-92**

This paper describes the development of the current United Kingdom stiffness requirements for the profile-wall flexible pipes and assesses their limitations. Laboratory testing of flexible pipes ranging in diameter from 100 to 375 mm (3.9 to 14.8 in) is described.

“United Kingdom Department of Transportation (DOT) Highway Advice Note HA40/89<sup>1</sup>, states that the DOT requires profile-wall, non-pressure drainage pipes to meet the minimum 50-year extrapolated stiffness of 1,400 Pa (0.2 lb/in<sup>2</sup>.) when tested in accordance with Appendix B of BS 4962: 1989, Specification for Plastics Pipes and Fittings for use as Subsoil Field Drains.

However, the approach of DOT Highway Advice Note HA40/89 is considered as an excessively conservative approach by accepting the traditional 5 percent diametral strain limit in addition to applying a factor of two to the pipe stiffness and assuming worst case installation conditions. This approach coupled with the long-term creep test requirements of BS4962 has resulted in the substantial overdesign of pipes to meet material and structural criteria.

In laboratory testing, twin-wall annular corrugated HDPE pipes with inside diameters ranging from 100 to 375 mm (3.9 to 14.8 in) were tested. Pipe with an internal diameter of 300 mm (11.8 in) or less were tested in a 1.0 x 1.1 x 1.0-m (3.3 x 3.6 x 3.3 ft) deep box, whereas larger pipes were tested in a 1.5 x 1.8 x 1.5 m (4.9 x 5.9 x 4.9 ft) deep box. The loading arrangement provided an approximately uniform vertical stress achieved using a rubber membrane mounted to the underside of the test box lids. The bed, surround, and

---

<sup>1</sup> Highway Advice Note HA40/89 Determination of Pipe and Bedding Combinations for Drainage Works. Department of Transport (Highway and Traffic), HMSO, London, UK, 1990.

backfill materials used were a well graded river sand and river gravel. Bedding layers were 100 mm (3.9 in) thick for all tests. The river sand surround and backfill were placed either virtually uncompacted or heavily compacted in layers not exceeding 150 mm (5.9 in) in depth.

Three loading phases were used in the test program:

i) Application of a static 70-kPa (10.15 psi) stress, to simulate a stationary heavy vehicle or burial to a depth of approximately 4 m (13.12 ft).

ii) Application of a cyclic 70-kPa (10.15 psi) stress, to simulate heavy vehicle loading over a shallow buried pipe. The frequency of the cycle was 0.01 Hz, 1000 cycles being applied.

iii) Application of a static 140-kPa (20.3 psi) stress, to simulate a burial depth of approximately 8 m (26.3 ft).

The static stresses were applied for 12 hours and, after unloading, a period of 4 hours was allowed for recovery. Table 1.6.1 shows some of the selected data at critical stages of tests (both vertical and horizontal diametral strains). Figs. 1.6.1 and 1.6.2 also show a set of vertical and horizontal test data for a pipe with an internal diameter of 375 mm (14.8 in) installed in uncompacted 10-mm (0.4 in) pea gravel (typical U.K. site practice).

### **Pipe deflections**

i) The test results indicate minimal deformations (less than 1 percent) during the installation phase.

ii) Tests using heavily compacted well-graded river sand demonstrated remarkably good performance.

iii) The best performance was achieved by the 100-mm (3.9 in) pipe, indicating that the pipe/soil system is superior.

iv) Nonuniformly filled trench with no compaction caused a compressive strain at springline.

## **Pipe wall strains**

Pipe wall strains were measured beneath the corrugation, or ridge (single wall) and the valley (twin wall) for the 375-mm (14.8 in) pipe. Strain gages were placed at the pipe crown ( $0^\circ$ ), invert ( $180^\circ$ ), springings ( $90^\circ$  and  $270^\circ$ ), haunches ( $135^\circ$  and  $225^\circ$ ), and shoulders ( $45^\circ$  and  $315^\circ$ ).

i) Fig. 1.6.3 shows the tensile strains at the crown, high compressive strains at the shoulders and lower compressive strains at the springings ( $90^\circ$  and  $270^\circ$ ). This is a clear demonstration of “heart-shaped” deformation.

ii) The elliptical deformation at twin wall section was expected as a result of constant rate of deformation parallel plate test

iii) The data for the 140-kPa (20.3 psi) static load sequence show relatively small additional strains which conform broadly to the 70-kPa (10.15 psi) static load sequence.

iv) The wall strain data for the single wall (i.e., beneath the ridge) were in all cases less extreme and exhibited a greater degree of hoop compression than those for the twin wall sections (Fig. 1.6.4).

v) The ridge and valley provide a large proportion of the resistance to external loading and the single wall beneath the ridges (corrugation) is structurally less important.

## **Discussion of the test results**

i) The shape of the deformed pipe is a function of the properties of the surround medium.

ii) Lightly compacted sand produced the largest deflections due to the inability of arching mechanisms to form in loose material and greater pipe deflections being required to mobilize equilibrium passive earth pressures.

iii) Pipes in gravel exhibit far less vertical diametral reduction and deform to a “heart” shape, because of the high degree of lateral support provided to all parts of the pipe circumference by this medium.

iv) The greatest tensile strains always occurred at the pipe crown.

v) The distribution of strain around the circumference depended on the type of surround and type of loading.

vi) Good support to the pipe typically resulted in deformation that deviated from an ellipse under static load.

vii) Cyclic loading appears to permit reorientation of the soil particles and cause deformations of a more elliptical nature to be superimposed on the deformed shape.

### **Conclusions**

i) The current specification and design criteria used in the United Kingdom are conservative in the light of laboratory and field data.

ii) The currently accepted limiting deflections of 5 percent of original diameter over the long-term are still widely used, in spite of evidence that it is considered as excessively conservative.

iii) The U.K. Water Research Center recommends a deformation limit of 6 percent 12 months after construction and accepts that the greatest degree of increase in deformation after installation will occur in the first 2 years.

iv) The test results additionally indicate that a wider range of soil surrounds could be used in practice

v) The currently available creep stiffness test method do not address the fundamentals of pipe-soil interaction.

vi) The pipe-soil interaction should also be considered using the finite element method.

**Table 1.6.1 Experimental Data at Critical Points of Tests**

<b>Pipe Size</b>	<b>Soil</b>	<b>Sidefill Compaction</b>	<b>VDS HDS</b>	<b>I</b>	<b>70S</b>	<b>70C</b>	<b>140S</b>	<b>END</b>
100	RS	Not compacted	VDS HDS	0.07 -0.12	0.8 -0.8	2.7 -2.4	2.8 -2.4	2.6 -2.4
100	RS	Heavily compacted	VDS HDS	0.17 -0.01	-0.11 -0.03	0.08 -0.19	0.10 -0.16	0.04 -0.17
100	RG	Not compacted	VDS HDS	0.03 -0.03	0.4 -0.3	1.2 -0.9	1.2 -0.9	1.2 -0.9
150	RS	Not compacted	VDS HDS	0.10 -0.10	1.6 -1.0	2.6 -1.9	3.3 -2.1	3.0 -2.1
150	RG	Not compacted	VDS HDS	.15 -0.05	1.3 -0.7	1.9 -1.1	2.3 -1.3	2.1 -1.3
225	RS	Heavily compacted	VDS HDS	-0.12 0.06	0.1 0.0	0.1 -0.1	0.2 -0.1	0.1 -0.1
225	RS	Not compacted	VDS HDS	0.04 -0.07	1.2 -1.0	2.0 -1.9	2.7 -2.1	2.1 -1.8
225	RG	Not compacted	VDS HDS	0.14 -0.11	1.0 -0.7	1.5 -1.1	1.9 -1.3	1.6 -1.2
300	RS	Heavily compacted	VDS HDS	-0.31 0.40	0.0 0.3	0.1 0.2	0.4 0.1	0.2 0.2
300	RS	Not compacted	VDS HDS	-0.01 -0.05	2.7 -2.6	4.2 -4.2	5.1 -4.7	4.1 -4.2
300	RG	Not compacted	VDS HDS	0.18 -0.08	1.5 -1.2	2.2 -1.9	2.8 -2.5	2.3 -2.4
375	RS	Not compacted	VDS HDS	0.14 -0.03	1.3 -0.6	3.9 -2.6	4.4 -2.7	4.0 -2.6
375	RS	Heavily compacted	VDS HDS	-0.70 0.80	-0.6 0.7	-0.6 0.7	-0.5 0.7	-0.7 0.8
375	RG	Not compacted	VDS HDS	-0.30 0.30	0.0 0.1	0.3 -0.1	0.6 -0.2	0.2 -0.1

**Legend and Sign Convention**

**Soil Types**

RS = Well graded river sand

RG = Relatively uniform, sub-rounded 10 mm gravel

**Deflection**

VDS = Vertical diametral strain (% of mean external diameter)

HDS = Horizontal diametral strain (% of mean external diameter)

(Positive diametral strain values indicate a decrease in pipe diameter)

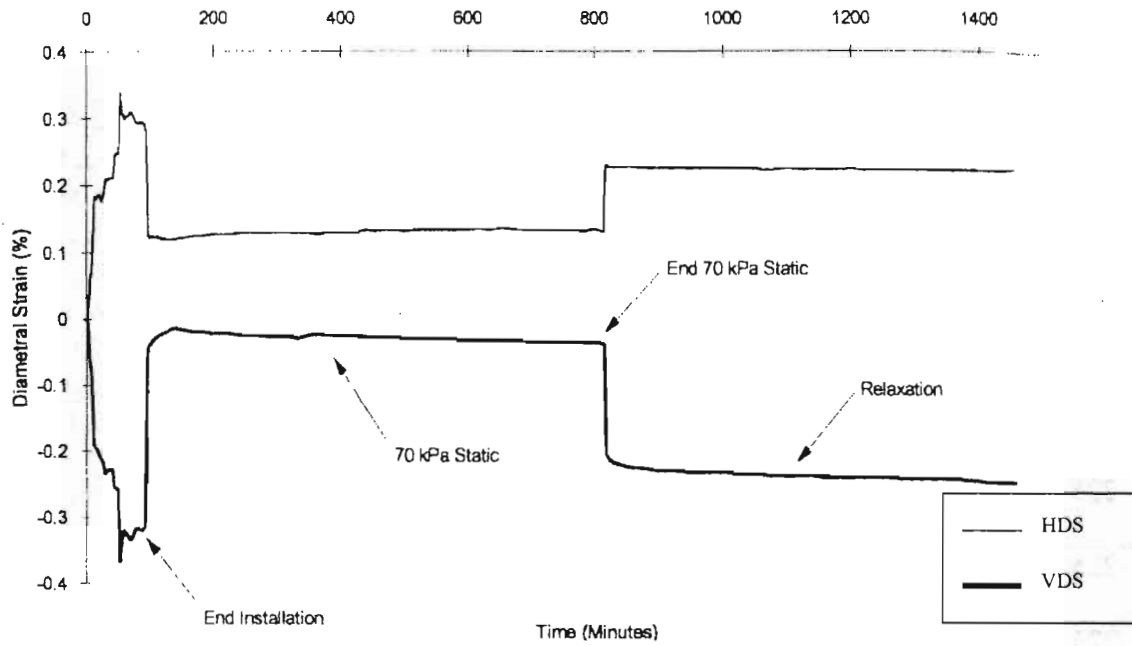


**Fig.1.6.1 Diametral Strains due to Installation and 70-Kpa Static Stress Phases**

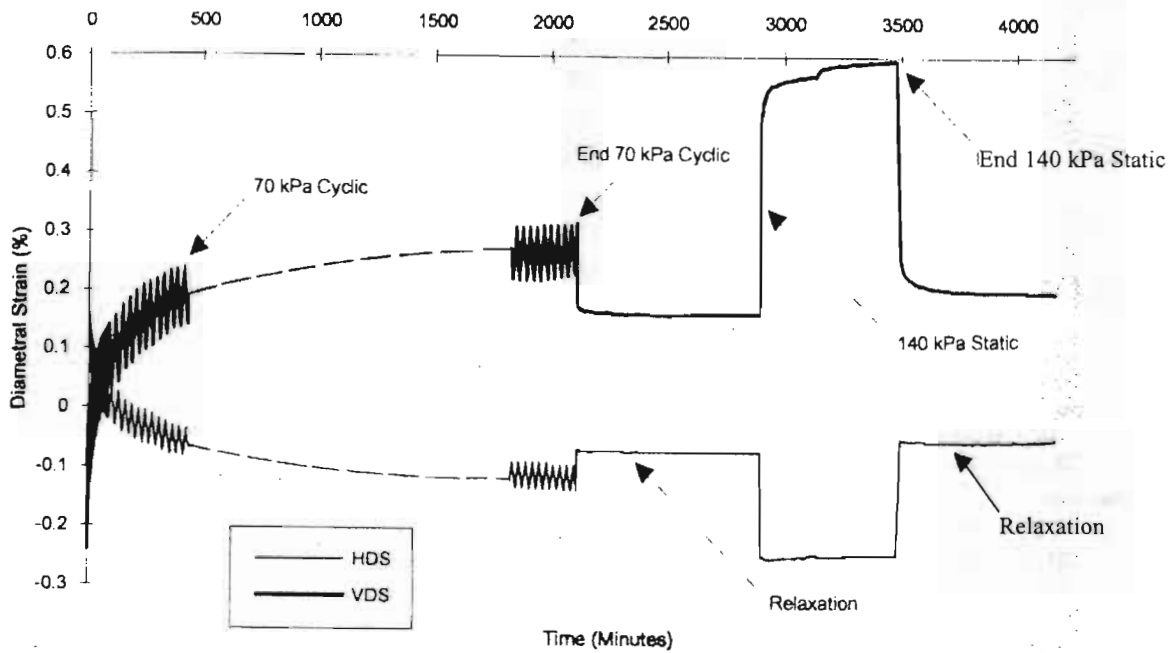


**Fig. 1.6.2 Diametral Strains due to Installation and 70-Kpa Cyclic and 140-Kpa Static Stress Phases**

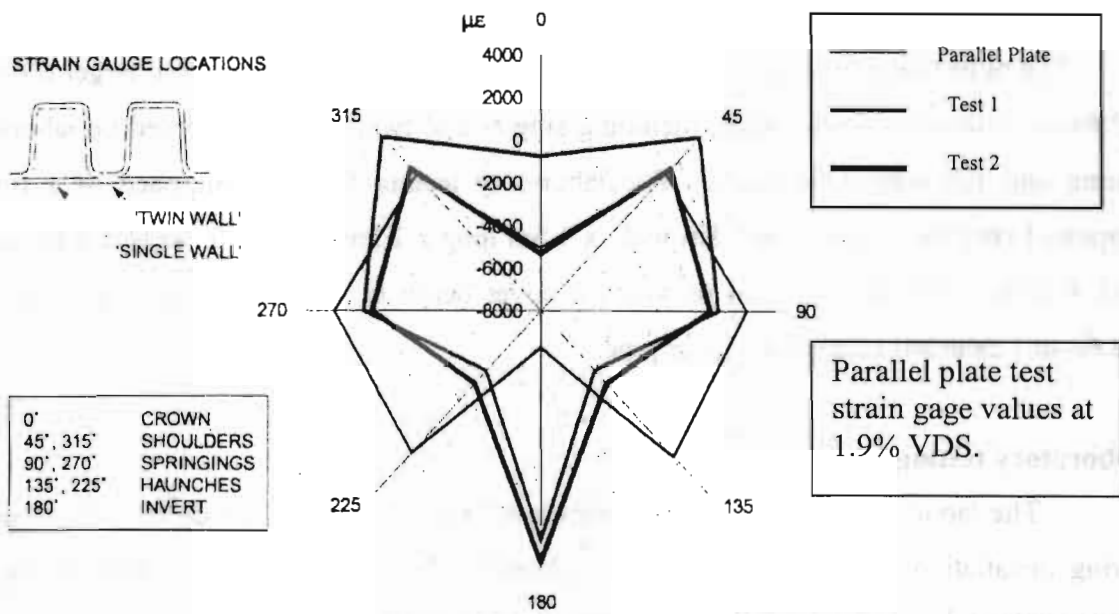


**Fig. 1.6.3 Twin Wall Strains Caused by the Complete Stress Sequence (End of Test Minus Installation) and Parallel Plate Testing**

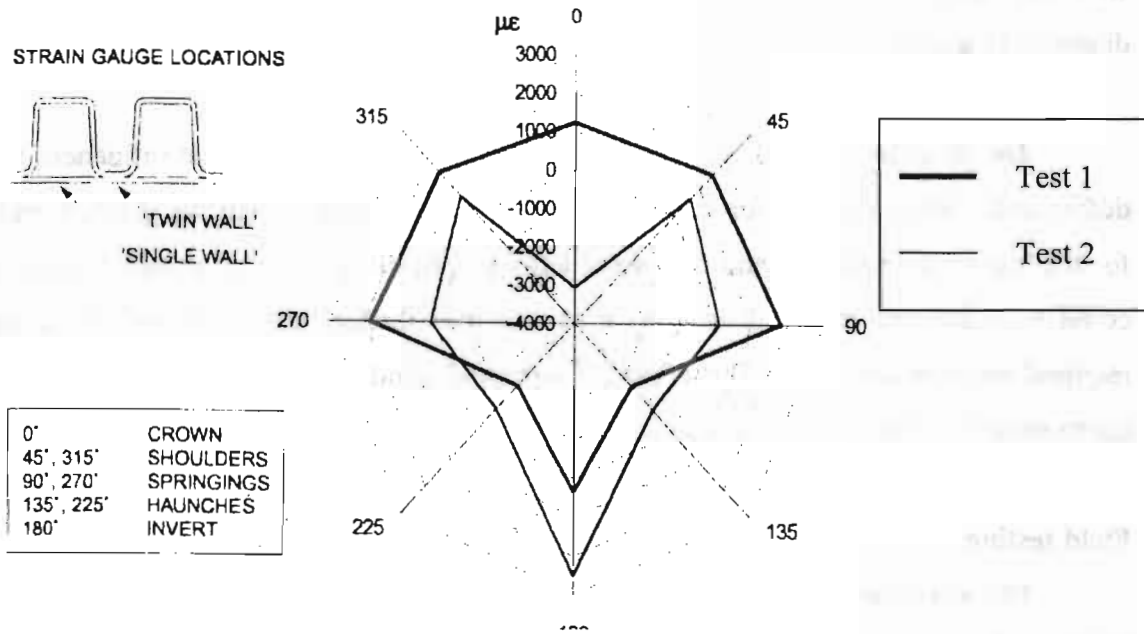


**Fig. 1.6.4 Single Wall Strains Caused by the Complete Stress Sequence (End of Test Minus Installation)**

**Laboratory and Field Testing of Large-Diameter Plastic Pipe**, *Fleming, P.R., Faragher, E., and Rogers, C.D.F., Transportation Research Record 1594, 1997, pp. 208-216.*

The objective of this paper was to examine the performance of selected larger 600-mm (23.64-in.) diameter plastic pipes, including single- and twin-wall types based on laboratory testing and full-scale field trials. The laboratory testing facility comprised of a rigidly supported steel box measuring 1.8m wide x 1.5m long x 2.2m high (6 ft. wide x 5 ft. long x 7.33 ft high). This arrangement provided a cover depth of 1.0m (3.33 ft.) for a 600-mm (23.64-in.) nominal internal diameter pipe.

### **Laboratory testing**

The laboratory test results are summarized in Table 1.6.2. The deflections recorded during installation were very small, never exceeding 0.3 percent. Pipes buried in slightly compacted sand and gravel deformed to an approximately oval shape, whereas those buried in heavily compacted sand showed elongation of the vertical diameter as filling proceeded from the bottom of the pipe level to the springline level. As filling proceeded, the vertical diameter shortened.

The static pressure phase demonstrated how the type of surround influences the pipe deformation. Deformations for the lightly compacted sand case were the greatest and those for the heavily compacted sand case were least as a result of the high passive pressures that could be mobilized in the denser material and the smaller movements of the springlines required to mobilize them. The effect of surround conditions on the pipe deformation is demonstrated in Figure 1.6.5.

### **Field testing**

The soil at the field test site was a stiff gravelly clay. The trench width was 1200 mm (47.2 in) the maximum allowable width in United Kingdom for a pipe with 600-mm (23.6 in) nominal internal diameter. Five pipes were installed with a 10-mm pea gravel bed and surround, and another five pipes with a trodden-in sand bed and surround. The depth of cover was 1.0 m (39.4 in) with a bed thickness of 150 mm (5.9 in). Strain gages were affixed to the

internal walls of the pipes. A conventional tractor and two-wheel, single axle trailer were used for the trafficking.

Table 1.6.3 shows the field test results. In general, the pipes buried in lightly or nominally uncompacted, trodden sand deformed to a greater extent than those buried in gravel. Gravel appears to give better support to the pipe and is an easier material to work with on-site. In some cases, the deflections did not differ by much, which suggests that installation techniques (especially compaction of the sand surround) affected pipe performance. Figure 1.6.6 indicates the accumulation of transient and residual strains recorded with the tractor axle directly above a corrugated twin-wall pipe.

## **Conclusions**

i) The current specification used for flexible pipes in the United Kingdom, which has a theoretical basis, leads to good performance of the pipes under normal and extreme loading conditions.

ii) During installation pipe deflections exceeded 1.01 percent under field conditions in only one case. In the laboratory deflections during installation did not exceed 0.31 percent. The lower deflections in the laboratory were attributed to the lower compactive effort used, the inability of the surround material to embed in the trench wall, and the closer control possible in the laboratory work.

iii) The pipes tested perform well under the loading conditions described herein, and this lends confidence to the fact that the theoretical methods used to derive the design charts used for pipe selection purposes will provide a safe design. However, there is a danger that the pipes could be over designed, and for this reason abnormally poor installations were examined.

iv) The generally good performance of all the pipes in all surrounds, in relation to the accepted deformation limit of 5 percent vertical diametral strain, suggests that the design criteria and installation conditions required in the United Kingdom are conservative and that other surround types (such as uncompacted sand) demonstrate good performance.

v) Typical pipe couplings have been subject to high overburden stress in very poor surround conditions and have been found to maintain airtightness, and thus fitness for purpose, at deformations in excess of the 5 percent limit. This could suggest that the 5 percent limit could be increased somewhat without a deleterious effect on pipeline integrity.

**Table 1.6.2 Vertical Diametrical Strains Recorded in Laboratory Tests**

REF	EOI VDS (%)	E70S DVS(%)	E70C DVS(%)	E140S DVS(%)	EOT VDS(%)
A-L	0.27	1.67	2.97	3.40	3.15
A-H	0.23	0.37	0.37	0.55	0.42
A-G	0.30	0.84	1.19	1.46	1.23
B-L	0.16	1.54	3.19	3.73	3.46
B-H	-0.35	-0.25	-0.18	0	-0.13
B-G	0.28	0.92	1.68	1.79	1.60
C-L	0.19	0.86	1.34	1.59	1.16
C-H	0.22	0.36	0.57	0.86	0.68
C-G	0.19	0.86	1.34	1.59	1.16
D-L	0.16	0.93	1.90	2.30	1.96
D-H	0.21	0.30	0.34	0.45	0.45
D-G	0.26	0.87	1.32	1.63	1.43
E-L	-0.11	1.12	2.44	2.81	2.53
E-H	-0.05	-0.01	0.01	0.17	0.10
E-G	0.31	0.86	1.34	1.59	1.43

**Key**

REF. Pipe type and backfill reference. The first letter indicates the pipe type (See table 1.6.3). The second indicates the type of backfill (L=lightly compacted sand, H=heavily compacted sand, and G=gravel)

VDS: Vertical diametral strain (shortening of vertical diameter/original vertical diameter).

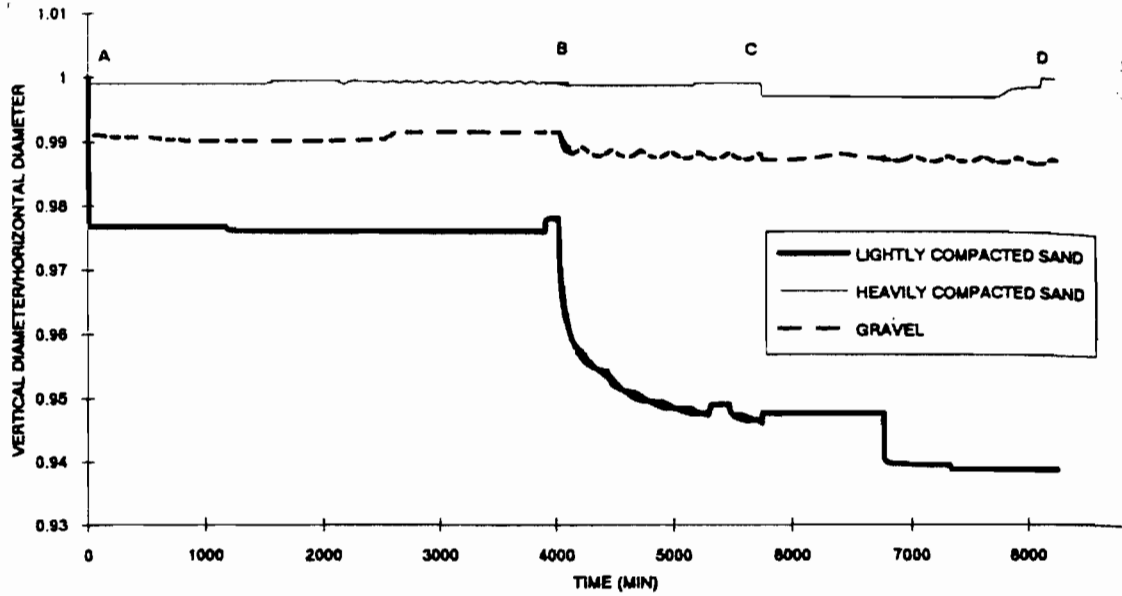
EOI: End of installation phase.

E70S: End of 70 kPa static pressure phase (load applied).

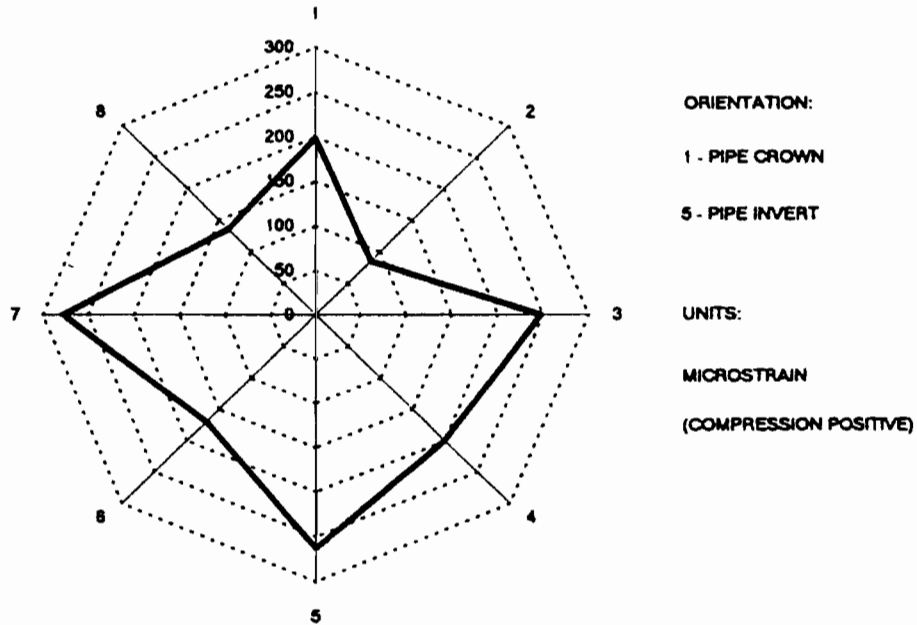
E70C: End of 70 kPa cyclic pressure phase (load released).

E140S: End of 140 kPa static pressure phase (load applied).

EOT: End of test (i.e., after load released).



Relative variation of vertical diameter to horizontal diameter for twin-wall pipe during laboratory test.



Strain distribution for a twin-wall pipe with uniform support from heavily compacted sand surround.

Figure 1.6.5 The Effect of Surround Conditions on the Pipe Deformation

**Table 1.6.3 Vertical Diametrical Strains Recorded in Field Test**

PIPE REF	EOI VDS(%)	EOT VDS(%)	AMPLITUDE (%)
A-S	1.01	3.24	0.10
A-G	0.70	2.17	0.10
B-S	0.92	4.32	0.13
B-G	0.51	2.12	0.15
C-S	0.78	2.32 <sup>1</sup>	0.13 <sup>2</sup>
C-G	0.71	2.45	0.11
D-S	0.66	1.91	0.07
D-G	0.36	1.48	0.09
E-S	0.48	1.42	0.09
E-G	1.58	3.72	0.11

Key

PIPE REF: As Table (1.6.2)

EOI VDS: VDS at end of installation phase.

EOT VDS: VDS at end of trafficking phase.

AMPLITUDE: Difference between transient and residual VDS during 1000<sup>th</sup> load cycle.

<sup>1</sup> VDS at 400<sup>th</sup> cycle (no further readings because of equipment problems).

<sup>2</sup> Amplitude at 400<sup>th</sup> cycle.

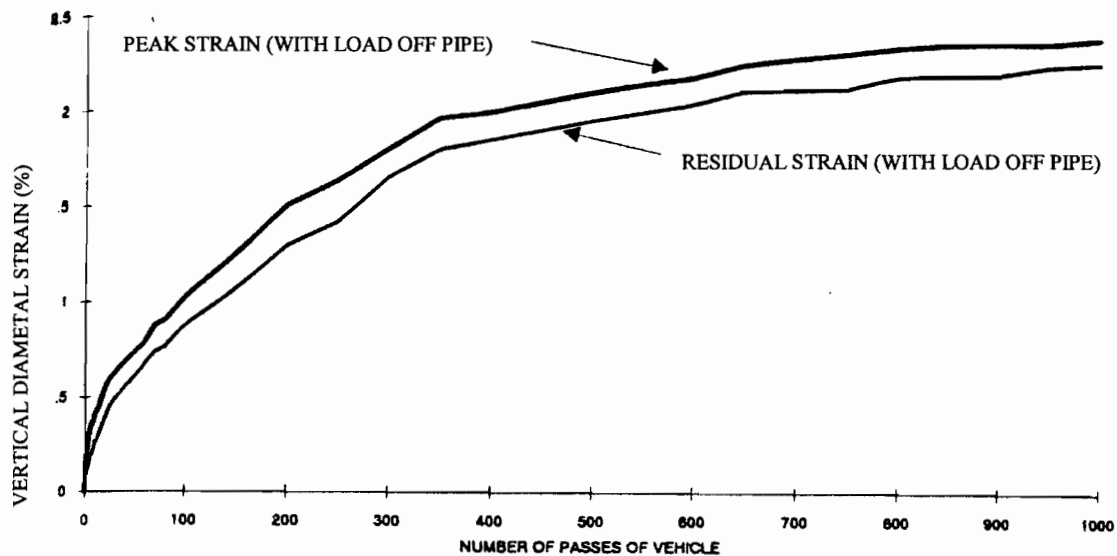


**Figure 1.6.6 Increase in Vertical Diametrical Strain for A Twin-Wall Pipe in A Trodden Sand Surround Under Repeated Loading in the Field Test**

**The Influence of Surrounding Soil on Flexible Pipe Performance, Rogers, C. D. F.,  
*Transportation Research Record 1129, 1987, pp. 1-11.***

The objective of the paper is to investigate the response of 160-mm-diameter, shallowly buried, unplasticized polyvinylchloride (uPVC) pipes to surface loading in full-scale tests. Surface loads of 5.5 and 7.0 tonnes were applied both statically and cyclically to simulate the loads applied by the rear wheel arrangement of a construction truck. The lower load was applied statically for 30 minutes, then removed for 45 minutes, and then cycled 150 times at approximately 12 cycles/minute, at the end of which pipe deformation was found to have stabilized.

### **Equipment and Instrumentation**

The first requirement was a facility of sufficient size to permit pipes to be tested free from boundary influences. A test pit was used with a testing area 3 m long, 2.1 m wide, and 1.9m deep and an inspection chamber at one end to allow access to the pipes during tests. Load was applied to the surface of the backfill through a 700-mm-diameter semiflexible platen by a hydraulic ram housed in a loading rig.

The backfill materials were concrete ballast (broad grading), washed quarry tailings, building sand (uniform), and reject sand (a silty sand). Each of the materials was used as a 50-mm bedding layer and uncompacted sidefill, and each installation was repeated with the exception of reject sand, which was a marginal material.

### **Experimental Results**

Preliminary tests were conducted to provide information on loading rates and duration, recovery periods, and boundary conditions. The tests showed that for installations subjected to large static surface loads for several days there was no apparent increase in the magnitude of pipe deformation under load, but that permanent deformation on removal of the load was significantly increased. It was also discovered that when a long recovery period of

24 hours or more was introduced during the cyclic load sequences, elastic recovery of the pipe was greater and was not wholly removed on the immediate application of the next cyclic load. Thus, accelerated cyclic loading is significantly worse than that applied at the more normal rates experienced at the site; extended static loads likewise provide a more severe case.

### The Influence of Soil Surround Type

The influence of sidefill type on the vertical diametral strain (VDS) of the pipe is demonstrated by the results of installations in which five uncompacted granular materials were used as sidefill and bedding, a summary of which is shown in Fig. 1.6.7. This figure shows the VDS values at various stages of the tests plotted using the point at which the pipe was positioned (PP) as the datum. Values thereafter are given at the end of installation (EOI), on application of the 55- and 70-kN loads (55 ON and 70 ON), and after they had been applied for 30 minutes (55 30 and 70 30). Values are also given after recovery at the end of the static load sequences (EO 55<sub>s</sub> and EO 70<sub>s</sub>) and the cyclic load sequences (EO 55<sub>c</sub> and EO 70<sub>c</sub>).

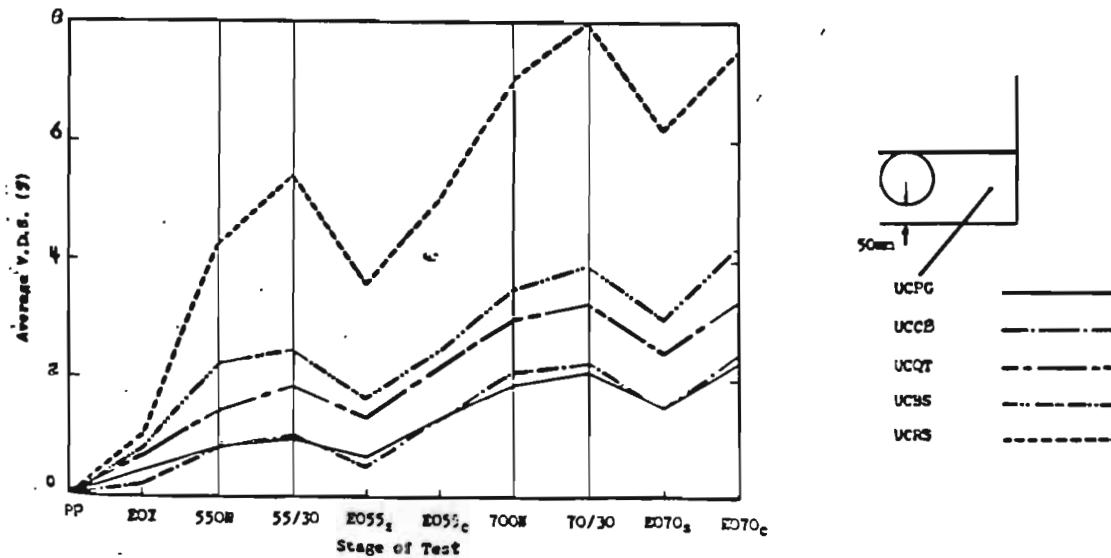


Fig. 1.6.7 Vertical Diametral Strains (VDS) for Five Sidefill Types in the Pit (Uncompacted Backfill / UCPG: Pea Gravel; UCCB: Concrete Ballast; UCQT: Quarry Tailings; UCBS: Building Sand; UCRS: Reject Sand)

## The Influence of Bedding

The influence of the bedding layer on pipe performance was investigated in three pit installations using uncompacted pea gravel sidefills with zero, 50-, and 100-mm-thick bedding layers (Fig. 1.6.8). These limited results indicate that where good support is afforded the performance of the pipe with the 50-mm-thick bedding layer is slightly better than that with the 100-mm-thick bedding. Omission of the bedding layer altogether leads to a worse case.

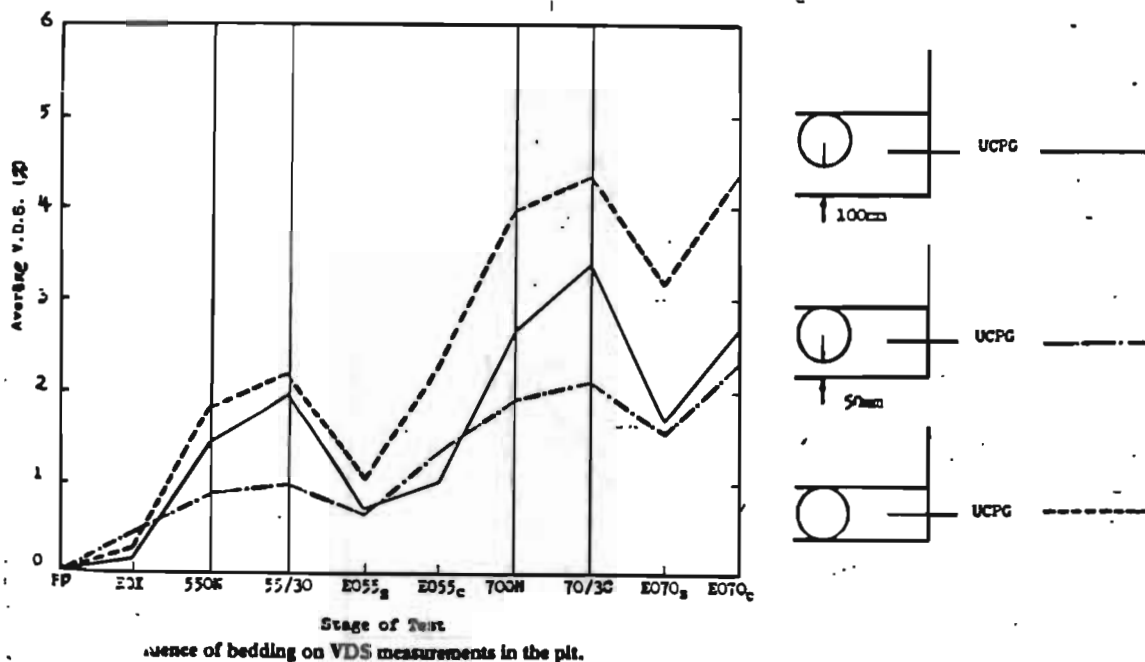


Fig. 1.6.8 Influence of Bedding on VDS Measurements in the Pit

## Compaction Fraction

British Standard<sup>1</sup> installation recommendations include the compaction fraction test, a method of fill selection, which relates the uncompacted and fully compacted heights of soil

<sup>1</sup> British Standards Institute, The Installation of uPVC Pipework for Gravity Drains and Sewers. British Standard BS-5955, Part 6, London, 1980

in a 250-mm-long, 160-mm-diameter tube. The difference between the two heights divided by the original height is known as the “compaction fraction” of the soil.

The average results of installations using five uncompact granular materials as sidefill and 50-mm-thick bedding were used for the comparison. The average compaction fractions were plotted against the VDS caused by the application of the 55-kN static load (55 ON) and the VDS at the end of the test (EOT), both related to the strains at the end of installation (EOI). These are presented in Figure 1.6.9, in which a clear relationship is apparent.

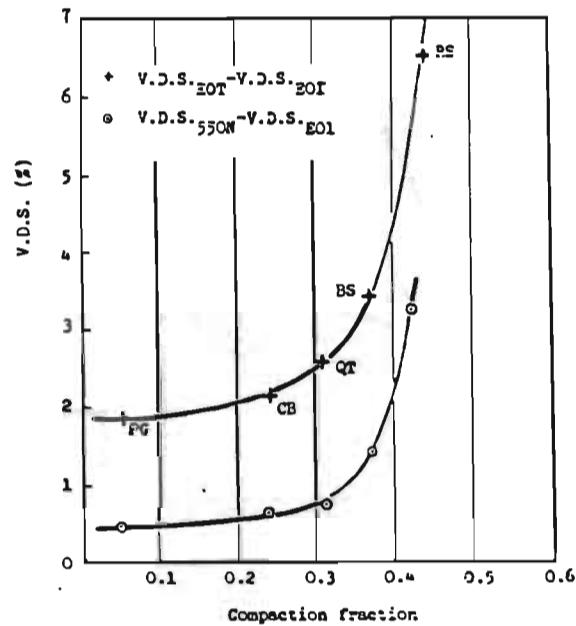


**Fig. 1.6.9 Influence of Empirical Soil Factor, Compaction Fraction**

### Conclusions

The better granular surrounds were more affected by the cyclic loads than the static loads, whereas the pipes in poorer soils were influenced more by the static load sequences. A bedding layer was found to be beneficial in reducing pipe deformation, although deformation increased as the bedding thickness increased from 50 mm to 100 mm.

**Some Observations on Flexible Pipe Response to Load, Rogers, C. D. F., *Transportation Research Record 1191, 1988, pp. 1-11.***

The objective of this paper was to investigate the performance of small-diameter uPVC pipes when buried at shallow depth. Surface load was applied to simulate the passage of site construction traffic.

The experiments were conducted in a reinforced box. The box was 750 mm long, 500 mm wide, and 550 mm deep, with a depth of cover to the pipe of 250 mm. Load was applied to the surface of the backfill through a 480-mm-diameter rigid platen, which represented the load caused by the rear wheel arrangement of a construction truck passing approximately 500 mm above the pipe crown.

Keuper marl (a silty clay having a liquid limit of 32 percent and a plastic limit of 19 percent) was used as backfill, the sidefill and bedding consisting of distinctly different soils. Pea gravel is a uniform rounded 10-mm gravel, concrete ballast is a well-graded aggregate of medium sand to medium gravel, and reject sand is a well-graded silty sand. The pipes were 160-mm diameter with a standard dimension ratio (diameter-wall thickness) of 41.

Three levels of compaction were used: no compaction, in which the material was dumped and leveled; light compaction, in which the sidefill was carefully compacted by foot after leveling; and thorough compaction by two passes of pneumatic tamper with a single head of 125 mm diameter.

Surface loads of 5.5 and 7.0 tonnes were applied both statically and cyclically to each experimental installation. The lower load was applied statically for 30 minutes, was removed for 45 minutes, and was then cycled 150 times at approximately 12 cycles/minute. After 150 cycles of load, the pipe deformation was found to have stabilized. The installation was allowed to recover for 2 hours before the process was repeated with the higher load, the final recovery period being at least 18 hours.

## Experimental Results

Fig. 1.6.10 shows the extrapolated pipe-wall strain profiles for the tests after the 55 kN static load was applied for 30 minutes. The curve for pea gravel was indicative of considerable action to relieve pressure in the top section of the pipe and consistently good support around the pipe. In uncompacted (UC) pea gravel sidefill, a maximum tensile strain occurred at the crown and a maximum compressive strain occurred at the shoulder (45°). Fig. 1.6.11 shows the curves for the tests using uncompacted pea gravel (UCPG) and well-compacted silty clay (WCSC) in different configurations around the pipe.

The pipe deforms approximately elliptically when surrounded by a relatively poor soil and load is applied to the soil; but the pipe-wall strain profile will tend to a V shape (Fig. 1.6.12 a). This is caused by the lateral restraint of the soil, or passive pressure developed therein, which includes a greater compressive strain in the pipe springings.

Where a buried pipe is bedded in a good quality stiff soil up to at least its horizontal axis and a vertical load is applied to the soil surface, the pipe will tend to deform to a heart shape, in which the pipe crown flattens and the shoulders become relatively more curved with a roughly even change in curvature below the shoulders (Fig. 1.6.12 b). Such a deformation is accompanied by high tensile wall strain at the pipe crown and high compressive strains at the shoulders. Diametrically opposite behavior can occur in cases where the soil around the haunches is poor and that above it is of good quality (Fig. 1.6.12 c).

In cases in which exceptionally good lateral restraint is provided at the pipe springings, deformation will tend to be square shaped, in which the pipe and invert flatten and the shoulders and haunches take up a smaller radius of curvature, the springings remaining largely unstrained (Fig. 1.6.12d). This behavior typically occurs only in cases in which thorough compaction is applied to the sidefill at the level of the pipe springings, thereby creating a locally stiff medium.

The description by Howard<sup>1</sup> of rectangular deflection is consistent with the square-shaped deflection referred to previously. In this respect, rectangular shape is perhaps a better description because the pipe undergoes flattening at the crown and invert, with no change in curvature (i.e., negligible strain) at the springings.

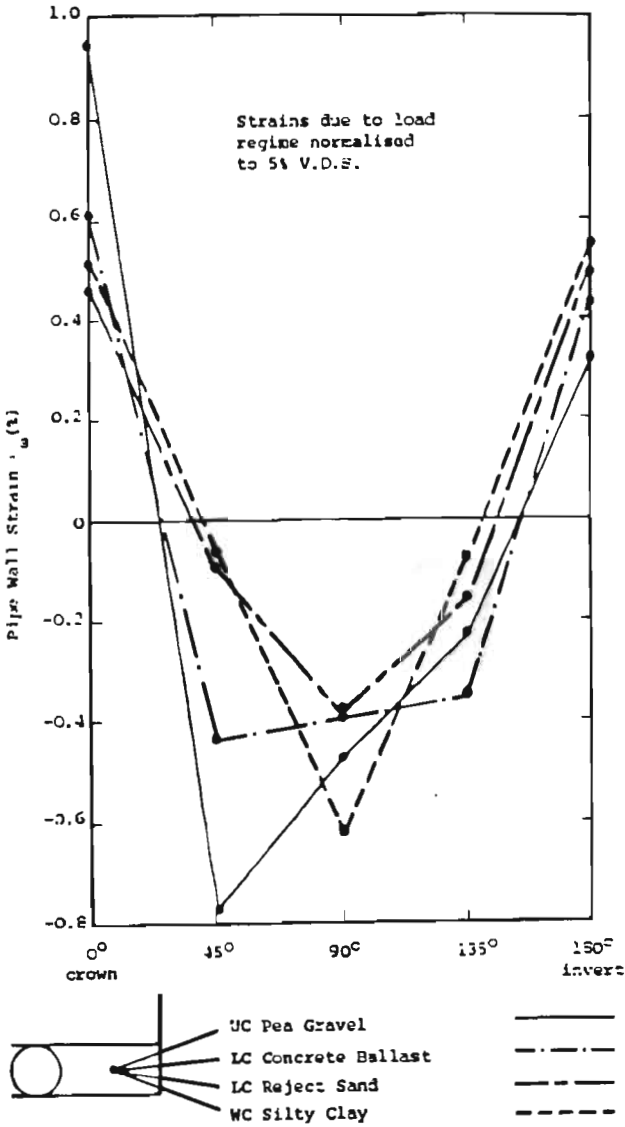


**Fig. 1.6.10 Pipe-Wall Strain Profiles Under 55 kN Static Load Using Four Sidefill Materials**

<sup>1</sup> Howard, A.K., Laboratory Load Tests on Buried Flexible Pipes, Progress Report No. 5, GRP, PE and PVC, USBR Report No. REC-ERC-73-16, Bureau of Reclamation (now Water and Power Resources Service)

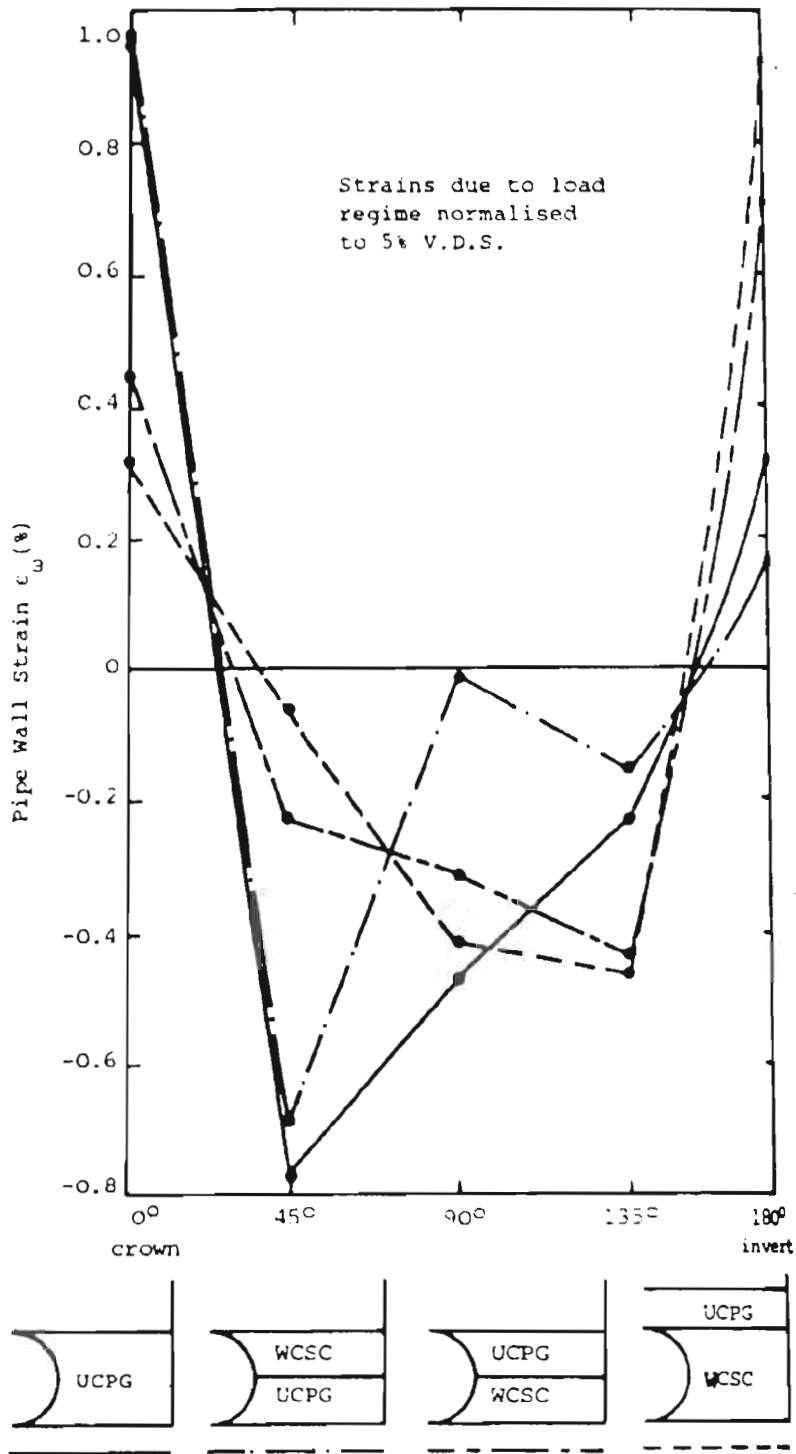


**Fig. 1.6.11 Pipe-Wall Strain Profiles Under 55 kN Static Load Using Four Combinations of Gravel and Clay**

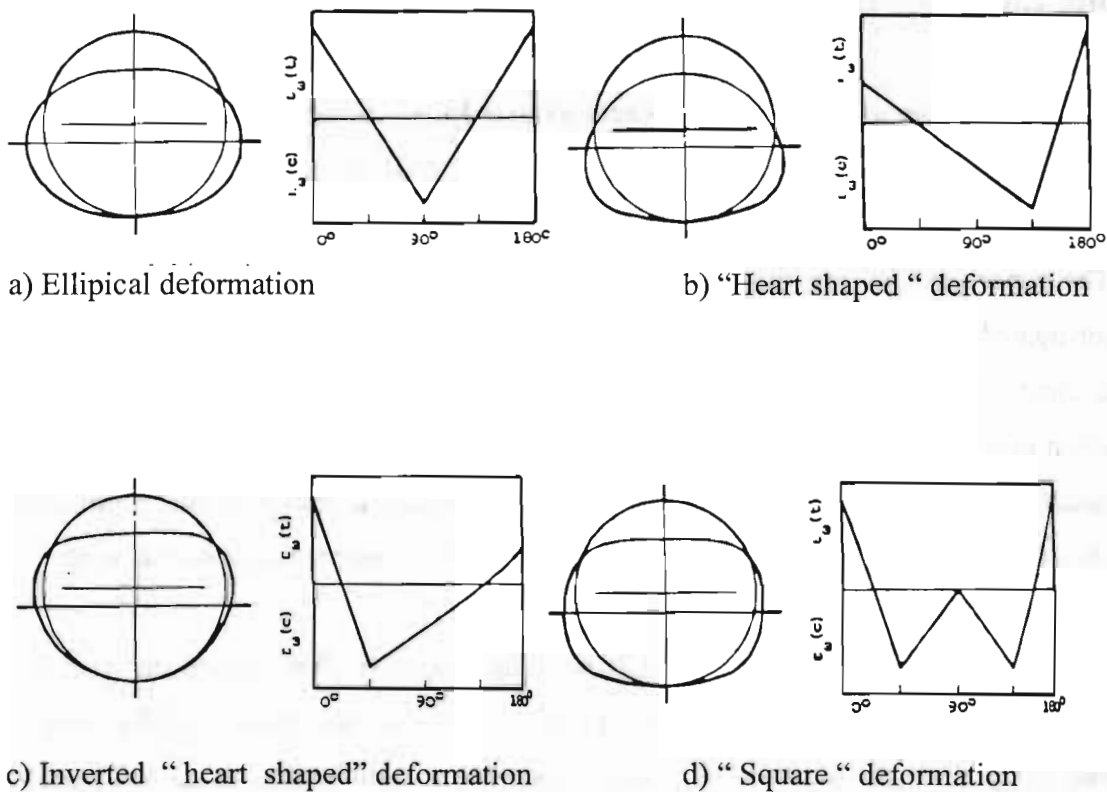


**Fig. 1.6.12 Types of Deformation and Associated Strain Profiles**

### Conclusions

The assumption of elliptical deformation in methods of prediction of pipe deformation is likely to be valid in cases where the pipe is subject to predominantly cyclic load or where the surrounding soil is not relatively stiff. Where applied load is predominantly static, the assumption could prove to be greatly in error. The assumption of elliptical deformation in experimental work should be avoided and measurement of pipe wall strain or wall movement, or both, should be made all around the circumference rather than solely across the vertical and horizontal axes.

## 1.7 Finite Element Analysis

**Nonlinear Finite Element Analysis for Thermoplastic Pipes, Zhang, C. and I. D. Moore.**  
*Transportation Research Record 1624, Paper No. 98-0701, 1998, pp. 225-230.*

The paper presents constitutive models for two HDPE materials, a plain HDPE pipe and a corrugated HDPE pipe. The models are used for predictions of plain HDPE pipe response under parallel plate loading and a section of corrugated HDPE pipe under hoop compression in a soil cell. The results of the finite element model are then compared with the experimental measurements. The effects of pipe response due to material and geometrical nonlinearity (large deformation and large strain) and backfill properties are also included.

Two nonlinear constitutive models were developed to characterize the nonlinear and time-dependent behavior of HDPE. The uniaxial nonlinear viscoelastic (NVE) model is formulated using a simple mechanical analogy featuring a combination of an independent spring with six Kelvin elements in series. The stiffness of the spring and the viscosity of the dashpot are defined as functions of stress. Creep data were used to calibrate the material functions.

The viscoplastic (VP) model is developed on the basis of the unified theory in which creep strain and plastic strain are described using the concept of inelastic strain. A state variable defined as a function of inelastic work and inelastic strain rate was introduced to describe the strain-hardening and rate dependent material behavior of HDPE. Data from constant strain rate tests were employed to determine the state variable and material parameters.

### **Analysis of plain HDPE pipe under parallel plate loading**

Both the NVE and VP models were used in the finite element simulation for the parallel plate tests. Pipe test segments 30 mm (1.2 in) long were cut from a thick plain HDPE pipe with an external diameter of 322 mm (12.7 in) and a wall thickness of 31 mm (1.2 in). During the tests a polytetrafluoroethylene (Teflon) sheet was used at the interface between the pipe wall and the steel plate to reduce friction. A plane stress condition was assumed for the finite element analysis. Only a quarter of the pipe was modeled using six-noded triangular elements due to symmetry of the problem.

Fig. 1.7.1 presents finite element predictions for the first test using both the NVE and VP models. The NVE and VP predictions for the second test are shown in Fig. 1.7.2. The VP and NVE predictions of relaxation response for the pipe fixed at 80 percent diameter are shown in Fig.1.7.3.

### **Analysis of corrugated HDPE pipe under hoop compression**

The corrugated HDPE pipe was tested under hoop compression by controlling the air pressure applied to a bladder placed between the backfill soil and the steel cell. The pipe was loaded by applying bladder pressure in 30-kPa (4.35 psi) increments. The finite element model was used to analyze the response of a corrugated HDPE pipe under axisymmetric compression.

The finite element predictions of the radius decrease vs. air bladder pressure are shown in Fig. 1.7.4. The VP prediction of the axial strains at both the valley and the crown of the corrugation are presented in Figs. 1.7.5 and 1.7.6 respectively.

The finite element model is capable of predicting the nonlinear time-dependent response of a pipe segment under bending and hoop compression for a range of load histories. The performance of the VP model is superior providing more accurate predictions.

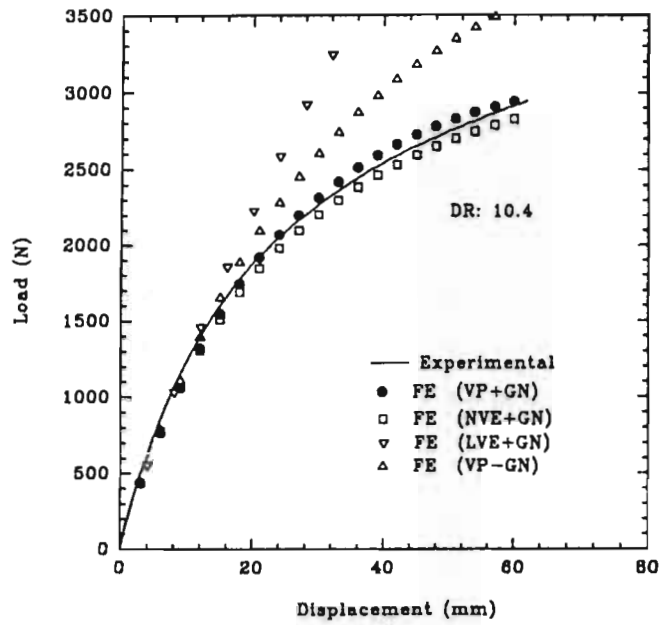


**Fig. 1.7.1 Load Deflection Response for Plain Pipe at 12-Mm/Min Vertical Deflection Rate Until 20 Percent Decrease in Vertical Diameter: Measurements and Finite Element Predictions**

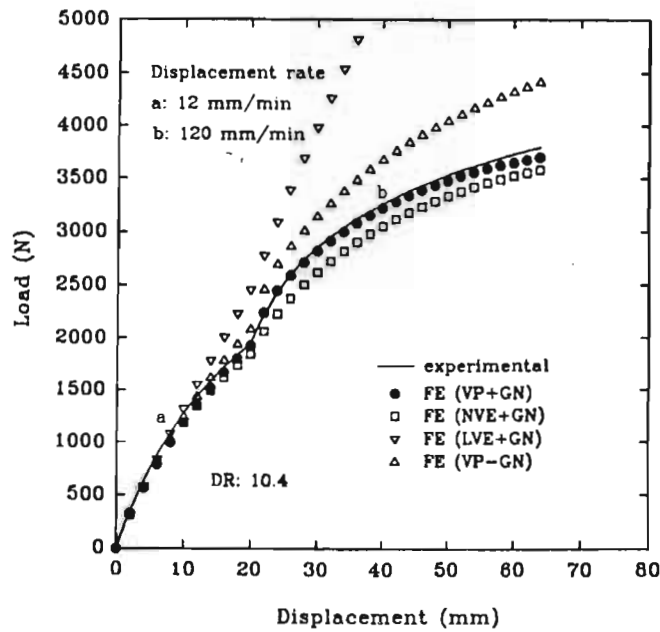


**Fig. 1.7.2 Load Deflection Response for Plain Pipe at Two Different Rates of Vertical Diameter Decrease: Measurements and Finite Element Predictions**

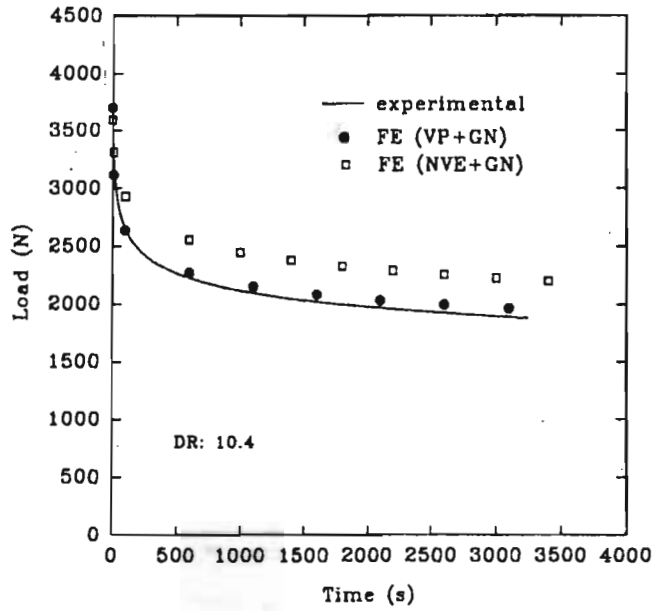


**Fig. 1.7.3 Load Relaxation with Time for Plain at Fixed Vertical Deflection after Abrupt Change Deflection Rate: Measurements and Nonlinear Finite Element Predictions**

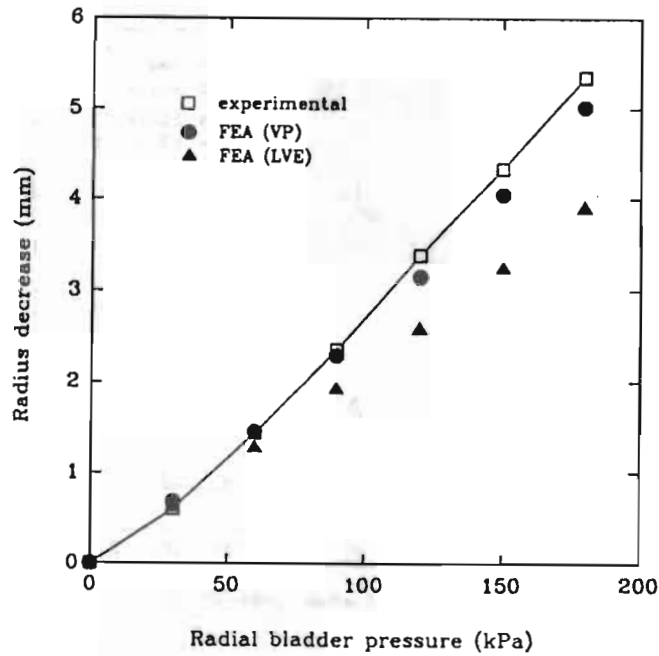


**Fig. 1.7.4 Radius Decrease Versus Air Bladder Pressure: Test Measurements and Finite Element Predictions**

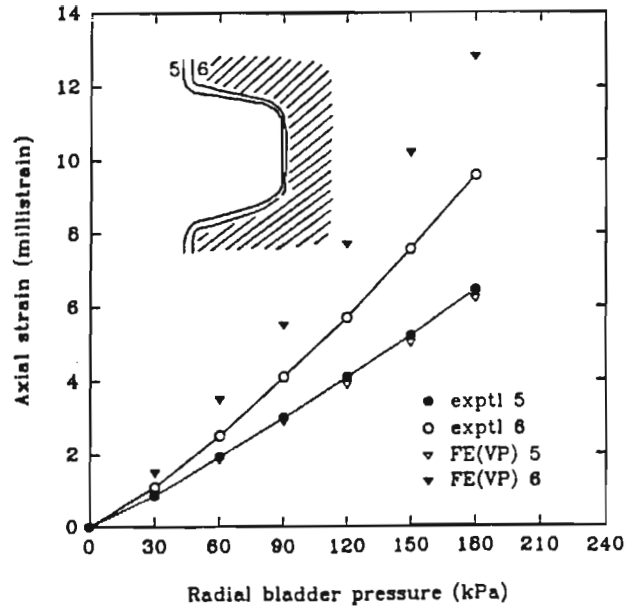


**Fig. 1.7.5 Axial Strain at Corrugation Valley: Finite Element Estimates and Experimental Measurements**

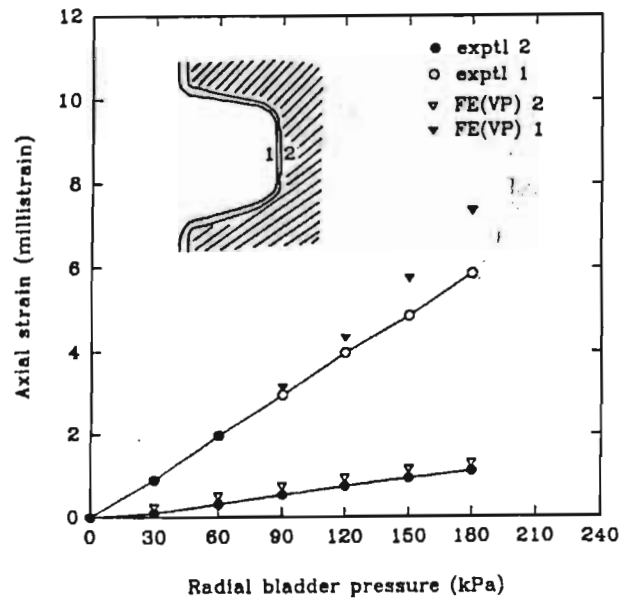


**Fig. 1.7.6 Axial Strain at Corrugation Crown: Finite Element Estimates and Experimental Measurements**

**Three-Dimensional Analysis of Flexible Circular Culverts, Moore, I.D., and Brachman, R.W., ASCE Journal of the Geotechnical Engineering, Vol. 120, No.10, 1994, pp.1829-1844.**

The objective of this paper was to develop an efficient three-dimensional finite element analysis for determining the long-term culvert response to vehicle loads. The limitations of this approach are evaluated by comparing the analytical results with the test data for the response of shallow buried culverts.

### Three dimensional analysis

Three-dimensional finite-element analysis was used to estimate the response of a shallow buried corrugated steel culvert to vehicle loads. Fig.1.7.7 shows a typical shallow buried culvert responding to tire pressures applied at various locations on the ground surface.

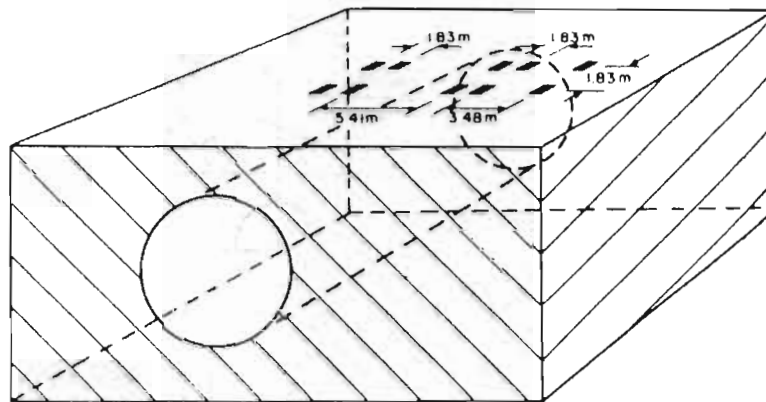


**Fig.1.7.7 Shallow Buried Culvert with Prismatic Geometry and Location of Tire Loads from Vehicle on Ground Surface**

A three-dimensional finite-element procedure was described that uses two-dimensional finite-element meshes in the xy plane and Fourier transform analysis in the direction of the culvert axis z. The analysis successfully predicted stresses for a three-dimensional problem with known solution. It was then used to estimate thrusts in a real culvert for which field-test data exist.

Fig.1.7.8 shows four perspectives of the buried pipe responding to surface loads, each illustrating a different feature of the analytical process.

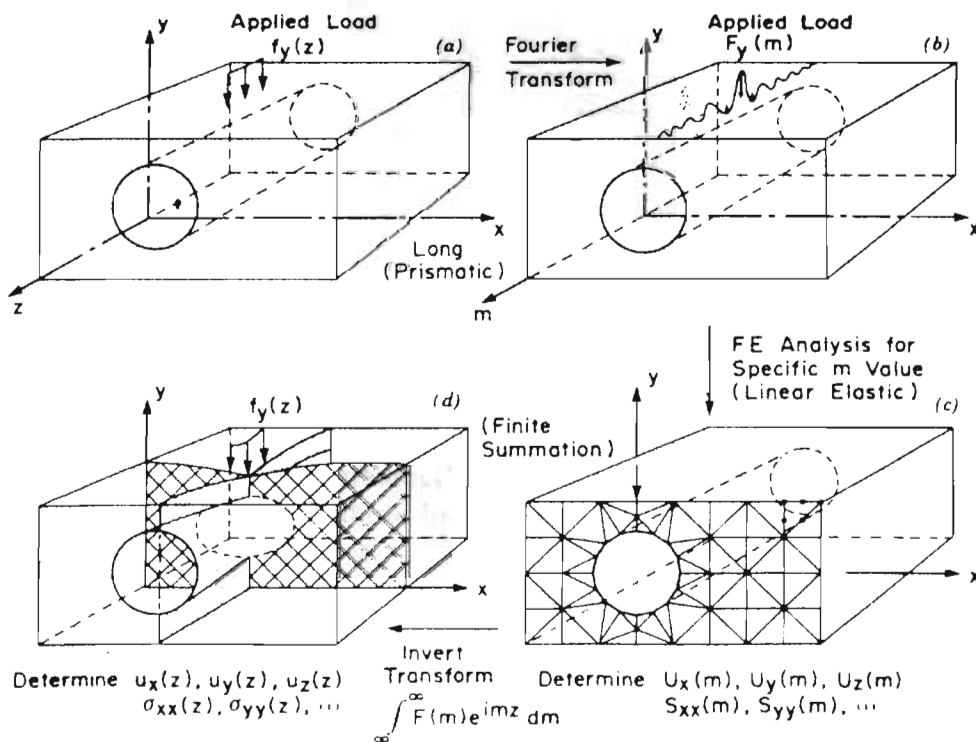
The loads from each individual tire or set of tires on each end of each axle of the test vehicle is modeled in the three-dimensional finite - element mesh. Fig. 1.7.9 shows the distribution of the axle loads for the vehicle, as they are applied in the direction of the road centerline. The load function is given by

$$F_c(m) = \frac{1}{m} [\sin(mz_s + mw) - \sin(mz_s)]$$

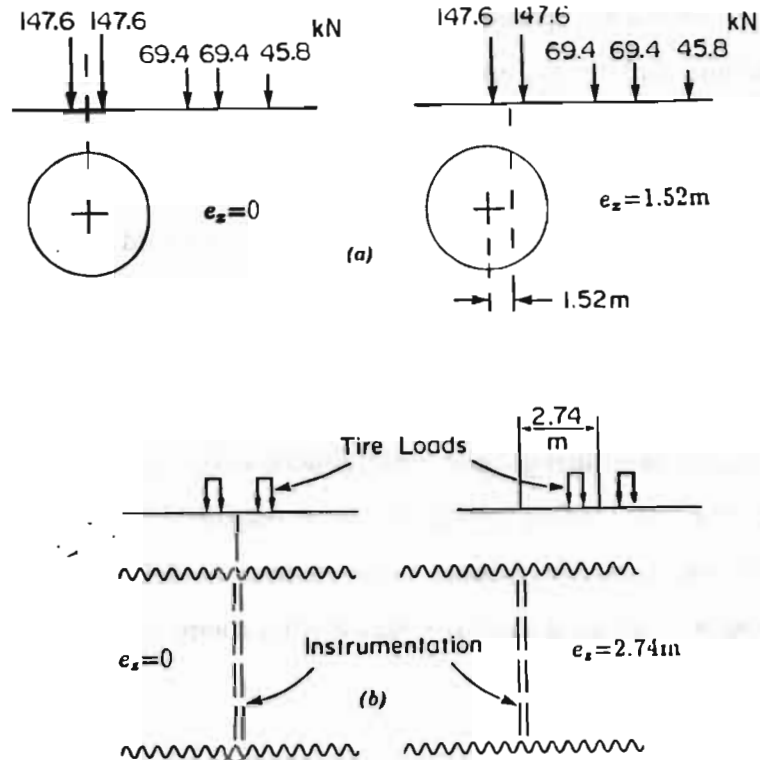
$z_s$  = a distance from the vehicle centerline

$m$  = the transform variable of Fourier series

$w$  = load patch of width (0.6 m)

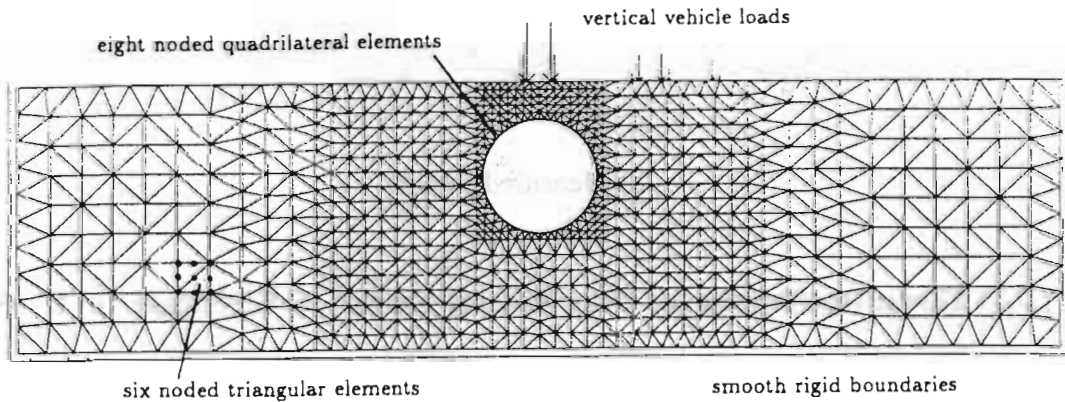


**Fig.1.7.8 Semianalytic Finite-Element Model for Shallow Buried Culvert**



**Fig.1.7.9 Axle and Wheel Loads under Test Vehicle: (a) x Direction, Eccentricity,  $e_x$  (b) z Direction, Eccentricity,  $e_z$**

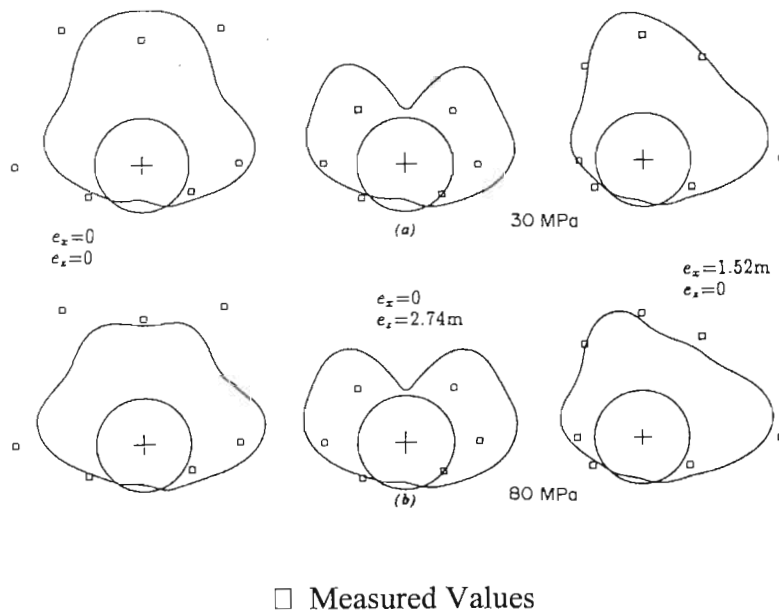
Fig. 1.7.10 shows the finite-element mesh use to analyze the Deux Rivieres structure. There were 1,700 six-noded triangles used to model the soil, and 64 eight-noded continuum elements were used to model the structure.



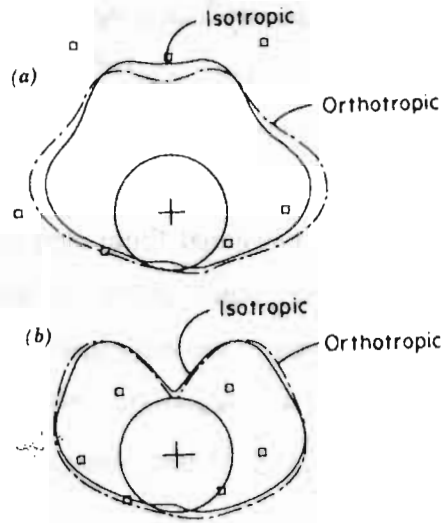
**Fig.1.7.10 Finite Element Mesh to Model Deux Rivieres Culvert**

Fig. 1.7.11 shows the measured and calculated thrust values. The comparison of theoretical predictions with measured response demonstrated that the general pattern of thrust distribution was predicted well, with the measured thrust variation due to changes in vehicle location being estimated successfully. Thrust at locations some distance down the culvert axis was found to be overestimated. Thrust estimates were found to be somewhat influenced by the modulus of the soil, although large adjustment to the soil modulus had reasonably small effect.

Analysis undertaken using orthotropic structural theory revealed that it may not be essential to model the low bending stiffness of the corrugated plate in the axial direction (Fig. 1.7.12). However, the three-dimensional finite-element model assumes the culvert is very long, and this appears to produce excessive thrust at locations away from the vehicle load.



**Fig. 1.7.11 Thrust Distribution for Deux Rivieres Culvert (a)  $E'=30\text{mpa}$  (b)  $E'=80\text{mpa}$**



**Fig. 1.7.12 Effect of Orthotropic Structural Theory on Thrust Predictions  $E_x=0$  (a)  $E_z=0$ ; (b)  $E_z=2.74$**

The improvements to thrust estimates that result from the use of three-dimensional analysis were demonstrated through comparisons with two-dimensional finite-element analysis. The results of the present study imply that thrust is not very sensitive to soil modulus (See Fig. 1.7.13), but quantities such as deflection and circumferential moment may be sensitive and the field-test data should include careful investigation of the soil conditions.

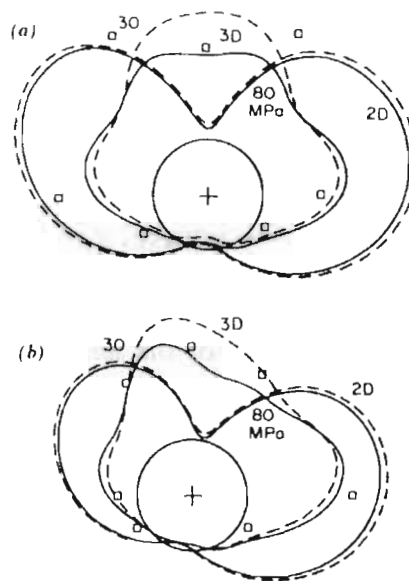


**Fig. 1.7.13 2D and 3D Thrust Predictions  $E_z=0$  (a)  $E_x=0$ ; (b)  $E_x=1.52m$**

**Three Dimensional Response of Deeply Buried Profiled Polyethylene Pipe, Moore, I.D., Geotechnical Research Center Report, GEOT-6-95, University of Western Ontario, London, ON, Canada, N6A 5B9, February 1995.**

The report presents a three dimensional finite element stress analysis to examine the response of profiled polyethylene pipe under various burial conditions. Radial, circumferential and axial normal stresses were examined for three pipes of different diameter buried at various depths in different soil materials. The implications for polyethylene pipe design are briefly examined in relation to arching, time-dependent pipe response and tensile rupture.

It was found that circumferential stresses are predominantly compressive, and can be predicted reasonably well using conventional two dimensional analysis. Tensile axial stresses develop in the inner liner of the pipe, which cannot be evaluated using three dimensional analysis. These tensions are greatest at the springline. This performance limit has been evaluated for three lined corrugated PE pipes under deep burial. The pipes considered have peak tension not more than half the AASHTO allowable value at 22-m (73.33 ft.) burial depth in very good quality (SW95) backfill material or 11m depth in the same soil at lower density (SW85).

Fig. 1.7.14a shows the pipe-soil system in which a circular pipe with annular corrugation and smooth internal liner is deeply buried within an earth embankment. The three dimensional nature of the problem is readily apparent given the geometry of the pipe profile ( Fig.1.7.14b). The stresses act in the circumferential  $\sigma_{tt}$ , radial  $\sigma_{rr}$  and axial  $\sigma_{zz}$  directions. Fig. 1.7.15 shows the finite element mesh used for the analysis in the vicinity of the 460-mm (18.11-ft.) diameter pipe. Six noded linear strain triangles are used to model the pipe as well as the soil material surrounding it. Figs.1.7.16-18 show contours of  $\sigma_{tt}$ ,  $\sigma_{rr}$ ,  $\sigma_{zz}$  for the pipe and the soil in the immediate vicinity of the pipe.

Stress in the section most distant from the pipe axis increases as one would expect at the crown/invert position, but remains close to the neutral axis values at the other two pipe locations. These extreme fiber stresses are less affected by bending than would be expected from calculations based on two dimensional analysis; it appears the mass of soil adjacent to the pipe at this location is acting with the HDPE material to carry much of the bending stress.

A stress concentration occurs at the point where the corrugation section and lining intersect. Stresses in the sections of lining spanning the corrugation decrease below the neutral axis values at each point around the pipe circumference.

The radial stresses are all relatively low. The tensile stresses develop in the pipe liner. These occur specifically as a result of local bending that develops. The tensions in the liner that develop close to the liner-corrugation junction represent an important performance limit for lined corrugated pipe under very deep burial.

Stresses within the pipe decrease as soil stiffness is increased, this is consistent with well known trends for buried flexible and rigid pipe. Pipe deformations decrease as backfill stiffness is increased, this is also consistent with the expectations for the flexible pipe where the pipe deformations are predominantly controlled by the soil, not the pipe itself.

Stresses in the pipe increase with burial depth, but at a rate, which is less than linear. As soil depth increases the soil stiffness also increases, so that additional 'positive arching' somewhat reduces the resulting loads. The only tensile circumferential stresses, which occur, develop at the crown of pipes deeply buried in the stiffer backfill, and the magnitude of these tensions is quite small.

Tensile radial stresses do develop in the pipes, but these are of relatively low magnitude except at the springline of the pipe deeply buried with lower density backfill. Axial tensions  $\sigma_{zz}$  develop in the liner of all of the pipes and are highest at the springlines.

The elastic continuum solution leads to the conclusion that decreases in effective HDPE modulus are beneficial. The stresses and pipe deformation are not greatly affected by the embankment material. The pipe diameter is not a particularly significant parameter.

The analysis reported in this paper indicated that at the springline of an 460mm diameter stormwater pipe buried 11m within dense granular backfill, a local axial tension of about 1.7 MPa can develop. As burial depth increases and/or backfill stiffness decreases the magnitude of this local axial tension rises. The zone of tension is located within the liner, and the corrugated component of the pipe profile is essentially unaffected.

Using the AASHTO short term tensile strength of 20.7 MPa (3000psi) for comparison with short term values (i.e. values calculated using short term HDPE modulus) and a long term tensile rupture stress of 6.2 MPa (900psi) for comparison with the long term stress values (i.e. values calculated using long term HDPE modulus), it appears that the pipes considered in this report have local stress not more than half the allowable value at 22m burial in very good quality (SW95) material or 11m in the same soil at lower density (SW85).

The analyses reported here suggest that increases in allowable burial depths may be possible for these profiled HDPE pipes in relation to the expected performance for deflection and local bending stress. This is conditional on careful construction of the soil envelope, sufficient soil quality to maintain stability against buckling and successful comparisons with field data to confirm the validity of the idealized soil-structure interaction model used in this study.

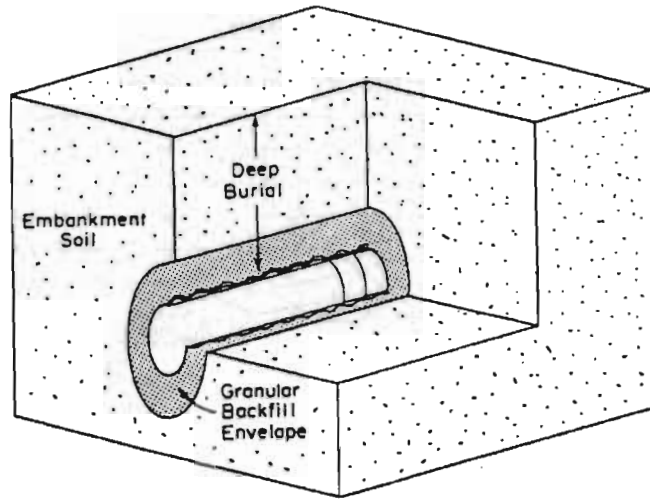


**Fig. 1.7.14a Exposed View Showing the Deeply Buried Pipe**

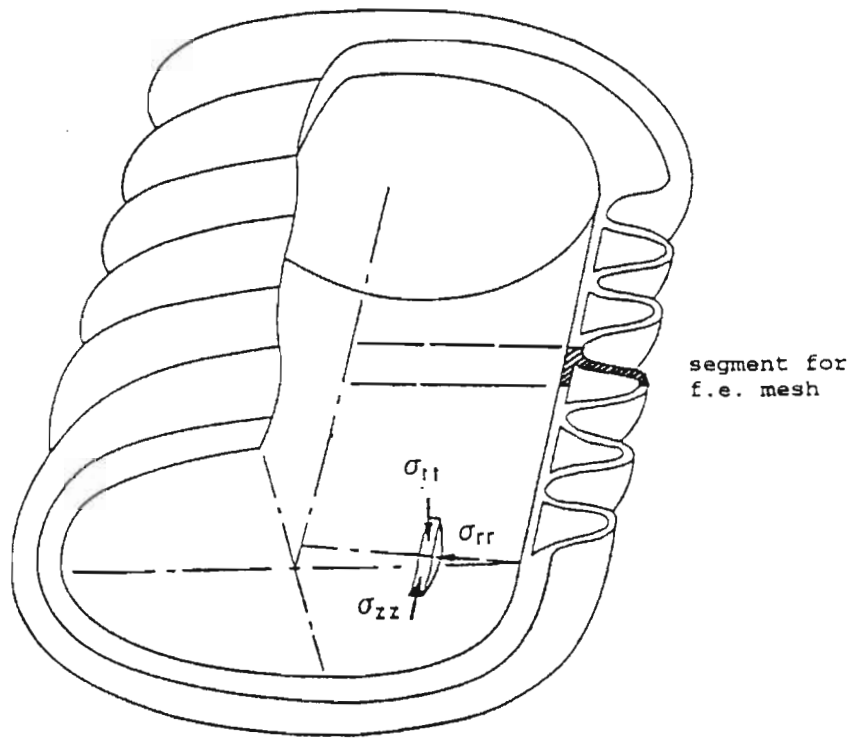


**Fig.1.7.14b Detail of the Pipe with Annular Corrugation and Smooth Internal Liner**

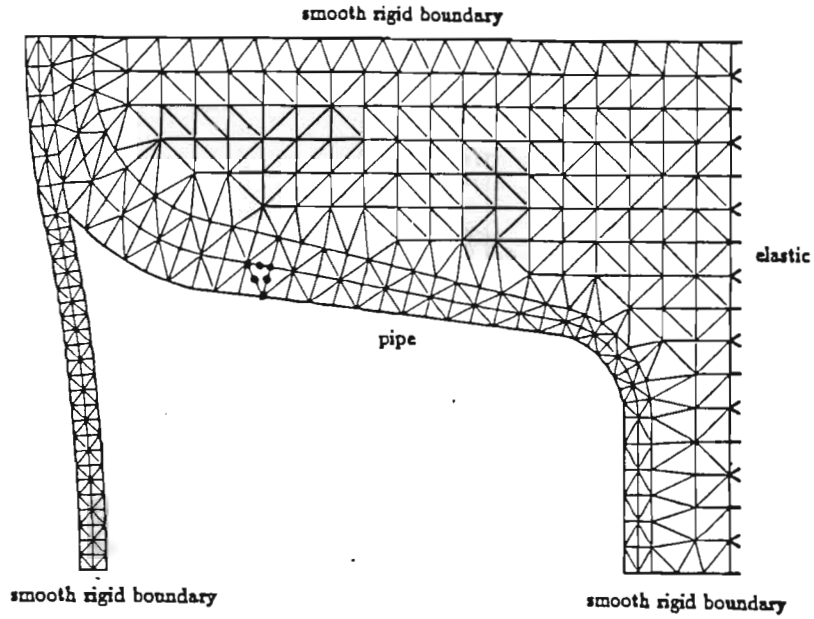


Fig.1.7.15 Finite Element Mesh Close to the 460mm Diameter Pipe

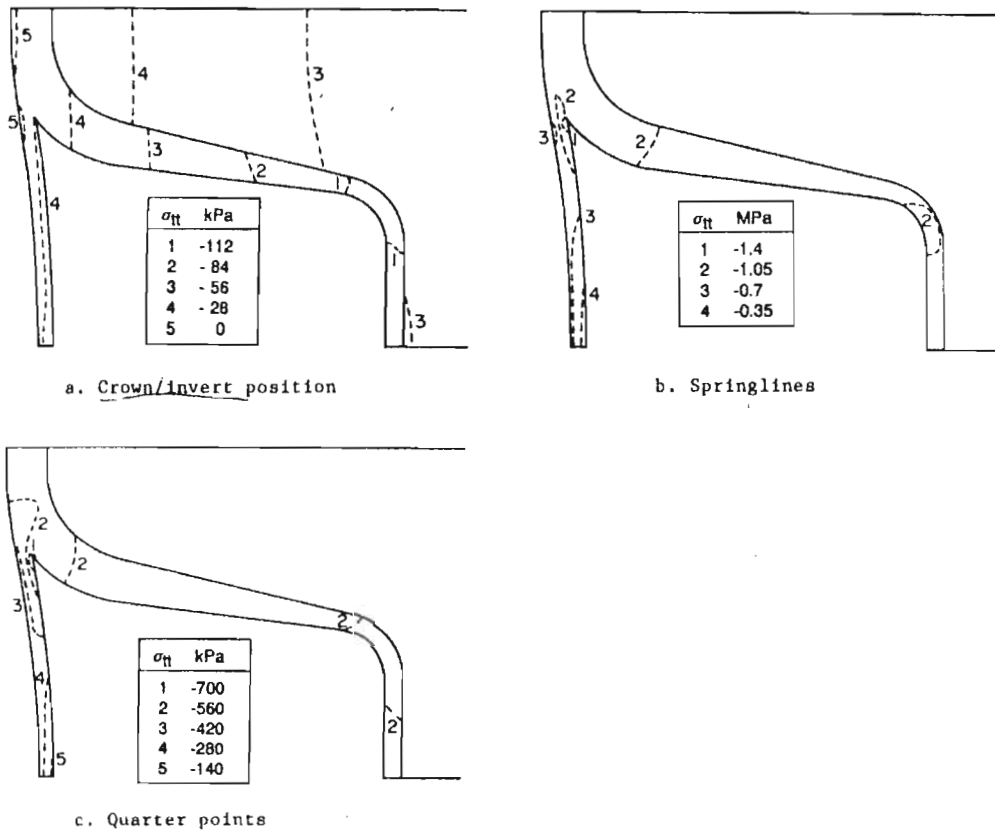
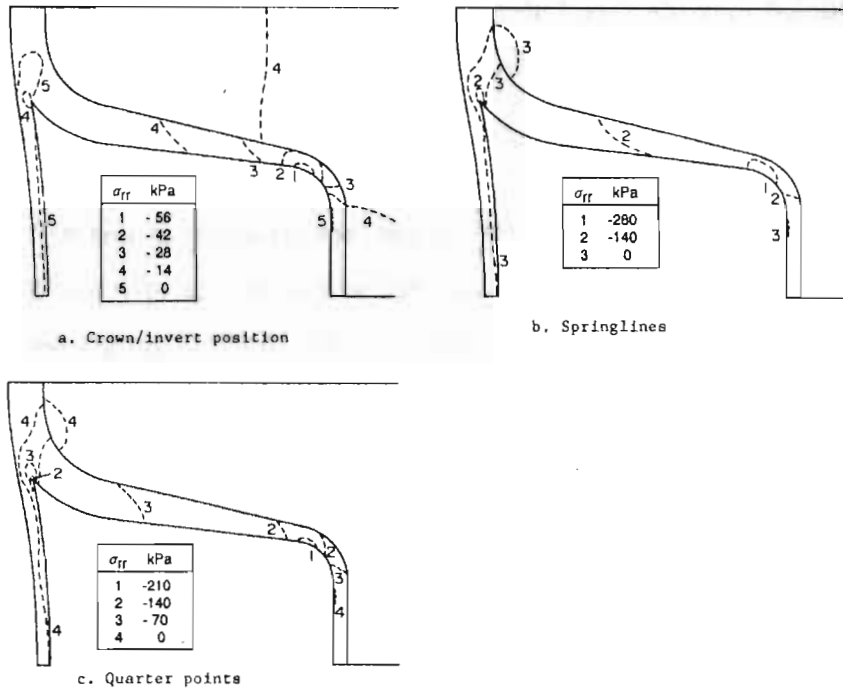
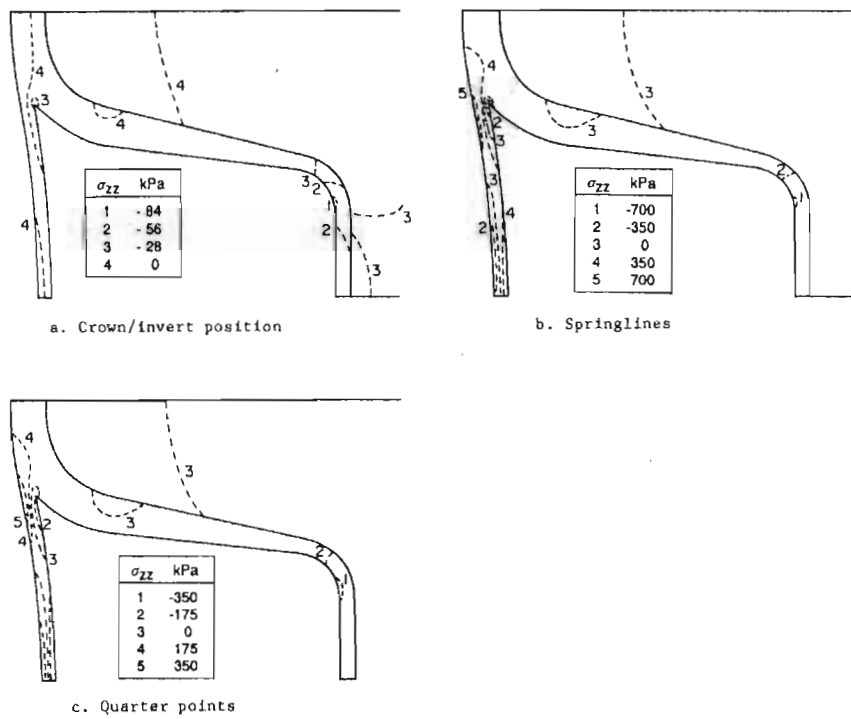


Fig.1.7.16 Circumferential Pipe Stresses at Crown/Invert, Springlines and Quarter Points



**Fig.1.7.17 Radial Pipe Stresses at Crown/Invert, Springlines and Quarter Points**



**Fig.1.7.18 Axial Pipe Stresses at Crown/Invert, Springlines and Quarter Points**

**Analysis of Buried Flexible Pipe Using CANDE and ANSYS**, Suleiman, M. T., Wipf, T. J., Klaiber, F. W., and Lohnes, R. A., *Transportation Research Board 81<sup>st</sup> Annual Meeting*, Jan. 2002, pp. 19.

The main objective of the theoretical analyses presented in this paper is to compare the results of CANDE with small and large deflection theories of ANSYS for the case of geostatic applied loads and develop a code using the ANSYS programming language to model the Duncan Chang soil model.

### Comparison of ANSYS and CANDE

A polyethylene (PE) pipe 610 mm (24 in.) in diameter with four different soil covers (1.5, 3.05, 4.6, and 6.1m) (5, 10, 15, and 20 feet) above the pipe springline was modeled using CANDE and small and large deformation analyses with ANSYS. In these models, the soil was assumed to be linear elastic material, no interface elements were used between the soil and pipe elements, and the pipe was assumed elastic with a smooth “no corrugation” uniform thickness. The soil and pipe properties used are given in Table 1.7.1

**Table 1.7.1 Pipe and Soil Properties Used in the Analysis**

Property	CANDE Plastic Pipe Properties	PE Pipe Property	Elastic Soil Properties
E (kPa)	11,024,000	757,900	6,890
$\mu$	0.3	0.45	0.35
T (mm)	12.7*	29.0	-----

\* assumed value.  
Soil  $\gamma = 1,920 \text{ kg/m}^3$

Fig. 1.7.19 shows the vertical deflection for different points on the pipe circumference for various depths of soil cover above the pipe springline. The three different analyses showed good agreement for the range of soil covers. Large deflection analysis using ANSYS has a very small effect on the pipe behavior.

The results from ANSYS utilizing the Duncan Chang model were compared with those from CANDE analysis for a pipe soil system. With the Duncan Chang model, Fig. 1.7.20 shows vertical deflection both at the crown and invert using Duncan Chang model for both CANDE and ANSYS. Fig. 1.7.21 shows the vertical deflection percent using CANDE and small and large deflection theories of ANSYS. Both ANSYS and CANDE have a good agreement for all soil covers with a maximum error of about 10%. Increasing the fill height from 4.6 to 6.1m (15 to 20 ft) increases the effect of large deflection theory on soil height. For these two cases of soil cover, ANSYS large deflection theory shows better agreement with the results from CANDE. However, the results from ANSYS small deflection theory differ more from those based on CANDE.

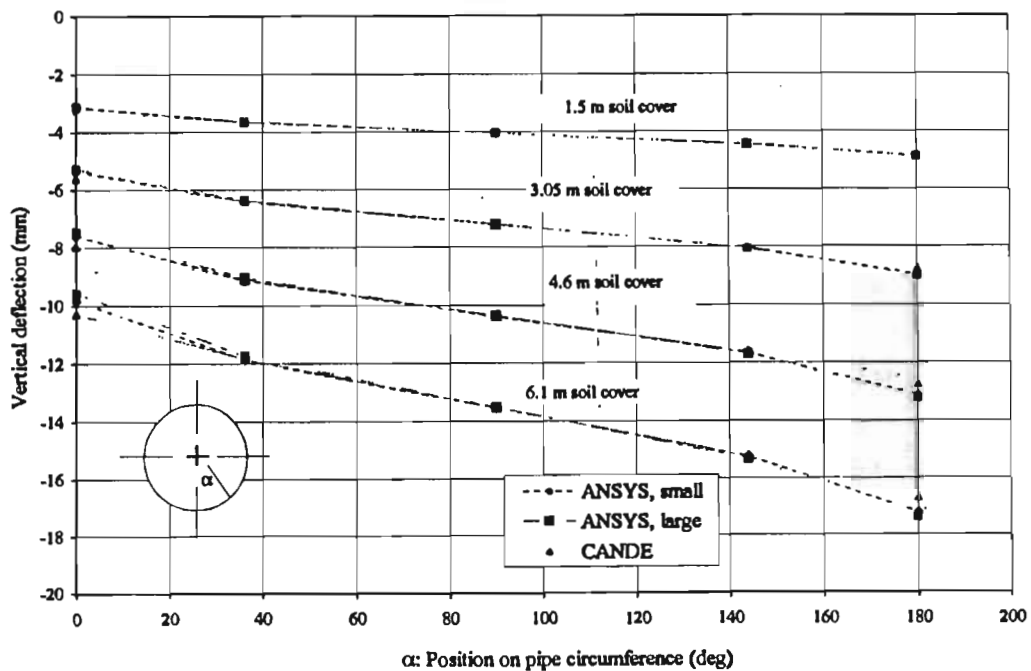


**Fig. 1.7.19 PE Pipe Crown Vertical Deflection with Respect to Position on Pipe Circumference for Different Height of Soil Covers (1 foot = 0.305m, 1 inch = 25.4mm)**

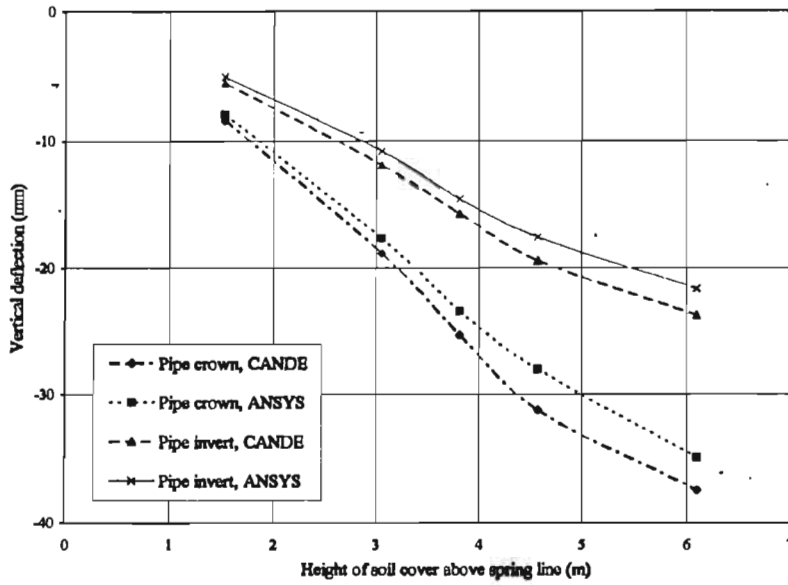


Fig. 1.7.20 PE Vertical Deflection using Duncan Chang Model for both ANSYS and CANDE (1 foot = 0.305m, 1 inch =25.4 mm)

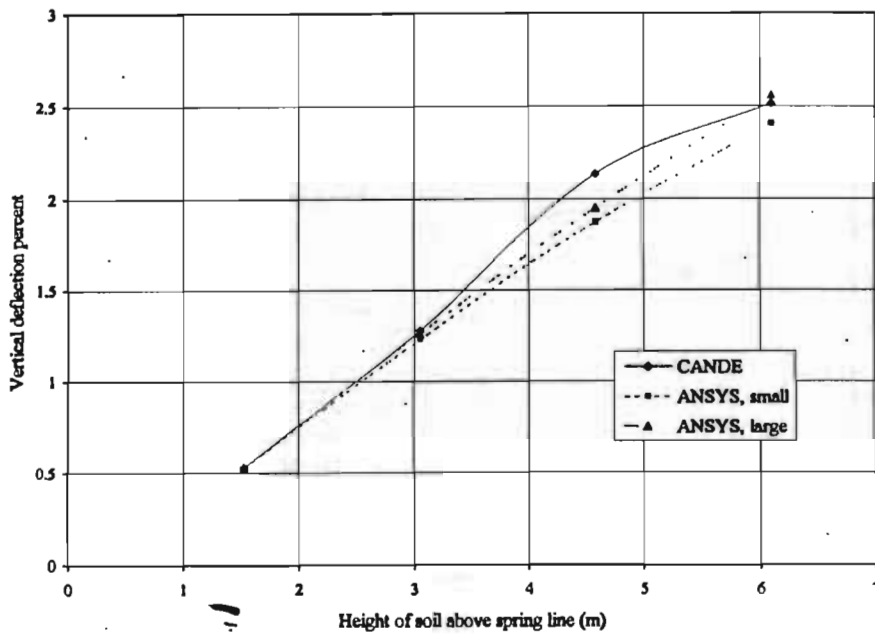


Fig. 1.7.21 PE Vertical Deflection Percent using Duncan Chang Model for both ANSYS and CANDE (1 foot = 0.305m)

## 1.8 Time-Dependent Behavior

**Time-Dependent Deflection of Thermoplastic Pipes Under Deep Burial**, Sargand, S. M., Hazen, G.A., White, K. and Moran, A. P., *Transportation Research Board 80<sup>th</sup> Annual Meeting, Paper No. 01-0292, Jan. 2001.*

The paper presents results of an experimental investigation on time-dependent deflection of thermoplastic pipe. The objectives were to determine the deflections of the pipe diameter in the vertical and horizontal directions and circumferential shortening at the time of installation and over the long term under actual field conditions.

Six different thermoplastic pipes, ranging in diameter from 762 mm to 1524 mm (30 inch to 60 inch) were buried under 12.2-m (40 ft.) cover and backfilled with Ohio Department of Transportation (ODOT) 304 crushed limestone or ODOT 310 river sand material. Table 1.8.1, Fig. 1.8.1 and Table 1.8.2 show the pipe properties, pipe cross-sections and stabilized deflections for the pipes respectively. The data reported herein was collected over a 8 month period after completion of construction and the deflection measurements will continue to be taken for a 2-year period.

The following conclusions are reported in this study:

i) The percent of horizontal deflection ranged from 0.7 to 1.3%. The percent circumferential shortening varied from 0.1% for the PVC pipes to 1.5% for the 60 in. HDPE pipe.

ii) The type of backfill did not seem to affect the magnitude of circumferential shortening (Table 1.8.2).

iii) Circumferential shortening of HDPE pipes was greater than that of PVC pipe (Table 1.8.2).

iv) A portion of the vertical deflection was mainly due to the circumferential shortening of the HDPE pipe.

v) For the PVC pipes, a portion of the vertical deflection corresponded to the change in horizontal diameter.

vi) The vertical and horizontal deflections and circumferential shortening stabilized within 45 days from completion of construction.

**Table 1.8.1 Pipe Properties**

Make*	Inside Diameter (mm)	Pipe Material	Corrug. Spacing (mm)	Wall Thickness			Moment of Inertia (mm <sup>4</sup> /mm)
				Outside Face (mm)	Inside Lining (mm)	Between Corrugations (mm)	
A	762	PVC	----	5.08	5.08	3.5	69.7
B	762	PVC	56.1	3.8	3.8	3.8	71.6
C	762	HDPE	106	2.7	2.7	4.2	142.6
D	762	HDPE	108	3.0	2.8	6.1	221.9
E	1050	HDPE	132.1	4.6	3.3	8.9	374.2
F	1524	HDPE	----	4.06	4.06	4.06	556.8

\*Pipe A: Lamson & Sessions Vylon – 30”

\*Pipe B: Contech A2000 – 30”

\*Pipe C: Lane HDPE – 30”

\*Pipe D: ADS N12 – 30”

\*Pipe E: ADS N12 – 42”

\*Pipe F: ADS HC– 60”

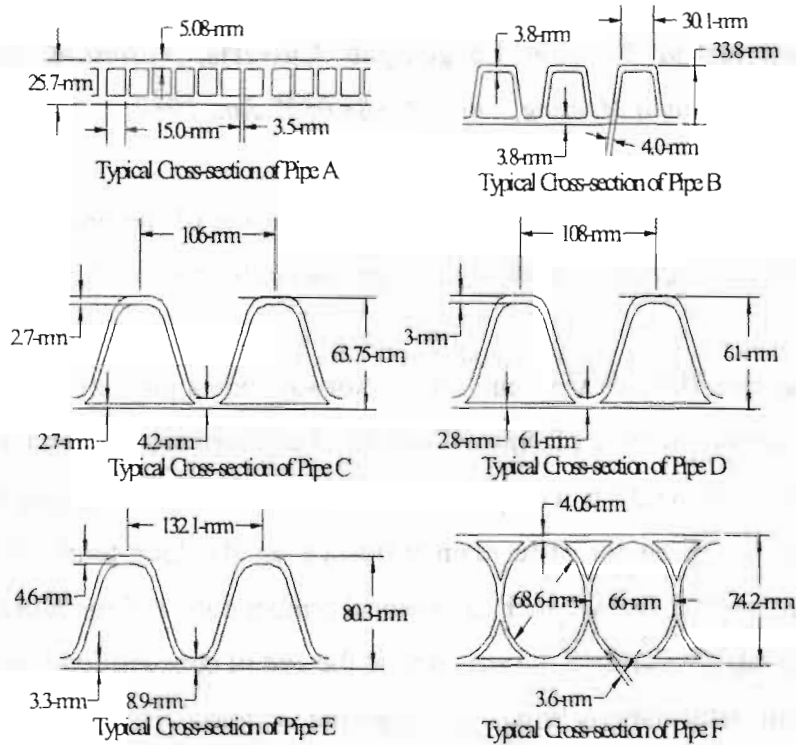


**Fig.1.8.1 Cross-Sections of The Test**

**Table 1.8.2 Stabilized Deflection for the Pipes.**

Pipe	Pipe Size (mm)	Backfill Type	Compaction (%)	Cover (m)	Stabilized Deflection (mm)**			
					Day*	Vert.	Horiz	Circum
A	762	ODOT 304	96	12.2	14	-13.7	6.35	-2.29
B	762	ODOT 304	96	12.2	30	-11.4	8.64	-2.54
C	762	ODOT 304	96	12.2	45	-22.9	5.08	-19.1
D	762	ODOT 304	96	12.2	30	-22.9	10.2	-12.7
E	1050	ODOT 304	96	12.2	35	-26.7	7.11	-23.4
F	1524	ODOT 304	96	12.2	50	-88.9	19.1	-72.4

\* The number of days is the difference between when the laying of cover was completed and when the values of pressure and deflection stabilized.

\*\* The value for the deflection is the absolute difference between the deflection at 0 feet of cover (at the top of the pipe) and the stabilized deflection after the construction of overburden.

**Long-term Behavior of Flexible Large-Span Culverts, Vaslestad, J., Transportation Research Board 68<sup>th</sup> Annual Meeting, Paper No.88 0337, Jan. 1989.**

On large-span culverts, long-term deflection increases of the order of 50% have been observed, and even failure has occurred on a large-span culvert after 10 years of service.

Two large-span flexible steel culverts in Norway, one a pipe arch with a span of 7.81 m (26.03 ft) completed in 1982 (Tolpinrud structure) and the second with a horizontal ellipse and a span of 10.78 m (35.37 ft) completed in 1985 (Dovre structure), are instrumented for monitoring long-term behavior. The main influence on the long-term effects is likely to depend on environmental factors such as seasonal temperature and moisture variations. The earth pressure distribution around the structure at the end of construction and after 18 months and the long term deformations from the Tolpinrud structure are shown in Fig. 1.8.2 and 1.8.3 respectively. Fig. 1.8.4 and 1.8.5 show respectively the measured thrust force and the earth pressure around the structure, Dovre. The long-term observation of the two flexible steel structures in this study shows that buried flexible steel culverts undergo changes in earth pressure distribution and structural response as time progresses after construction.

The earth pressure distribution around the pipe arch shows that the earth pressure is greatest at the springline. The lateral earth pressure at the springline increases considerably during the first six months after the end of construction, even reaching values above the vertical overburden pressure. The earth pressure at the haunch area is much lower than the earth pressure at the springline. Earth pressure distribution from the ring-compression theory, predicts greatest earth pressure at the haunch.

In the cold climate where the structure is located, the earth pressure around the pipe arch changes with temperature over the year. The earth pressure distribution around the horizontal ellipse also shows some variations over the year. At the springline the horizontal earth pressure has increased to 1.3 times the vertical overburden pressure. On the lower part of the structure the earth pressure is relatively small and varies little with temperature over the year.

In the horizontal ellipse the measured circumferential thrust force in the steel has increased considerably after construction. After six months the maximum thrust force increased 50%, and the maximum observed thrust in 1989 is almost twice the value measured at the end of the construction. The moment distribution also varies with time, but not as much as the thrust.

Positive arching is measured over the center of the crown. The arching effect is nearly constant, and is 30% of the vertical earth pressure over the observation period of almost three years, although the measured thrust in the steel indicates negative arching for the structure as a whole.

The long-term deflection and stresses in large-span flexible steel culverts can be controlled by using high quality backfilling material and established construction procedures.

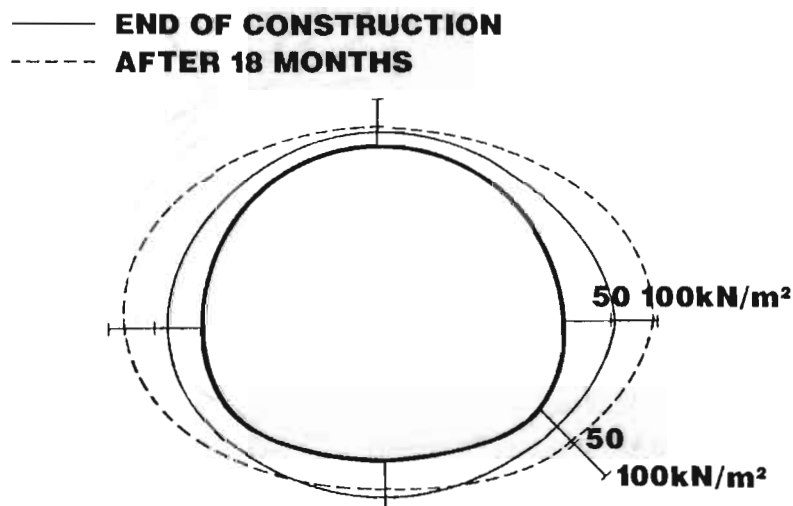


**Fig. 1.8.2 Measured Earth Pressure Around the Structure (Tolpinrud)**

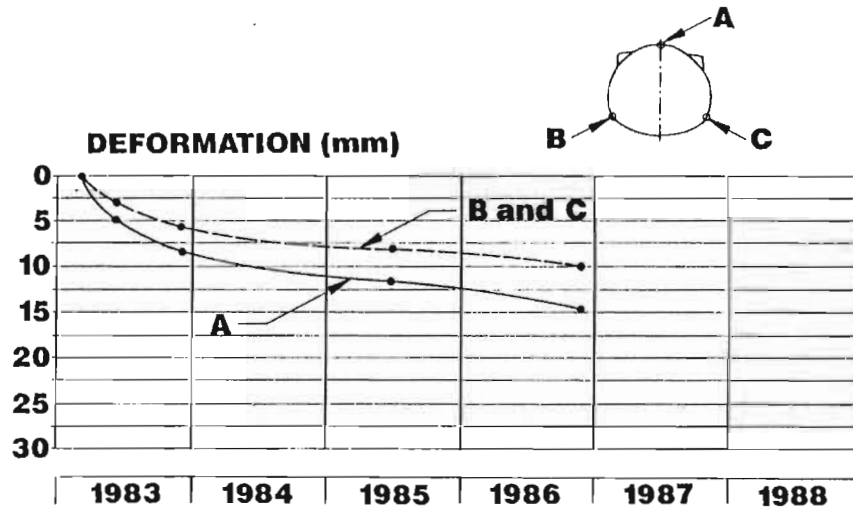


Fig. 1.8.3 Long-Term Deformations (Tolpinrud)

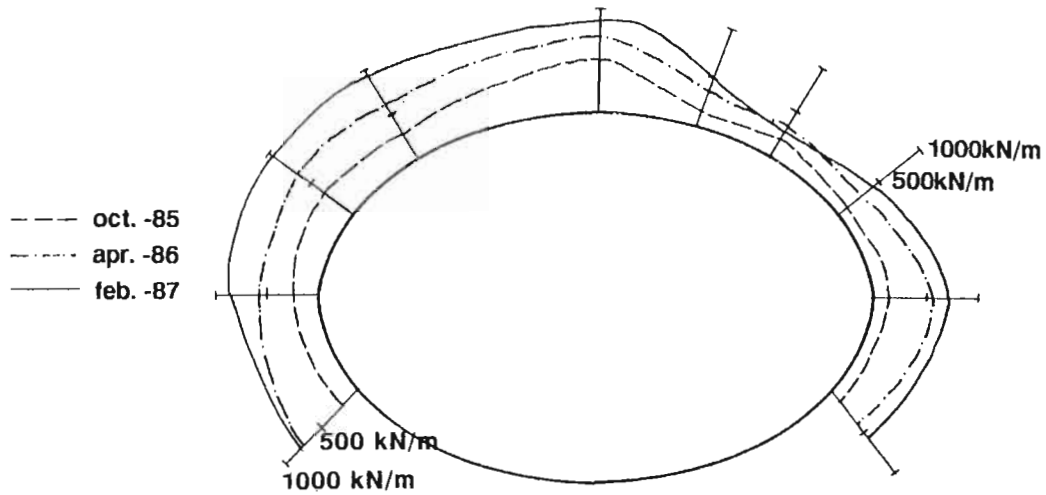


Fig. 1.8.4 Measured Thrust Force in the Steel Structure (Dovre)

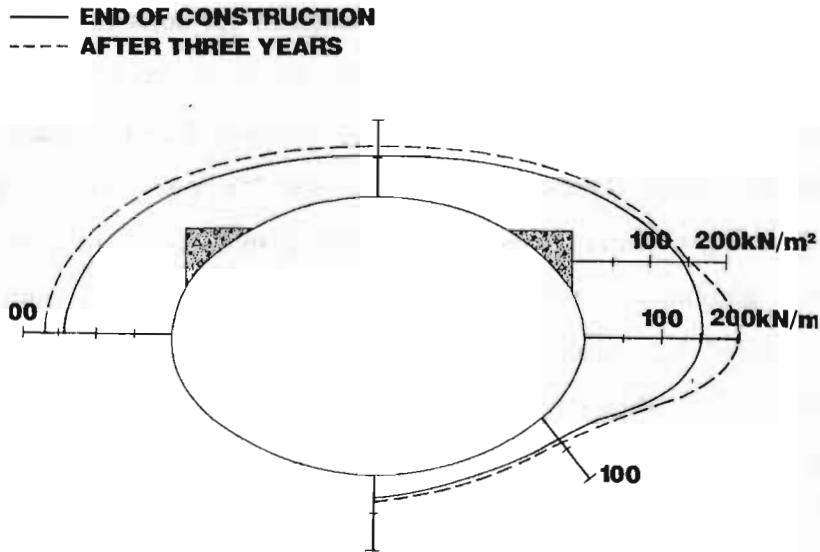


Fig. 1.8.5 Measured Earth Pressure around the Structure (Dover)

**New Method of Time-Dependent Analysis for Interaction of Soil and Large-Diameter Flexible Pipe**, *Chuo, K.M. and Lytton, R.L., Transportation Research Record 1315, 1991, pp. 58-66.*

All materials are known to experience a reduction in stiffness with time under an applied load. The reduction in stiffness is usually referred as relaxation. This property is pronounced for the plastic pipe, although it is less obvious in concrete and most metallic pipes. Hence in the design and use of plastic pipes, the ability to predict the effects of relaxation of the pipe and soil on the soil-pipe system is an important consideration.

The objective of this paper was to develop design equations to predict the pre-yield deflections, stresses, and strains in buried flexible plastic pipes over time. The design equations are obtained by regression analysis and the results are generated by a nonlinear finite element program. The main factors affecting the soil-pipe system were identified. They include pipe characteristics, properties of the different types of soils, arching in the soil, trench width, and presence of groundwater. The time-dependent behavior of the soil-pipe system was also presented, and the results were obtained by using the viscoelastic form of the design equations.

The hyperbolic stress-strain model was assumed for soils in the three zones (see Fig.1.8.6). Pipe stiffness, the properties of the embedment, the backfill, and the native soil, the cover depth, soil arching, trench width, and the presence of ground water were identified as the influential parameters in the soil-pipe system. The design solutions were obtained from a factorial study using CANDE (a nonlinear finite element code) to generate a database based on a large number of cases. The design equations obtained from the regression analysis were verified by using several sets of field measurements and the literature. Predictions that can be obtained using the design equations include the pipe vertical deflection with or without groundwater, the ratio of the pipe vertical deflection to its horizontal deflection, the soil vertical and lateral stress at the springline, the soil support modulus, the bending moment of the pipe wall at the crown, the thrust in the pipe wall at the crown, and the strain in the pipe wall at the crown. The elastic design equations were then transformed into a viscoelastic form yielding the results as a function of time.

The pipe vertical deflection expressed as a ratio to the average pipe diameter is given by

$$\frac{\Delta D}{D} = \frac{\frac{(1-v_e)}{3(3-4v_e)}(1-A_f)\gamma.z.W_f}{\frac{8.E_p.I_p}{(1-v_p^2)D^3} + \frac{(3-2v_e)(1-2v_e)}{12(3-4v_e)(1-v_e)}}$$

Where

- $A_f$  = factor representing the amount of arching,
- $\gamma$  = the unit weight of the soil,
- $z$  = the depth of cover to the springline,
- $W_f$  = a factor to correct for the presence of a water table,
- $v_e$  = Poisson's ratio of the elastic medium,
- $v_p$  = Poisson's ratio of the pipe,
- $E_p$  = the elastic modulus,
- $I_p$  = the moment of inertia of the pipe wall,
- $D$  = the pipe diameter,
- $E'$  = the soil modulus.

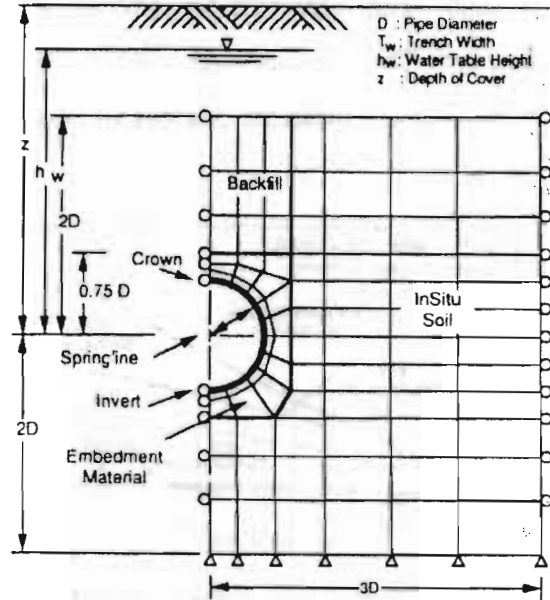


**Fig.1.8.6 Typical Configuration of A Pipe Trench**

**Factors Influencing Pipe Deflection**

Pipe Stiffness ( $PS=8E_pI_p/D^3$ ) is a function of the elastic modulus or relaxation modulus, the diameter of the pipe, and the moment of inertia of the pipe wall. Fig 1.8.7 shows the reduction in pipe deflection when the stiffness of a 1219 mm (48 in) diameter pipe is increased from 8.27 to 27.58 kPa (1.2 to 4.0 psi).

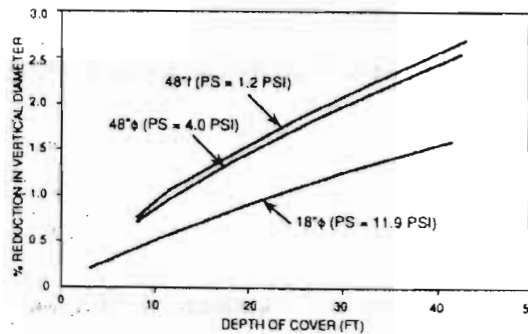


**Fig. 1.8.7 Vertical Deflections for Pipes of Different Stiffness**

## Soil Stiffness

Fig.1.8.8 shows how pipe deflections can be reduced by increasing the degree of compaction on the embedment soil. The soil modulus resulting from the interaction between the different types of native soil and the different degrees of compaction of the embedment soil is shown in Fig. 1.8.9

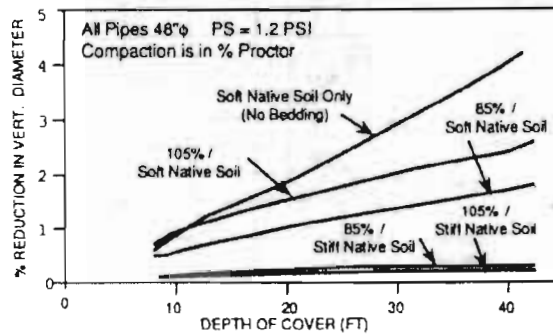


Fig. 1.8.8 Vertical Deflection of Pipes in Different Soils

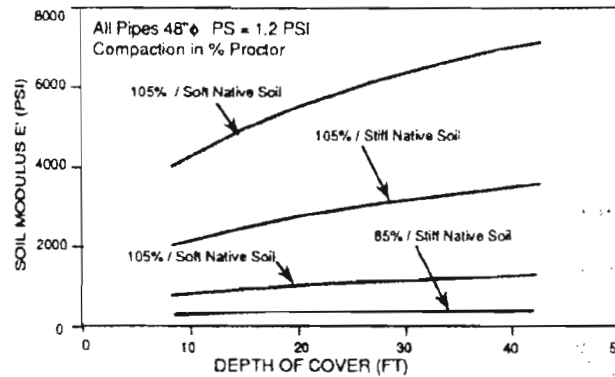


Fig.1.8.9 Soil Moduli for Different Depths of Cover

## Soil Arching

The degree of soil arching is described by the term  $A_f$ , which can take values ranging from 1.0 to negative values.

$$A_f = [1 - (1 - A_{fo})A_{fc}]$$

where,

$A_{fo}$  (function of a representative soil exponent number,  $K_r$ ) and  $A_{fc}$  (function of  $K_r$ , Trench width,  $T_w$ , and soil modulus,  $E'$ ) are listed in Chua (1991).

Fig. 1.8.10 shows the arching values that can be obtained for various degrees of compaction in different native soils.

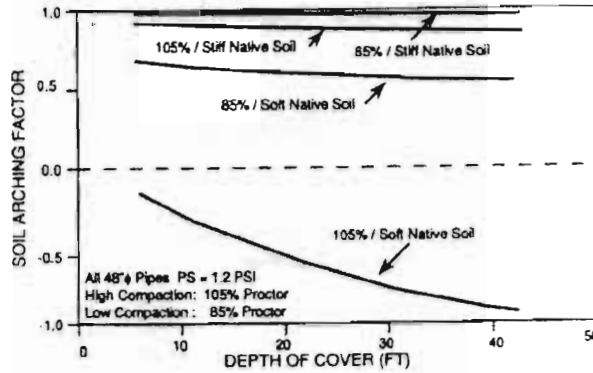


**Fig.1.8.10 Arching Factor of A Soil-Pipe System in Different Soils**

### Trench Width

Generally, a trench width of about 1.5 times the pipe diameter is preferred when using a flexible pipe. An increase in the trench width will weaken the arch to be formed.

### Groundwater

The presence of groundwater will increase deflection only beyond a specific head, which varies with soil modulus (Fig. 1.8.11).

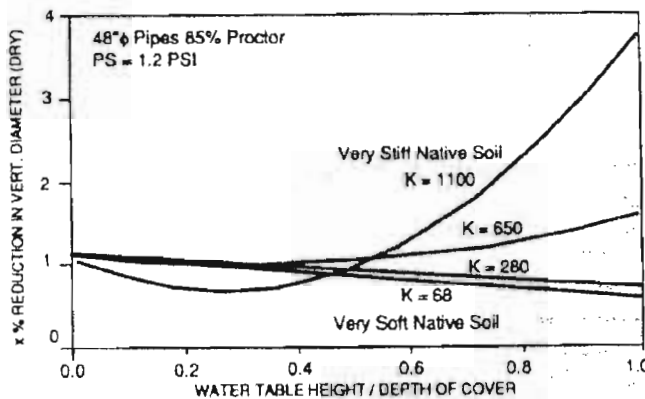


**Fig. 1.8.11 Effects of Groundwater on Pipe Deflection**

### Ratio of Vertical to Horizontal Deflection ( Fig.1.8.12)

The inaccurate notion among pipe design engineers is that all pipes will approach failure, if they do not conform to the elliptical shape, where the  $D_v/D_h$  or  $D_h/D_v$  ratio is unity.

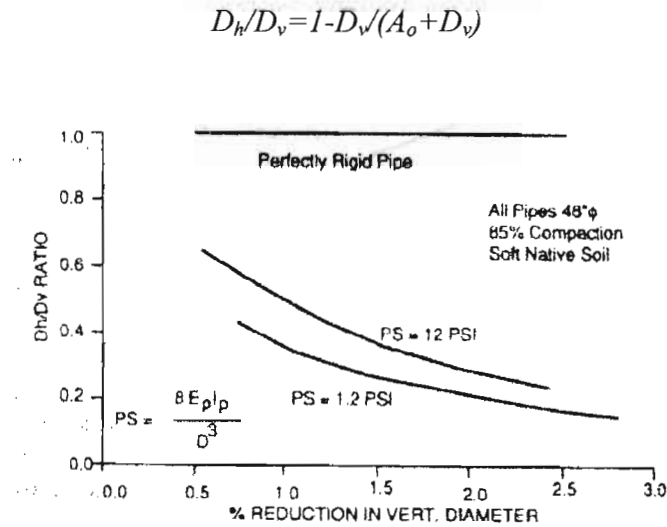


**Fig.1.8.12 Ratio of Pipe Horizontal Deflection to Vertical Deflection**

### Bending Moment, Thrust, and Strain in the Pipe Wall

The bending moment at the crown can be expressed as  $M = D_f 4E_p I_p (\Delta D / D) / D$

where  $D_f$  = the deformation factor.

The thrust at the pipe crown, T, is given by

$$T = (C_1 \sigma_x + C_2 P_w \gamma_w z) D / 2$$

Where

$\sigma_x$  = horizontal earth pressure at the springline

$\gamma_w$  = the unit weight of water

$P_w$  = pore water pressure

D = the pipe diameter

z = the depth of cover to the springline

$C_1 = 0.7285$

$C_2 = 0.9145$

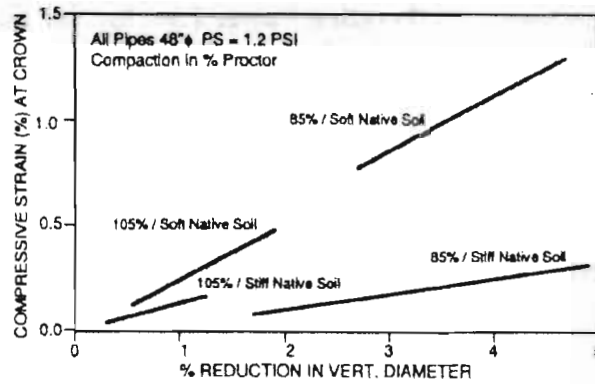


**Fig.1.8.13 Pipe Strains at Crown for Different In Situ Soils**

Fig 1.8.13 shows the variation of the strain at the crown at different levels of vertical deflection of a 48-in.-diameter HDPE pipe for various installation cases after 1 year.

### Time-dependent Design Equation

The Laplace-transformed time-dependent pipe vertical deflection is given by

$$\mathcal{L}\left\{\frac{\Delta D}{D}\right\} = \frac{1}{s} \cdot \frac{B_f(1-A_f)\gamma.z.W_f}{8.E_p.I_p/(1-\nu^2)D^3 + S_c.E'}$$

where,

$s$  = a variable of integration of Laplace-Transform

$\nu$  = Poisson's ratio.

The Laplace-transformed time-dependent bending moment in the pipe wall is given by

$$\mathcal{L}\{M\} = 4D_f E_p I_p (\Delta D / D) / SD$$

Relaxation in a soil-pipe system, pipe vertical deflection with time, bending moment pipe strains with time are shown respectively in Table 1.8.3, Figs. 1.8.14 and 1.8.15.

**Table 1.8.3 Exponents of Relaxation Power Law for Soils and Pipe Materials**

Descriptions	m Values	Remarks
Allenfarm (ML)	0.106	Texas Soil at optimum Moisture Content
Moscow (CH)	0.101	
Floydada (CL)	0.079	
Mississippi Delta (CH)	0.082 to 0.104	
Louisiana Coast (MH)	0.029 to 0.104	
Haney Clay N.C.	0.300 to 0.600	
Seattle Clay O.C.	0.500	
Redwood City Clay	0.250	
Osaka Clay	0.000	
Tonegaw Loam	0.200	
Bangkok Mud	0.200	
Concrete	0.028	
High Density Polyethylene	0.098	
Polyvinyl Chloride	0.031	
Reinforced Plastic Mortar	0.048	

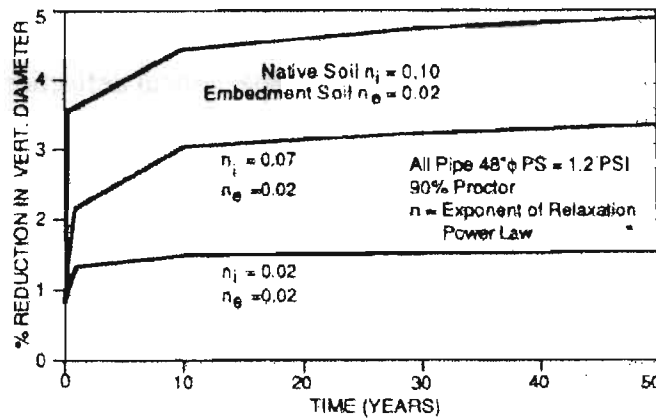


**Fig.1.8.14 Variation of Pipe Vertical Deflection over Time**

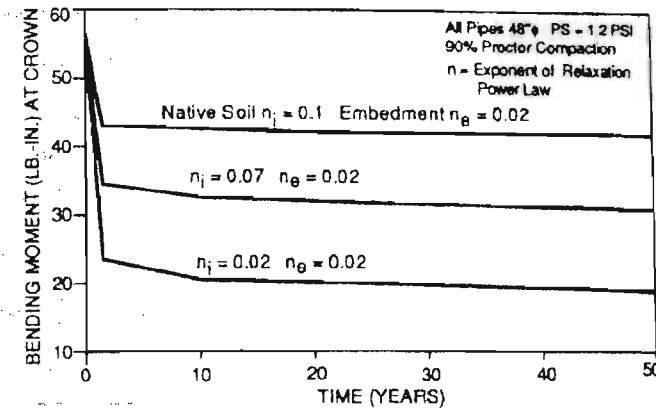


**Fig.1.8.15 Variation of Bending Moment at Crown over Time**

The results of the design equations and Spangler's equation are compared in Fig. 1.8.16 with the average of five pipe vertical deflections per section. The pipe deflections measured during the 10-month period are shown in Fig. 1.8.17.

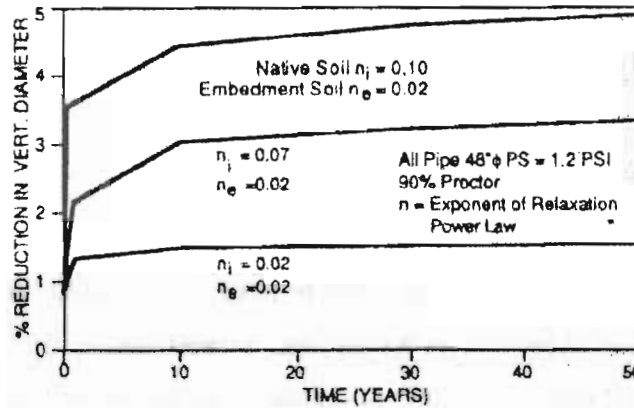


**Fig.1.8.16 Predicted and Measured Pipe Vertical Deflection for Different Depths of Cover**

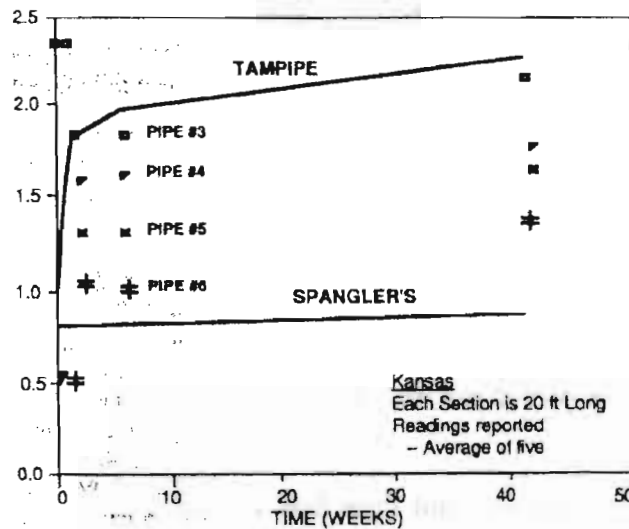


**Fig.1.8.17 Predicted and Measured Pipe Vertical Deflection for Different Time Periods**

The authors have shown that it is possible to quantify the effects of various factors on pipe deflections over time and that the design equations were able to match field measurements. The ability to describe the details of soil-pipe behavior with a sound engineering approach can be expected to provide a major benefit to the design, construction, and performance of buried flexible pipes.

**Stress Relaxation Characteristics of the HDPE Pipe-Soil System**, Petroff, L.J., *Proceedings of the International Conference sponsored by the Pipeline Planning Committee of the Pipeline Division of the American Society of Civil Engineers, 1990, pp.281-294.*

The paper summarizes the viscoelastic behavior of pipe-soil system. High density polyethylene (HDPE) pipes under deep burial may undergo a relief in load with time due to creep and deflection.

### **Viscoelasticity of Soil**

Creep is deformation that occurs with time under constant load and stress relaxation. The soil creeps due to deformation within the microstructure of its fabric, where stress concentrations break down the fabric or cause rearrangements and compression of the particles. Creep occurs in both fine and coarse grained soils. When the load required to maintain a constant deformation decreases, or relax with time, stress relaxation takes place in the soil. For most material at strains below yielding the relaxation modulus,  $E(t)$  is given by the power law<sup>1</sup> in time as:

$$E(t) = E_1 t^{-m}$$

where,  $E_1$  = initial modulus  
 $t$  = time  
 $m$  = the power law exponent.

### **Viscoelasticity of Pipe Materials and Pipe-Soil System**

HDPE pipe materials are viscoelastic. Fig. 1.8.18 shows the stress relaxation curve for HDPE. A large portion of the total creep deformation for HDPE structures occurs within a few weeks after initial loading.

---

<sup>1</sup> Chua, K.M. and Lytton, R.L., A Method of Time-Dependent Analysis Using Elastic Solutions for Nonlinear materials, Int. J. for Numerical and Analytical Methods in Geomechanics, Vol. 11, pp. 421-431

The application of load to a pipe-soil system initiates a reaction/counteraction effect between soil and pipe. The specific response of the system is determined by the viscoelastic properties of soil and pipe

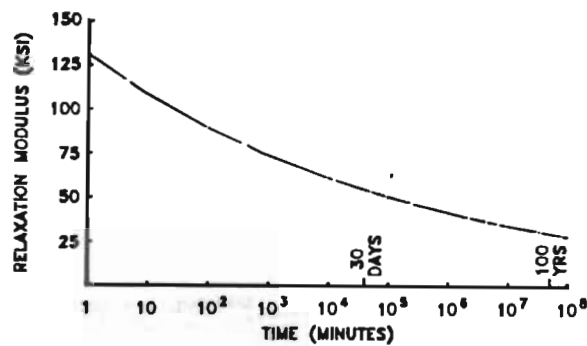


Figure 1.8.18 Stress Relaxation Modulus vs. Time for HDPE

### Load on Flexible Pipe

Flexible pipes deflect under load and are usually less stiff or only slightly stiffer than the surrounding soil. Where pipe and soil are of equal stiffness, the trench load is spread uniformly over the pipe and soil. Where the pipe is less stiff than the soil, the pipe carries proportionately less load. This is a consequence of the pipe's deflection and the internal shear resistance of the soil.

Arching can occur in all soils that have an angle of internal friction greater than zero. Viscoelastic behavior of soils and pipe promote arching. If the pipe creeps under load faster than the surrounding soil, the soil picks up that load through arching, followed by a decrease of stress with time in the pipe. Conversely, if the soil creeps faster than the pipe, the stress will increase with time.

Fig. 1.8.19 shows the change of bending moment in the pipe wall with time for a 48" HDPE profile pipe under two different backfill conditions. The stress in the pipe decreases with time for the sand backfill, which undergoes less creep than the pipe. Conversely, the

pipe experiences increasing stress when installed in the clay backfill, which creeps at a faster rate.

Pipe can be designed to take advantage of the viscoelasticity of the soil, if it can be made more flexible than the soil. This can be accomplished with HDPE since it is a ductile material with a high strain capacity (design strain equals 0.042) and thus can deform to relieve stresses.

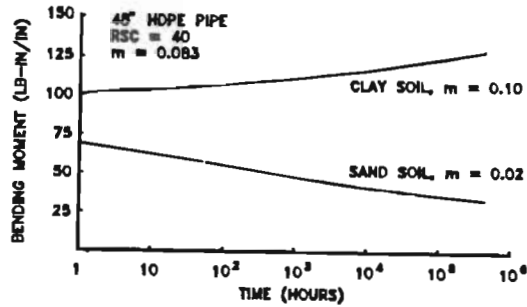


**Figure 1.8.19. Crown Bending Moment vs. Time for HDPE Pipe in Clay and in Sand**

### Conclusions

i) Time-dependent deformation and strain in a buried HDPE pipe are controlled by the stress relaxation and creep characteristics of the embedment soil and pipe.

ii) The flexural stress and thrust in the pipe wall depend on the viscoelastic properties of pipe and soil. Whether the load remains constant, increases, or decreases with time depends on the relative values of the relaxation modulus of soil and pipe materials.

iii) For HDPE pipes, embedded in compacted granular material, the highest stresses occur at completion of installation and decrease with time.

iv) For HDPE pipes the consequences of creep deflection are insignificant, when compared to the benefit gained from stress relaxation with its consequent load reduction.

**Three Dimensional Time Dependent Model for Buried HDPE Pipe, Moore, I.D., *The Proceedings of the Eighth International Conference on Computer Methods and Advances in Geomechanics, Vol.2, 1994, pp. 1515-1520.***

This paper estimates the three dimensional stress and strain fields in the buried pipe to assess the likelihood of material failure and time dependent deformation. Three dimensional viscoelastic solutions are developed for a buried HDPE pipe. Axisymmetric geometry and linear viscoelasticity of annular pipes are used and predictions from the model are compared with laboratory and field measurements of load, strain and displacement.

A semi-analytic finite element solution is described to investigate the mechanical response of the pipe. Fig. 1.8.20 shows features of soil-pipe system. The time dependent nature of HDPE response should be modeled and the soil surrounding the pipe in different zones must be represented, which contribute in varying measure to the overall pipe-soil interaction.

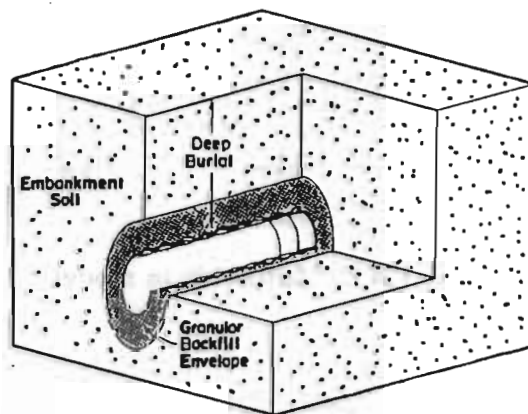


**Fig. 1.8.20 Typical Buried HDPE Pipe**

Axisymmetric geometry can be used to simplify analysis of corrugated pipes with annular design and linear material response. A two-dimensional finite element mesh is used to model the geometry and strain fields in  $r, z$  planes as shown in Fig.1.8.21, and a Fourier series is used to model load variations around the pipe circumference.

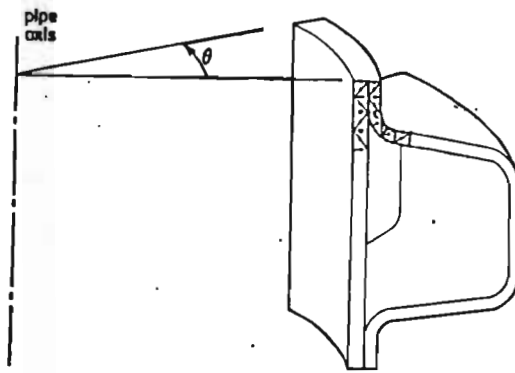


**Fig.1.8.21 Finite Element Model for Axisymmetric Pipe Analysis**

A linear viscoelastic finite element analysis utilizing sets of springs and dashpots, known as multi-Kelvin model is used, with one independent spring and a series of K Kelvin elements as shown in Fig. 1.8.22.

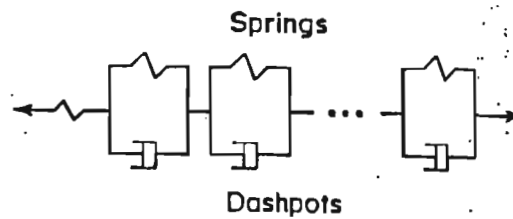


**Fig.1.8.22 Multi-Kelvin model**

The uniaxial 'secant' creep modulus  $E(t) = \sigma/\epsilon(t)$  (psi) is expressed as a power law model for HDPE given by

$$E(t) = mt^{-n}$$

where, time  $t$  is expressed in minutes,  $m$  equals 2059 psi and  $n$  equals 0.0197 providing the creep modulus in psi.

The load path experienced by pipe is modeled with a multilinear approximation for applied forces  $F(t)$  given by

$$F(t) = F_1 + g_1(t-t_1)$$

Where,  $g_1$  = load gradient

$F_1$  = net load at time  $t_1$ .

### Analysis of Laboratory Test

A parallel plate test was performed to investigate the effectiveness of the three-dimensional viscoelastic finite element model. This parallel plate test involves a 320 mm length of 450 mm diameter pipe subjected to load across the vertical pipe diameter as shown in Fig. 1.8.23a.

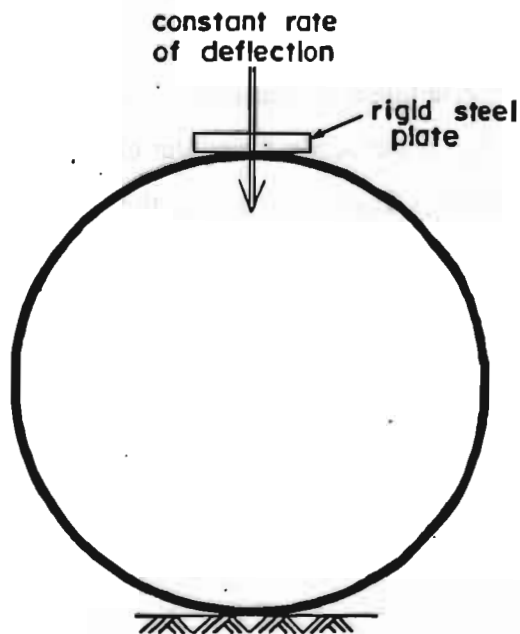


**Fig. 1.8.23a. Loading Conditions for the Parallel Plate Test**

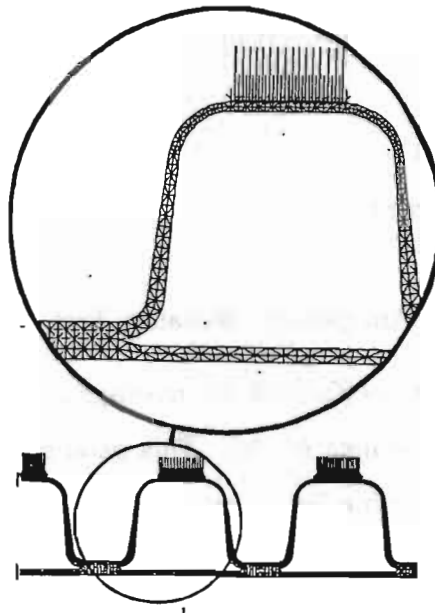


**Fig. 1.8.23b Finite Element Mesh for the Parallel Plate Test**

The two-dimensional finite element mesh used for the HDPE pipe is shown in Fig. 1.8.23b, featuring 1200 six noded linear strain triangular elements. Fig.1.8.24 shows a finite element estimate of the strain versus load response together with experimental measurements at two gages located at the crest of the corrugation and oriented in a circumferential direction (denoted by D and J). The comparison reveals that the three-dimensional finite element analysis with viscoelastic properties provides very reasonable estimates of strain versus load for this parallel plate test. At the peak load, the discrepancy of  $600\mu\epsilon$  (12%) is similar to those for all other strain locations and directions.

### **Depth Burial Field Study**

In order to examine the performance of this three-dimensional pipe-soil mode, experimental data<sup>1</sup> on the installation of a 600 mm diameter corrugated HDPE pipe beneath a 30.5m embankment are compared with the predictions from the model.

Fig. 1.8.25 shows a schematic of the installation. Fig. 1.8.26 shows that both measured circumferential strain and deflection correlate well with the theoretical model.

<sup>1</sup> Hashash, N.M.A. and Selig, E.T., Analysis of the Performance of a Buried High Density Polyethylene Pipe, In Mitchell Sargand and Hurd, Editors, Structure Performance of Flexible Pipes, Page 95-103, Balkema, Rotterdam, 1990

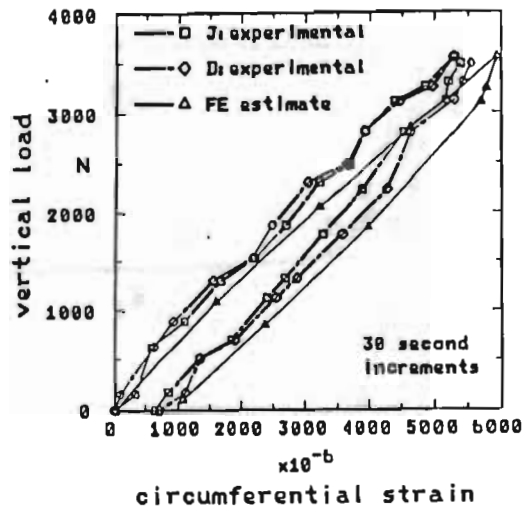


Fig.1.8.24 Experimental Measurement and Finite Element Predictions for the Parallel Plate Test

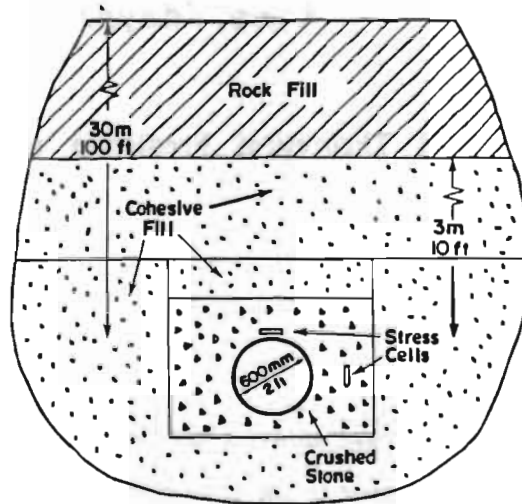


Fig.1.8.25 Field Installation for Deeply Buried HDPE Pipe<sup>1</sup>

<sup>1</sup> Hashash, N.M.A. and Selig, E.T., Analysis of the Performance of a Buried High Density Polyethylene Pipe, In Mitchell Sargand and Hurd, Editors, Structure Performance of Flexible Pipes, Page 95-103, Balkema, Rotterdam, 1990

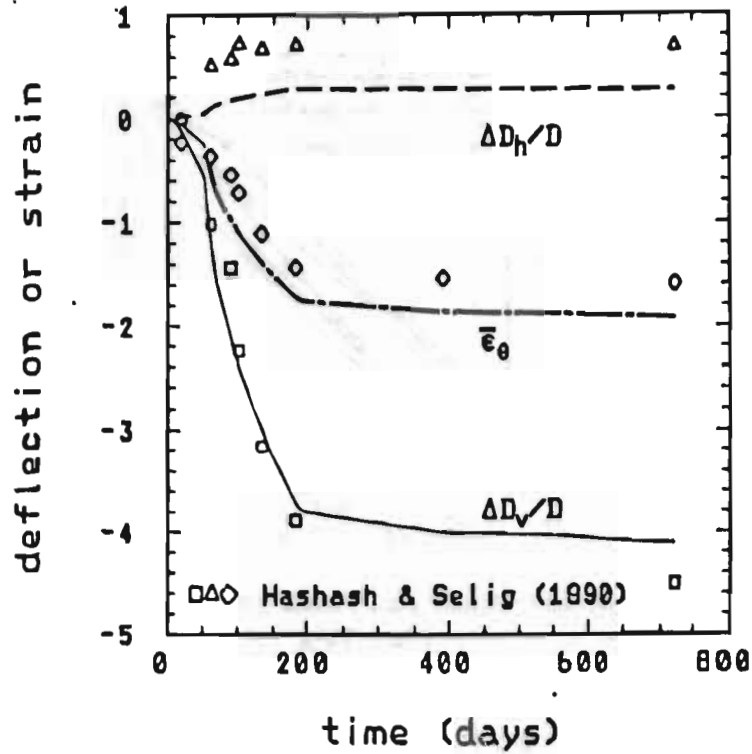


Fig. 1.8.26 Measurement and Theoretical Prediction of Pipe Deformation and Circumferential Strain

### Conclusions

Three dimensional finite element analysis has been presented for use in investigating the performance of profiled HDPE pipe in the laboratory and under deep burial conditions. The model appears to perform well, providing good predictions for both the laboratory test and field study. However, improvements to the rheological parameters for HDPE appear necessary since the model is underpredicting the rate of stress relaxation and creep over extended periods of time.

## 1.9 Lifetime Prediction of Polyethylene Pipes

**New Method of Lifetime Prediction for Brittle Fracture of Polyethylene**, Chudnovsky, A., Shulkin, Y., Baron, D., and Lin, K. P., *Journal of Applied Polymer Science*, Vol. 56, 1995, pp. 1465-1478.

The paper proposes a new method of lifetime prediction for polyethylenes (PEs) under creep. The method is based on the crack layer concept. The crack layer (CL) is a system consisting of the closely coupled crack and process zone (PZ). The CL is characterized by the crack and PZ lengths and is, therefore, a system of two degrees of freedom. This results in the existence of various scenarios for the fracture process and more realistic modeling of slow crack growth behavior in PEs.

Fracture in the ductile mode occurs as a result of macroscopic shear rupture, and the time to failure in this process is mainly determined by the rate of viscoelastic deformation. The brittle mode of failure is associated with slow crack growth induced by a preexisting defect. The lifetime in this case is the time during which the crack initiates and slowly propagates, up to the ultimate instability leading to catastrophic failure.

### Crack Growth Modeling

In simple tension tests, most PEs exhibit cold drawing (necking) with constant drawing stress  $\sigma_{dr}$  and natural draw ratio  $\lambda_n$ . The simplified model of the crack layer developed is characterized by two parameters, the crack length ( $l$ ) and the crack layer length ( $L$ ) shown in Fig. 1.9.1. The bulk material surrounding the CL is the original material, while the PZ consists of the drawn material. The process of CL propagation is governed by the following equations:

$$\frac{dl}{dt} = k_1 X_{CR} \quad \frac{dL}{dt} = k_2 X_{PZ}$$

where

$X_{CR}$  is the driving force for the crack advance

$X_{PZ}$  is the driving force for the PZ advance

$k_1, k_2$  are kinetic coefficients

Solving the above equations by a numerical method, the lifetime ( $t_f$ ), or the elapsed time until the cartographic failure, can be obtained.

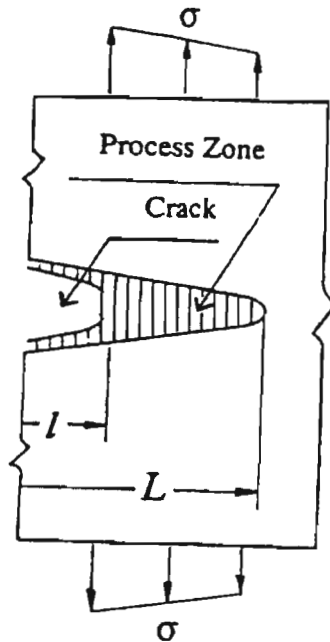


**Figure 1.9.1 Schematic Presentation of Crack Layer in PEs**

### **Time-Stress-Temperature Relation**

If the material properties, specimen geometry, and applied stress are prescribed, a computer simulation of slow CL growth can be constructed by means of the numerical solution of the above equations. Analyzing the data from the numerical calculations, the following approximate relation is obtained between the lifetime and applied stress:

$$\log \tau_f = B - \beta \log \sigma'$$

where,  $\tau_f$  is the time to failure normalized by the rupture time (elapsed time until fiber creep rupture,  $t_r$ ) of the drawn material

$\sigma'$  is the applied stress normalized by the drawing stress  $\sigma_{dr}$

$B$  and  $\beta$  are general functions of both temperature and specimen geometry obtained in the computer simulation.

The above relation can also be reduced to the following form:

$$t_f = t_0 \left( \frac{\sigma}{\sigma_{dr}} \right)^{-\beta} \exp \left( \frac{Q_0 - \chi \sigma_{dr}}{RT} + b \right)$$

where,

$b = B / \log e$

$t_0$  = characteristic time

$Q_0$  = activation energy

$\chi$  = coefficient

$R$  = universal gas constant

$T$  = temperature

$\sigma$  = applied stress.

If activation energy  $Q_0$  is taken as 100 kJ/mol (this value is reported as the average for PEs), then the other two parameters,  $t_0$  and  $\chi$ , can be determined from the experimental data. The data of the direct measurements<sup>1,2</sup> (points) and the theoretical predictions (lines) are combined and shown in Fig. 1.9.2. The dashed lines correspond to the adjustment temperatures 70 and 50°C. The theoretical results agree with the experimental results (within scatter of the data), not only at 60°C (the temperature of interpolation) but also at 80 and 42°C (the temperatures of extrapolation). Experimental data for temperature at 24°C does not exist. Evidently, the CL kinetic model can be used to describe the stress lifetime relationships for brittle fracture at various temperatures.

### Accelerated Testing for Lifetime

The CL kinetic model can be determined from tests that do not involve slow crack growth. Two types of tests are needed for the material characterization. The first type is simple ramp test, which provide Young's modulus  $E_0$ , Poisson's ratio  $\nu$ , drawing stress  $\sigma_{dr}$ , natural draw ratio  $\lambda_n$  and drawing energy  $\gamma_{dr}$ , at various temperatures.

<sup>1</sup> Huang, Y.L. and Brown, N., J. Polym. Sci., Part B: Phys., 28, 2007(1990)

<sup>2</sup> Lu, X. and Brown, N., J. Mater. Sci., 25, 29(1990)

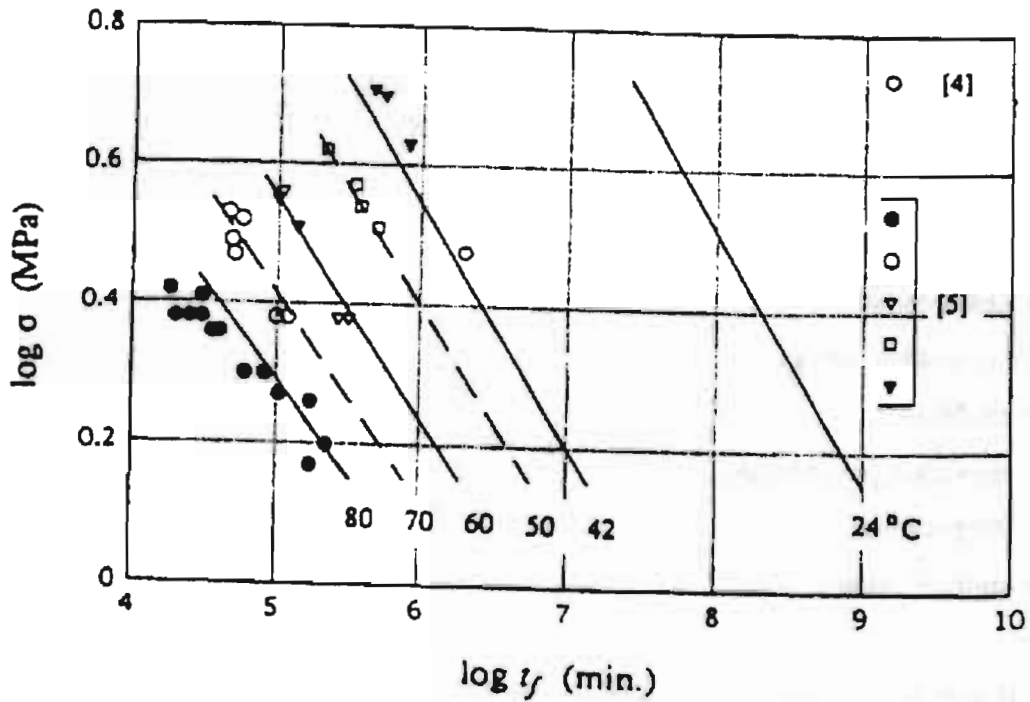


**Figure 1.9.2 Experimental Observations (points) and Theoretical Predictions (lines)**

The second type includes the creep tests of the drawn fibers under  $\sigma_{dr}$ . The characteristic time  $t_0$ , activation energy  $Q = Q_0 - \chi \sigma_{dr}(T)$ , and specific rupture energy  $\gamma_0(T)$  should be extracted at various temperatures. Both test types can be performed on unnotched specimens.

The temperature dependence of the material characteristics leads to the determination of the temperature dependence of rupture time  $t_r$ . Then, computer simulations of slow crack growth based on the CL kinetic model result in the determinations of parameters  $B$  and  $\beta$  as functions of temperature. Thus, all quantities are known, and predictions of lifetime can be computed for a range of temperatures.

**Methodology for Durability Analysis of HDPE Pipe**, Chudnovsky, A., Sehanobish, K., and Wu, S., *American Society of Mechanical Engineers, Pressure Vessels and Piping Division (Publication) PVP, Vol. 388, ASME 1999, pp. 405-412*

This paper presents defect characterization, the correlation of the defect properties and long-term performance of HDPE pipes. The short-term and long-term properties of HDPE are investigated experimentally by evaluating the creep behavior of original and drawn materials. These properties are used as basic parameters for lifetime prediction using the crack layer theory.

### **Defect Characterization**

Two HDPE pipes which had been subjected to long-term pressure testing at 80°C with internal pressure of 5 MPa have been examined by scanning electron microscopy (SEM), energy dispersive X-ray (EDX), micro transmittance infrared spectroscopy, and hot-stage microscopy to determine the size distribution and compositions of defects present in the pipes. The fracture surface shown in Fig. 1.9.3 was produced by freeze fracturing an arch-shaped section of the pipe which contained the site at which a leak was first observed when the pipe failed the long-term test. A particle approximately 75µm in diameter is located at the center of the round domain. This particle appears to have been the main initiator of failure in this pipe.

### **Defect size distribution**

Figure 1.9.4 shows the particle size distribution obtained from two types of fracture surfaces in a tested pipe. Most of the particles below 10 µm were located on a fracture surface produced by notching and fracturing pipe in liquid nitrogen, where no externally visible cracks were located. All but one of the particles > 50 µm in diameter appeared to have been the main initiator of the failure which caused externally visible cracks. While the relative populations of defects in these two pipes cannot be determined accurately from this information, it is clear that a pipe, which has a longer lifetime, also contains a significant number of defects, often as large or larger than pipes, which exhibited a shorter lifetime.

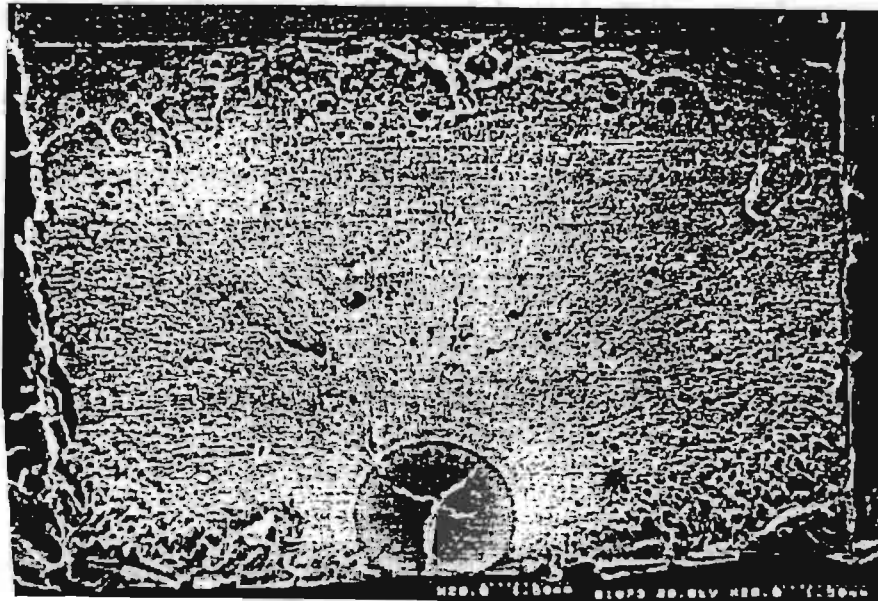


Fig. 1.9.3 SEM Image of Fracture Surface. The Primary Crack Initiation Site is Located at Bottom-Center in the Figure and is Near the Inner Wall of the Pipe.

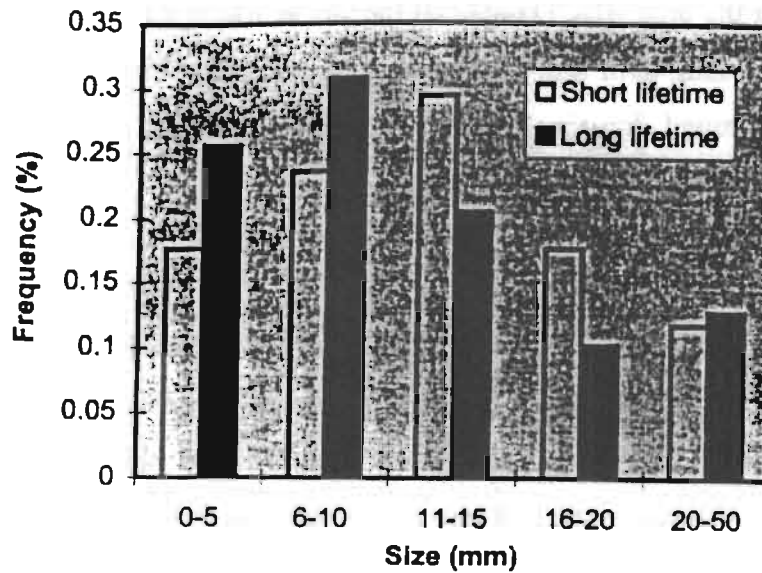


Fig. 1.9.4 Particle Size Distribution of Defect Particles Observed From Fracture Surfaces of Two Pipes with Quite Different Lifetimes (6 Times Difference) Under Test

### Crack Sizes vs. Defect Size in Tested Pipes

For the tested pipes, there are many natural cracks, which initiated during testing, in addition to the major crack that caused failure of the pipe. In most cases, these natural cracks were initiated from defects distributed inside the pipe. Natural cracks in two tested pipes have been analyzed by cryogenic fracture of tested pipes. The results and their correlation with defect sizes are shown in Fig. 1.9.5. These results suggest that the crack size is not proportional to the defect size in the pipes.

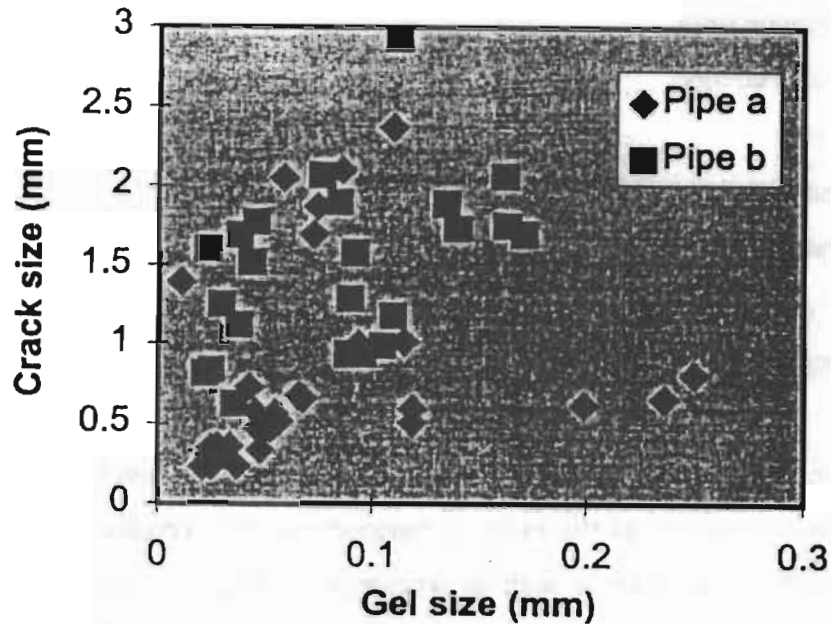


Fig. 1.9.5 The Defect Sizes vs. the Crack Sizes in Tested Pipes

## Prediction of Crack Initiation and Propagation by the Crack Layer Method

The procedure for lifetime prediction is based on the crack layer concept. The lifetime,  $t_f$ , of high density polyethylene under creep can be expressed as:

$$t_f = t_0 \left( \frac{\sigma}{\sigma_{dr}} \right)^{-\beta} \exp \left( \frac{Q_0 - \chi \sigma_{dr}}{RT} + b \right)$$

where,

$b$  and  $\beta$  are kinematic model parameters

$t_0$  = characteristic time

$Q_0$  = activation energy

$\chi$  = coefficient

$R$  = universal gas constant

$T$  = temperature

$\sigma$  = applied stress

$\sigma_r$  = drawing stress.

Lifetime prediction, within the framework of the crack layer, depends on experimental measurements of the material parameters, and computer simulations of slow crack growth with the conditions such as temperature, specimen geometry and load level. Two types of physical tests are performed to determine the material parameters. One is a simple ramp test, which provide the elastic modulus, yield stress, drawing stress at various temperatures. The second test is a creep test of drawn material under the stress  $\sigma_{dr}$  at various temperatures. The characteristic time  $t_0$  and activation energy  $Q_0$  can be extracted from the results of these creep tests.

The test samples for the ramp tests are compression molded ASME D638 standard, type IV specimen and they are run at temperature of 23°C with the strain rate of 0.009/second. Several materials for pipe application have been run and they have a similar drawing stress (~15 MPa) and natural draw ration (~6). Tensile creep tests for the pipe material have been run at 23°C and under the draw stress. The specimen is standard ASTM D638 type IV specimen. Fig. 1.9.6 shows typical creep strain as a function of time.

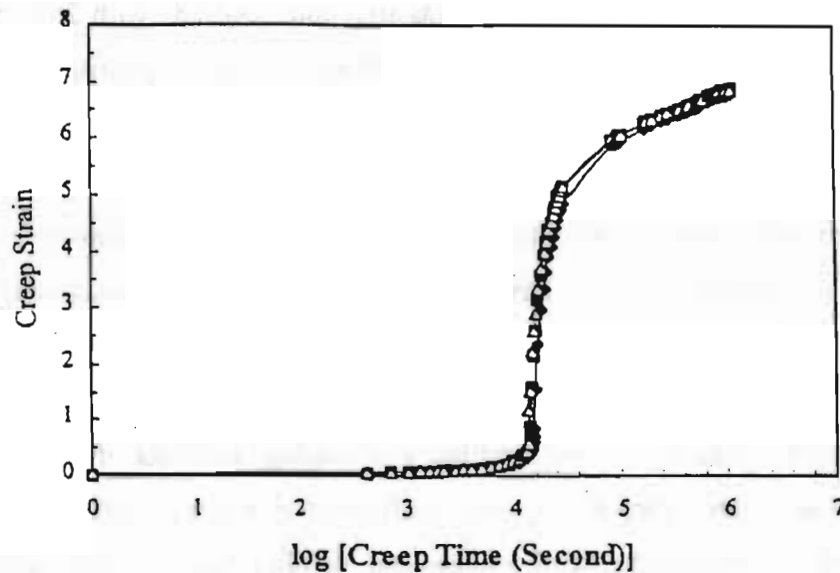


**Figure 1.9.6 Creep Behavior of a HDPE Material Under the Stress of Drawing Stress**

### Conclusions

Fractographic analysis of tested pipes shows that cracks are mostly initiated from large (>50µm) defect particles. The results show that pipes with smaller defect particle size (less than 20µm) have a better long-term property. However, pipes with a similar defect particle size do not necessarily have a similar long-term performance.

**Accelerated Fracture Mechanics Evaluation of Slow Crack Growth Potential in Corrugated Polyethylene Pipes**, *Kuhlman, C. J., Weed, D. N., and Campbell, F. S., Final Report No. 06-15378 submitted to Corrugated Plastic Pipe Association, 1995.*

The primary objective of this study was to make quantitative estimates of the service lifetimes of both virgin and recycle corrugated polyethylene (PE) pipes for gravity flow applications. The virgin material was AASHTO M294 cell classification 324420C, while the recycle material was AASHTO M294 cell classification 324420C with 25% post-consumer resin content. Lifetimes were assumed to be controlled by the long-term failure mechanism of slow crack growth (SCG).

Lifetime estimates for both virgin and recycle corrugated PE pipes of 12, 18, and 30-inch diameter were calculated as a function of burial depth, pipe size, initial defect depth, defect geometry, and service temperature.

The fracture mechanics-based lifetime methodology consists of two broad elements. The first element is laboratory testing and analysis of pre-notched PE test samples. Tests were performed to replicate the SCG process and develop data necessary to determine the SCG material properties. The second element is the calculation of service-induced stress intensity factors (SIF), which govern the SCG process in these materials. SIF solutions incorporated stress data generated from finite element simulation of soil loading of PE corrugated pipes. Stress data were supplied to South West Research Institute (SWRI) by the University of Western Ontario.

**Slow Crack Growth Mechanism**

In order for SCG to occur in PE, the following two elements must exist: a defect in a component and a local tensile stress acting to open the defect. If either of these two is absent, then SCG will not occur.

## Stress Intensity Factor

The initiation of SCG and crack growth rate have been rigorously correlated with linear elastic stress intensity factor<sup>1</sup> from first principles. The stress intensity factor (SIF), denoted as  $K$ , also called “crack driving force”, is calculated as a function of the applied remote stress, the crack geometry, and the overall component or structure geometry. It can be represented by the general expression<sup>2</sup>:

$$K = F\sigma_{rem}\sqrt{\pi a}$$

where,  $\sigma_{rem}$  is the remote or global stress,  $a$  is the absolute crack size, and  $F$  is a dimensionless correction factor associated with the crack and overall component geometries.

## Test Articles

Due to the curvature inherent in a round pipe, and the need for precise laboratory test samples, test specimens were machined from compression molded, flat panels of PE. Panels each of virgin and recycle PE were sent to SWRI. Table 1.9.1 lists the alphabetical character that corresponds to each of the four panels used in this program.

## Test Samples

Three test specimens, each 7 inches long by 1 inch wide (0.1 inch thick), were machined from each of four panels. This sample is commonly referred to as the single-edge notch tension (SENT) specimen. In this sample, the precrack was 0.5 inch deep. This precrack, or prenotch, is important for the crack growth tests.

---

<sup>1</sup> Kanninen, M.F., O'Donoghue, P.E., Popelar, C.H., and Kenner, V.H., A Viscoelastic Fracture Mechanics Assessment of Slow Crack Growth in Polyethylene Gas Distribution Pipe Materials, Engineering Fracture Mechanics, Vol. 36, No. 6, 1990 pp. 903-918.

<sup>2</sup> Kanninen, M.F., and Popelar, C.H., Advanced Fracture Mechanics, Oxford University, Press, New York, 1985

**Table 1.9.1 Correspondence Between Notation on Panels and Panel Designations**

Panel Notation upon Receipt SWRI	Panel Designation Used in This Program
AASHTO M294 Compound with 25% PCR	A
AASHTO M294 Compound with 25% PCR	B
AASHTO M294 Virgin Compound Compression Molded ASTM D-1928 Proc. C. 0.10"	C
AASHTO M 294 Virgin Compound	D

**Test Equipment**

The SCG test setup is shown schematically in Fig. 1.9.7. The SENT sample is loaded with a constant weight. The displacement of the point of application of the load is measured as a function of time with an LVDT. The (time, displacement) data pairs are stored on computer (data logger) for post-test analysis.

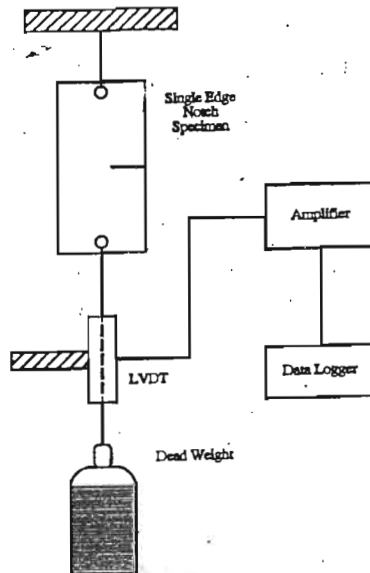


**Fig. 1.9.7 Schematic of the SCG Experimental Setup**

## Test Data

Test number, specimen ID, material type, test conditions, and initial defect size (nominal initial  $a_0/w$  ratio) are given in Table 1.9.2. Under “Specimen number,” A-1, means, for example, sample 1 of panel A.

**Table 1.9.2 Information of Slow Crack Growth Tests**

Test Number	Specimen Number	Type of Polyethylene	Nominal Initial ( $A_0/W$ )	Load (Lb)	Test Temperature ( $^{\circ}F$ )	Test Status
3	A-1	Recycle	0.5	21.0	73	Complete
4	C-3	Virgin	0.5	21.0	73	Complete
5	B-2	Recycle	0.4	10.4	70	In progress
6	D-2	Virgin	0.4	10.4	70	Complete
7	D-1	Virgin	0.5	7.4	73	Complete

Sample A-1 was tested at room temperature and lasted roughly 19 days (456 hours). Data for this specimen, machined from the recycle PE, are shown in Fig. 1.9.8. Figure 1.9.8 is a plot of the displacement of the prenotched test sample in time at the point at which the load was applied. The initial portion of the curve (up to about 89 hours) is due to the viscoelastic response of the material. If no initial cracks were present in the specimen, then the curve would very nearly plateau at about 0.040 to 0.050 inch of displacement for the time scale of this plot. However, because a crack exists, the curve starts to turn upward at about 89 hours, indicating the beginning of crack growth in the sample. This inflection point denotes the transition from incubation to the onset of crack growth or propagation. The time corresponding to this inflection is called the “incubation time”; it is the time from application of a load to a sample or structure containing a defect to the time that the crack begins to grow.

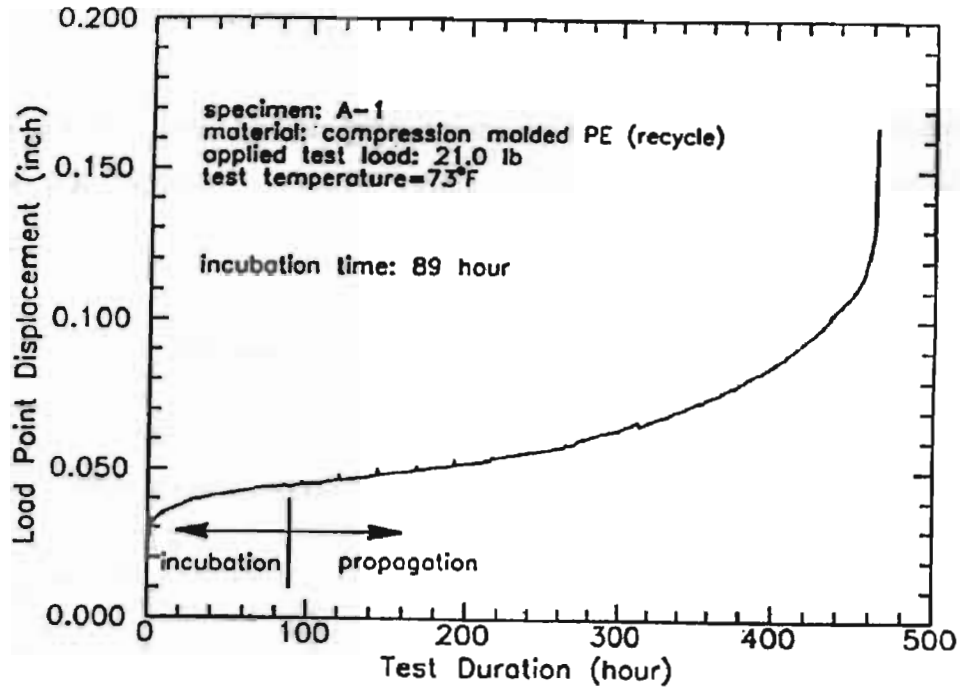


Fig. 1.9.8 Raw SCG Test Data for Recycle Sample A-1. The Point of Inflection at 89 Hours Denotes Transition from Incubation to Crack Propagation

#### Determination of Crack Incubation Material Constants

The initial stress intensity factor,  $K_0$ , is calculated for the SENT specimen geometry<sup>1</sup>:

$$K_0 = \sigma_{rem} \sqrt{\pi a_0} \sqrt{\frac{2w}{\pi a_0} \tan\left(\frac{\pi a_0}{2w}\right)} \left[ \frac{0.752 + 2.02\left(\frac{a_0}{w}\right) + 0.37\left(1 - \sin\frac{\pi a_0}{2w}\right)^3}{\cos\left(\frac{\pi a_0}{2w}\right)} \right]$$

where  $\sigma_{rem}$  is the remote applied stress,  $a_0$  is the initial crack length, and  $w$  is the specimen width. The value of  $K_0$  for each sample is listed in Table 1.9.3.

<sup>1</sup> Tada, H., Paris, P.C. and Irwin, G.R., The Stress Analysis of Cracks Handbook, Del Research Corporation, Hellertown, PA, 1985.

**Table 1.9.3 SCG Post Test Data**

Test	Specimen Number	Type of Polyethylene	Test Temperature (°F)	Measured Initial Defect Depth (in.)	Incubation Time (hours)	Initial Stress Intensity Factor, $K_0$ (psi $\sqrt{\text{inch}}$ )
3	A-1	Recycle	73	0.503	88.6	832.8
4	C-3	Virgin	73	0.515	12.4	880.9
5	B-2	Recycle	70	0.4*	>4000*	274.8*
6	D-2	Virgin	70	0.401	2784	270.4
7	D-1	Virgin	73	0.504	3199	286.7

\* Estimates, due to in-progress test

The incubation time and initial stress intensity data of Table 1.9.3 are plotted at a temperature of 70°F in Fig.1.9.9 for each of the recycle (circles) and virgin materials (triangles). Note that the recycle sample B-2 test is in progress, so that the data point for the incubation time is denoted by the filled circle, with arrow.

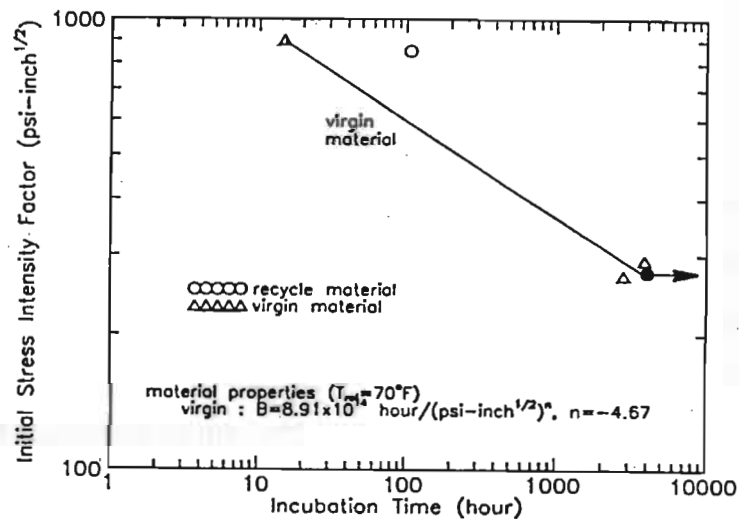


**Fig. 1.9.9 SCG Incubation Test Data For Virgin and Recycle Material Tests. The Line Represents The Best Power Law Fit to the Virgin Material Data**

Data for the virgin material in Fig. 1.9.9 can be represented by the equation

$$t_i = BK_0^n$$

where,  $t_i$  is the incubation time,  $K_0$  is the initial stress intensity factor, and B and n are material parameters. It is the goal of the analyses to determine these material parameters B and n. A power law fit to the virgin material data is shown in Fig. 1.9.9 by the line and results in the constants listed in Table 1.9.4

**Table 1.9.4 SCG Incubation Material Parameters for Virgin PE Material at A Reference Temperature of 70°F. Parameters for Virgin Material are used as Lower Bound Estimates for Those of Recycle PE Material**

Material	B $\left( hr / [psi \sqrt{inch}]^n \right)$	N (--)
AASHTO M294 virgin compound	$8.91 \times 10^4$	-4.67

### Service Lifetime Analysis Procedures

The lifetime forecasting procedures consist of three elements:

- i) Determination of stresses developed in corrugated PE pipes due to service conditions
- ii) Calculation of in-service crack driving forces that result from applied stresses and defects in pipe liners
- iii) The construction of the lifetime forecasting equation using the SCG incubation properties.

## **In-Service Crack Driving Forces**

Just as a SIF solution was needed for the SENT test sample to develop the SCG incubation material parameters, SIF solutions (SIFs) were also needed to characterize the in-service crack driving force. In order to obtain SIFs, tensile stresses that develop in corrugated pipes due to soil overburden were required for input to the crack driving force equation,  $K$ , (through the  $\sigma_{rem}$  term). Stress inputs were provided by the University of Western Ontario.

Sophisticated computer software, developed at SWRI, was used to make the in-service crack driving force calculations. The program employs the weight function approach whereby arbitrary stress fields, acting in the presence of a crack, are used to determine the SIFs for actual structural components.

## **Service Lifetime Equation**

The Popelar bi-directional time-temperature shift factors were used to make lifetime estimates that account for different service temperatures and are given by

$$a_T = \exp\{-0.0606(T_s - T_i)\}$$

and

$$b_T = \exp\{0.0064(T_s - T_i)\}$$

where,  $T_s$  is the service temperature of interest and  $T_i$  is the reference temperature corresponding to that of the SCG incubation properties. Both temperatures are in degrees Fahrenheit.

The incubation lifetime is the time from the application of tensile stress to a defect in a structure up to the time that the defect begins to grow. It is given by

$$t_i = a_T b_T^n B K_0^n$$

where,  $a_T$  and  $b_T$  are the Popelar shift functions,  $B$  and  $n$  are the SCG incubation material parameters (Table 1.9.4), and  $K_0$  is the in-service crack driving force corresponding to the initial defect depth,  $a_0$ . This equation is used to make incubation lifetime estimates for recycle and virgin corrugated PE pipes.

### Service Lifetime Estimates

Failure of a corrugated pipe is defined as the onset of crack growth; i.e., the time from application of tensile stress to a defect in a pipe until the time at which the defect starts to grow. Plots of service lifetime are presented as a function of initial crack depth, service temperature, and initial defect geometry. All defects are assumed to be oriented in the radial-circumferential plane, such that tensile axial stress acts to initiate crack growth. Furthermore, the defects are assumed to exist at the inner surface of the liner, where the axial tensile stresses are largest. The lifetime plots are therefore “worst case” scenarios.

Fig. 1.9.10 is a plot of incubation life versus service temperature for 18 inch diameter, virgin corrugated PE pipe buried at 36 feet. In this figure, temperature ranges from 45 to 65°F, while the resulting lifetime spans 0 to 100 years. The three initial defect depths range from 0.015 inch to 0.025 inch (compared to the liner wall thickness of 0.071 inch).

Data in Fig. 1.9.10 can be used by corrugated pipe manufacturers, as well as the gravity flow corrugated pipe industry. For example, in Fig. 1.9.10, if a design life of 60 years is desired for 18 inch diameter virgin pipe buried to a depth of 36 feet, and if ground temperature in the geographic region where the pipe will be installed is about 52°F, then the maximum allowable defect depth that can be tolerated in the liner of the pipe is 0.020 inch.

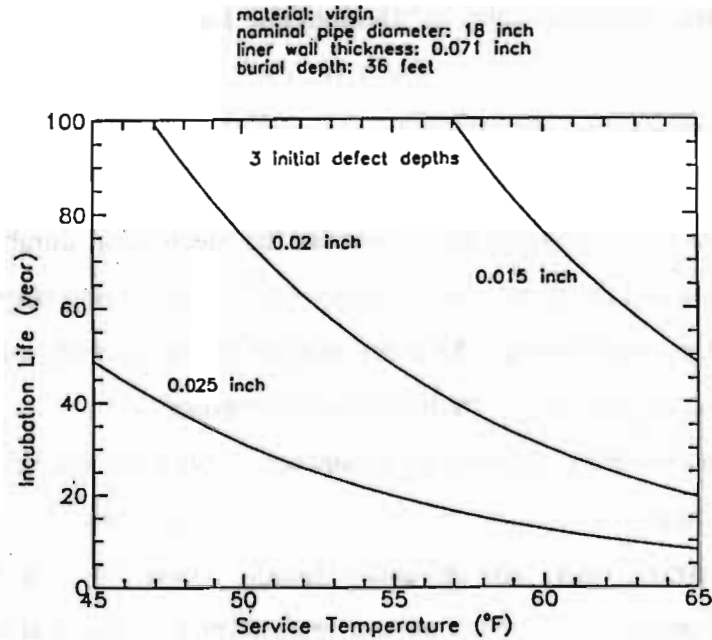


**Fig. 1.9.10 Estimated Lifetime of 18 Inch Diameter Virgin Pipe Buried at A Depth of 36 Feet versus Service Temperature for Three Defect Depths**

This 60 year life starts from the time at which the defect is introduced into the liner, under load. For instance, in this example, if the pipe was in operation for 5 years, and at the end of the fifth year, the 0.020 inch defect was introduced, then the total lifetime would be approximately 65 years (5+60).

### Conclusions

Lifetime calculations were made for corrugated PE pipes in service. The total lifetime of a PE structure is the sum of the incubation life and the propagation life. This study addressed the incubation life exclusively. This approach of neglecting the propagation life contributes to the conservatism in the lifetime graphs.

It was found that the linear elastic-fracture mechanics lifetime estimation procedures developed for natural gas pressurized PE pipe can be applied to corrugated pipe.

All data consistently show that the recycle material is more SCG resistant than the virgin material. Thus, the lifetime plots for virgin pipe can be taken as lower bounds on the lifetimes for recycle pipe.

**Time-Temperature Superposition in Mechanical Durability Testing of Polyethylene Geomembranes**, Lord, Jr., A. E., Hsuan Y.G., and Koerner, R.M., *Geotechnical Testing Journal*, v 16, n 2, June 1993, pp.259-262.

The objective of this paper is to consider the mechanical durability of polyethylene (PE) geomembranes and check whether the universal factors of polyethylene plastic pipe can also be applied to geomembranes. As a supplement to the currently used notched constant tensile load tests, crack growth rate studies are also proposed.

The time-temperature superposition concept in polymer science allows one to shift high-temperature data (which takes relatively short time to obtain) to a lower-temperature (where data acquisition times are extremely long). These lower temperatures represent typical service temperatures for many natural applications. Popelar et al.<sup>1</sup> showed that the shift factor can be applied to a variety of stress vs. failure time data in the HDPE pipe area. It is of significant importance to see if the same shifting factors in polyethylene pipe can be used for polyethylene geomembranes as well.

### **Crack Growth Rate Theory**

The theory of linear elastic fracture mechanics is used for crack growth rate evaluation. An attempt is made to provide suitable parameters for analyzing material failure under mechanical load. It is assumed that all materials have flaws (defects, cracks). The strength of the stress field at the crack tip is described by a stress intensity factor  $K$  given by

$$K = c\sigma(a)^{\frac{1}{2}}$$

where,  $c$  = a geometrical stress-raising factor which is a complicated function of the (crack length) / (specimen thickness) ratio; its value for the single edge notch shown in Fig. 1.9.11 can be found in Kinlock and Young<sup>2</sup>

$\sigma$  = applied stress  
 $a$  = crack length.

---

<sup>1</sup> Popelar, C.H., Kenner, V.H. and Wooster, J.P., An Accelerated Method for Establishing the Long Term Performance of Polyethylene Gas Pipe Materials, *Polymer Engineering and Science*, Vol. 31, No. 24, pp. 1693-1700.

<sup>2</sup> Kinlock, A.J. and Young, R.J., *Fracture Behavior of Polymers*, Elsevier, London, p. 102.

The stress intensity factor  $K$  depends on external stress, crack size, specimen geometry and crack geometry. Experiments in a large number of crack growth studies show that “ $K$ ” and the rate of crack growth “ $da/dt$ ” are related by the following equation

$$\frac{da}{dt} = a = BK^n$$

where,  $B$  and  $n$  are empirical constants, which depend on the material, temperature, and stress. By integrating the above equation we get

$$t_f = \frac{1}{B} \int_{a_0}^w \frac{da}{K^n} + t_i$$

where,  $t_f$  = failure time

$a_0$  = initial crack depth

$w$  = sheet thickness, and

$t_i$  = time to initiate slow crack growth (SCG).

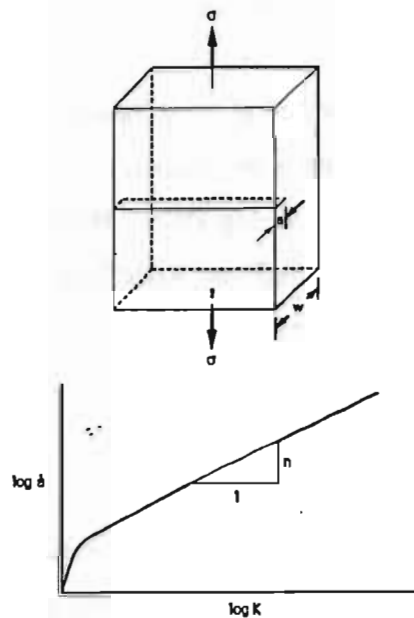


**Fig.1.9.11 Notched Constant Load Specimen and Crack Growth Rate  $\dot{a}$  ( $da/dt$ ) versus Stress Intensity Factor ( $K$ ) Curve**

SCG can be monitored in a notched geomembrane (sheet) specimen at a constant elevated temperature. The constants  $B$  and  $n$  would be determined, and the incubation time,  $t_i$ , for the start of crack growth would also be established. The SCG results can then be shifted to the lower ambient site-specific temperature of the geomembrane by means of the universal time-temperature shift factors. Failure times will be calculated from the equation above at ambient temperature for various assumed initial crack sizes  $a_0$  and sheet thickness  $w$ .

### **Time-Temperature Superposition in PE Geomembranes**

The modified version of constant load test called the notched constant tension load (NCTL) test is used to study the ductile-to-brittle behavior of semi-crystalline geomembranes including those made from polyethylene. This test uses ASTM Test Method for Tensile-Impact Energy to Break Plastics and Electrical Insulating Materials (D 1822-89) shaped dumbbell specimens. These specimens are notched to a depth of 20% of thickness at their midpoint and subjected to constant load.

A series of tests are performed at temperatures of  $50^{\circ}\text{C}$ ,  $40^{\circ}\text{C}$  and  $25^{\circ}\text{C}$  using an PE geomembrane. The responsive curves are shown in Fig. 1.9.12, which display a piece-wise linear behavior plotting log stress vs. log failure time. If the transition points (i.e., break point of these curves sometimes called the “knee”) are shifted horizontally and vertically, a single master curve can be determined.

### **Conclusions**

It is found that both the vertical and horizontal shift factors for the geomembrane sheet materials are precisely the same as those universal factors determined for HDPE pipe materials. The results obtained in the NCTL test can be shifted to ambient temperatures with some degree of confidence.

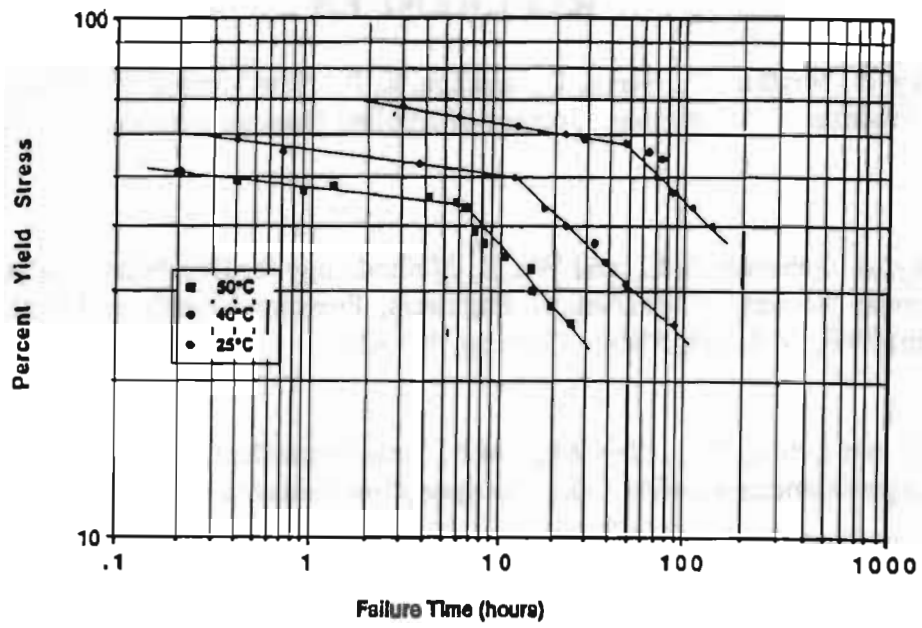


Fig.1.9.12 Experimental NCTL Test Results for a HDPE Geomembrane

## REFERENCES

- Chudnovsky, A., Shulkin, Y., Baron, D., and Lin, K. P., New Method of Lifetime Prediction for Brittle Fracture of Polyethylene, *Journal of Applied Polymer Science*, Vol. 56, 1995, pp. 1465-1478.
- Chudnovsky, A., Sehanobish, K., and Wu, S., Methodology for Durability Analysis of HDPE Pipe, American Society of Mechanical Engineers, Pressure Vessels and Piping Division (Publication) PVP, Vol. 388, ASME 1999, pp. 405-412
- Chuo, K.M. and Lytton, R.L., New Method of Time-Dependent Analysis for Interaction of Soil and Large-Diameter Flexible Pipe, *Transportation Research Record* 1315, 1991, pp. 58-66.
- Conard, B. E., Lohnes, R. A., Klaiber, F. W., and Wipf, T. J., Boundary Effects on Response of Polyethylene Pipe Under Simulated Live Load, *Transportation Research Record* 1624, Paper No. 98-0588, 1998, pp. 196-205.
- Dhar, A. S. and Moore, I. D., Corrugated HDPE Pipe: Laboratory Testing and Two-Dimensional Analysis to Develop Limit States Design, *Transportation Research Board 81<sup>st</sup> Annual Meeting*, Jan. 2002, pp. 22.
- Duryee, W.A., The Peripheral Movement of Soil Around a Buried Flexible Pipe ,Master's Thesis, Department of Civil Engineering, Kansas State University, 1974.
- Faragher, E., Rogers, C.D.F., and Fleming, P.R., Laboratory Determination of Soil Stiffness Data for Buried Plastic Pipe, *Transportation Research Record* 1624, Paper No.98-0773, 1998, pp. 231-236.
- Fleming, P.R., Faragher, E., and Rogers, C.D.F., Laboratory and Field Testing of Large-Diameter Plastic Pipe, *Transportation Research Record* 1594, 1997, pp. 208-216.
- Havens, B.T., Klaiber, F.W., Lohnes, R.A., and Zachary, L.W., Longitudinal Strength and Stiffness of Corrugated Steel Pipe, *Transportation Research Record* 1514, 1995, pp. 1-9.
- Howard, A.K., Modulus of Soil Reaction Values For Buried Flexible Pipe, *ASCE Journal of the Geotechnical Engineering Division*, Vol.103, No.GT1, January 1977, pp.33-43.

Katona, M.G. and Akl, A.Y., Structural Design of Buried Culverts With Slotted Joints, ASCE Journal of Structural Engineering, Vol .113, No.1, 1987, pp. 44-60.

Klaiber, F.W., Lohnes, R.A., Zachary, L.W., Austin, T.A., Havens, B.T., Mccurnin, B.T., Design Methodology for Corrugated Metal Pipe Tiedowns: Phase 1, Iowa DOT Project HR-332, ISU-ERI-Ames-9340, Engineering Research Institute, Iowa State University, 1993.

Kuhlman, C. J., Weed, D. N., and Campbell, F. S., Accelerated Fracture Mechanics Evaluation of Slow Crack Growth Potential in Corrugated Polyethylene Pipes, Final Report No. 06-15378 submitted to Corrugated Plastic Pipe Association, 1995.

Lohnes, R.A., Klaiber, F.W., Kjartanson, B.H., Austin, T.A., Heilers, G.A., Morgan, B.C., Peiffer E.A., Design Methodology for Corrugated Metal Pipe Tiedowns: Phase 2, Iowa DOT Project HR-362, ISU-ERI-Ames-9640, Engineering Research Institute, Iowa State University, 1995.

Lord, Jr., A. E., Hsuan Y.G., and Koerner, R.M., Time-Temperature Superposition in Mechanical Durability Testing of Polyethylene Geomembranes, Geotechnical Testing Journal, v 16, n 2, June 1993, pp.259-262

McGrath, T.J., Calculating Loads on Buried Culverts Based on Pipe Hoop Stiffness, Transportation Research Record 1656, Paper No.99-0909, 1999, pp.73-79.

McGrath, T. J., DelloRusso, S. J., and Boynton, J., Performance of Thermoplastic Culvert Pipe Under Highway Vehicle Loading, Transportation Research Board 81<sup>st</sup> Annual Meeting, Jan. 2002, pp. 14.

Moore, I.D., and Brachman, R.W., Three-Dimensional Analysis of Flexible Circular Culverts, ASCE Journal of the Geotechnical Engineering, Vol. 120, No.10, 1994, pp.1829-1844.

Moore, I.D., Three Dimensional Time Dependent Model for Buried HDPE Pipe, The Proceedings of the Eighth International Conference on Computer Methods and Advances in Geomechanics, Vol.2, 1994, pp. 1515-1520.

Moore, I.D., Three Dimensional Response of Deeply Buried Profiled Polyethylene Pipe, Geotechnical Research Center Report, GEOT-6-95, University of Western Ontario, London, ON, Canada, N6A 5B9, February 1995.

Moser, A.P., Structural Performance of HDPE Profile-wall Pipe, Buried Structures Laboratory, Utah State University, Logan, Utah, October 1999.

Petroff, L.J., Stress Relaxation Characteristics of the HDPE Pipe-Soil System, Proceedings of the International Conference sponsored by the Pipeline Planning Committee of the Pipeline Division of the American Society of Civil Engineers, 1990, pp.281-294.

Rogers, C. D. F., The Influence of Surrounding Soil on Flexible Pipe Performance, Transportation Research Record 1129, 1987, pp. 1-11.

Rogers, C. D. F., Some Observations on Flexible Pipe Response to Load, Transportation Research Record 1191, 1988, pp. 1-11.

Rogers, C.D.F., Fleming, P.R., Loeppky, M.W.J., and Faragher, E., Structural Performance of Profile-Wall Drainage Pipe-Stiffness Requirements Contrasted with Results of Laboratory and Field Tests, Transportation Research Record 1624, 1995, pp. 83-92.

Sargand, S. M., Hazen, G.A., White, K., and Moran, A.P., Time-Dependent Deflection of Thermoplastic Pipes Under Deep Burial, Transportation Research Board 80<sup>th</sup> Annual Meeting, Jan. 2001, pp.12.

Sargand, S.M., Hazen, G.A., and Moran, A.P., Comparison of Structural Response of 762 mm (30 in.) Diameter Thermoplastic Pipes under Deep Burial, Transportation Research Board 80<sup>th</sup> Annual Meeting, Jan. 2001, pp.24.

Sargand, S. M., Hazen, G.A., White, K., and Bhargava, A., Comparison of Tests and Analysis of 1050 mm (42 in.) Diameter High Density Polyethylene (HDPE) Thermoplastic Pipe, Transportation Research Board 80<sup>th</sup> Annual Meeting, Jan 2001, pp.18

Seed, R. B. and Duncan, J. M., Earth Pressure and Surface Load Effects on Buried Pipelines, Advances in Underground Pipeline Engineering, Jeyapalan, J.K. ed., 1985, pp. 320-329.

Suleiman, M. T., Wipf, T. J., Klaiber, F. W., and Lohnes, R. A., Analysis of Buried Flexible Pipe Using CANDE and ANSYS, Transportation Research Board 81<sup>st</sup> Annual Meeting, Jan. 2002, pp. 19.

Zhang, C. and Moore I. D., Nonlinear Finite Element Analysis for Thermoplastic Pipes, Transportation Research Record 1624,1998, pp. 225-230.

Vaslestad, J., Long-term Behavior of Flexible Large-Span Culverts, Transportation Research Board 68<sup>th</sup> Annual Meeting, Paper No.88 0337, Jan.1989.